The University Of Zielona Góra

DOCTORAL THESIS

The Effect of Spread –Spectrum Modulated EMI on the Power Line Communication Systems

Wpływ EMI modulacji widma rozproszonego na systemy komunikacji linii elektroenergetycznych

Author:
M.Sc.Waseem Elsayed

Supervisors:
prof. dr hab. Eng. Robert Smoleński
(University of Zielona Góra)
Signature:.....
prof. Frank Leferink
(University of Twente)
Signature:.....
prof. Dave Thomas
(University of Nottingham)
Signature:.....

Faculty of Computer, Electrical and Control Engineering

Automation, Electronics, Electrical Engineering and Space Technologies

Zielona Góra, May, 2023

Contents

List of Figures

List of Tables

Acronyms

ADC	Analoge to Digital Converter
AFE	Analogue Front End
ARIB	Association of Radio Industries and Businesses
AV	Average detector
AWGN	Additive White Gaussian Noise
BER	Bit Error Rate
CAN	Controller Area Network
CFL	Compact Florescent lamp
CM	Common Mode
CP	Cyclic Prefix
D8PSK	Differential 8-bit Phase Shift Keying
DBPSK	Differential Binary Phase Shift Keying
DDC	Digital Down Converter
DPSK	Differential Phase Shift Keying
DUC	Digital Up converter
DM	Differential Mode
DQPSK	Differential Quad Phase Shift Keying
EMC	Electromagnetic Compatibility
EMI	Electromagnetic Interference
EN	European Norm
FCC	Federal Communications Commission
FEC	Forward Error Correction
FER	Frame Error Rate
FFT	Fast Fourier Transform
FIR	Finite Impulse Response
FSK	Frequency Shift Keying
GSM	Global System for Mobile
IF	Intermediate Frequency
IFBW	Intermediate Frequency Band Width
IFFT	Inverse Fast Fourier Transform
ISI	Inter Symbol Interference
LED	Light Emitted Diode
LISN	Line Impedance Stabilization Network
MAC	Medium Access Control
OFDM	Orthogonal Frequency Division Multiplexing
PAM	Pulse Amplitude Modulation
PHY	Physical Layer
PLC	Power Line Communication
PRIME	Power line Related Intelligent Metering Evolution
PSK	Phase Shift Keying
PWM	Pulse Width Modulation
QP	Quasi Peak detector
RBW	Resolution Bandwidth
RCFMFD	Random Carrier Frequency Modulation with Fixed Duty cycle
RCFMVD	Random Carrier Frequency Modulation with Variable Duty cycle
RPPM	Random Pulse Position Modulation
RPWM	Random Pulse Width Modulation
SCENT	Smart Cities EMC Network for Training
Si	Silcon
SiC	Silicaon Carbide
SNR	Signal to Noise Ratio
SRRC	Square Root Raised Cosine
SSM	Spread Spectrum Modulation
TI	Texas Instrument

Chapter 1

Introduction

1.1. Electromagnetic Compatibility in the Smart grid

Nowadays, the interest in using green sources of energy like solar and wind energies [1, 2] has amplified due to the well-known adverse impact of using fossil fuels on the environment. Furthermore, the rapid increase in technological inventions helps in creating a smart grid environment to raise grid efficiency and reliability. However, due to the complexity of the smart grid systems, various problems may exist — including the Electromagnetic Compatibility (EMC) between the smart grid elements.
The EMC according to the International Electrotechnical Commission (IEC), means "EMC is the process in which such electromagnetic interferences are contained so that all surrounding equipment can operate safely and reliably.". From the EMC perspective,there is a source of Electromagnetic Interference (EMI) affects a certain victim/s through a parasitic coupling path. Therefore, EMC is the successful avoidance of these interferences. The interference could be conducted or radiated, also the interference could occurs internally in the same device due to the parasitic coupling between the components. In the case of the radiated EMI, the emissions source generating high-frequency components travels through the air and affects the victim. However, in the case of conducted emissions, the coupling path exists in the electric circuit. Generally, the conducted emission could be inductive or capacitive or a combination between them, also it can be through direct galvanic conduction.

In this thesis, we will only focus on the effect of EMI on the performance of the victim devices. Electromagnetic Interference is generated from several energy receivers such as electric drives, lighting, household appliances, and computers. Most of these devices use power electronic converters in their operation. Hence, the power electronic converters are a common source of EMI and they could affect the operation or even cause the malfunctioning of some devices in the grid if a parasitic coupling path has existed.

1.2. Motivation

Most of the EMC challenges in the smart grid appear due to the complexity of the smart grid, which results in a closer interaction between the electrical power and power electronics with information technology and communications equipment. This happens because a lot of electrical devices were designed as compact devices that include both power and communication capabilities. Moreover, most power converters utilise switching frequencies that falls in the same bandwidth utilised by the low frequency communication systems, especially in CISPR A band. The communication standards deal with the communication channel performance under the effect of noise. Therefore, a lot of digital communication technologies have been implemented like the Orthogonal Frequency Division Multiplexing (OFDM) to assure the robustness of the communication systems under the presence of noise.
For decades, EMC and communication standards have dealt with the amplitude and the frequency of the signal as the dominant factors that control the behaviour of the devices. Nevertheless, in a complex environment, the relationship between devices is much deeper than what is considered in the standards. In addition, there appears to be a lack of research investigating

the effect of the SSM modulated EMI on the communication channel behaviour.

Generally speaking, we can divide the devices in the electric systems into two types — devices with communication and those without communication [3]. Thus, the possibility of conducted interference could take place intentionally or unintentionally in four forms (A-D):

A) Interference between devices with communication

This occurs when two or more devices that have communication features and work together, affect each other causing an increase in the bit error rate. As their interaction is intentional, these devices are designed to work with a specific signal-to-noise ratio (SNR). Consequently, this type of interference is not considered as it is not expected that they will disturb each other in an undesired manner.

B) Interference of devices without communication by devices with communication

In this type of interference, the communication equipment (e.g: Power Line Communication (PLC)) can have a great impact on the device without communication. This type of interference was stated in [4],for example, the PLC works between 42 and 88 kHz frequency band, in this case, the PLC can affect the loads that work with a switching frequency between this range, which may cause the malfunction of the working device and additional heating of internal components of the affected device, thereby reducing its lifetime [5]. As the signalling frequencies of the communication devices are usually above 20 kHz, the generation of audible noise is not an issue for interference type. In addition, the communication signal power is usually less than the power of the EMI signal, this type of interference seldom happens, however, the interference may exist in case of a high-frequency converter.

C) Interference of devices with communication by devices without communication

In this case, the victim is the communication device (e.g: PLC), the interference causes the decrease of the SNR below the level of noise-free communication, respectively, causing the presence of bite error and sometimes failure of communication [6–9].This could happen for two reasons. The first is due to the low input impedance of the non-communicating device, which leads to a decrease in the level of the communication signal causing the receiver to not decode the data accurately. The second reason is the non-intention emission generated by the device without communication, which may lay between the PLC frequencies working range. Depending on the location and the number of the EMI sources, the communication may fail in one or multiple communication devices in the low voltage network.

D) Interference between devices without communication

Interferences of this type always include at least one device with non-intentional emission. The interaction between devices is mainly determined by their input impedance characteristic. High non-intentional emission levels combined with low input impedances of the affected equipment can increase the probability of interference significantly. Usually, this could happen in the case of aggregated EMI in the smart grid where there are several sources of EMI. Thus, the effect of the EMI could appear in the form of frequency-beating phenomena, if two or more converters are operating with the same switching frequency [10].

Figure 1.1 shows the four possible interference types between devices. As in most cases, the power devices are much stronger than the communication devices, type C is the most common interference in the smart grid systems. Usually, this type of interference occurs in the low-frequency range between 9 to 150 kHz, as most the power devices (e.g: power electronics converters) utilize a switching frequency in the same frequency range.

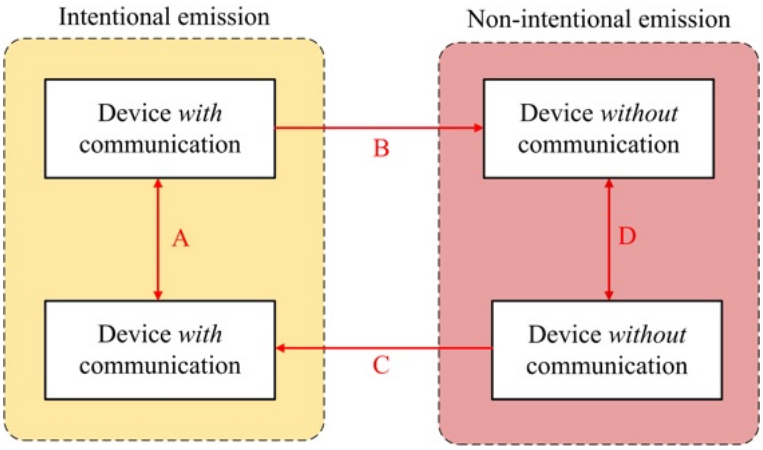

Figure 1.1: Types of interference between devices.

1.2.1. PLC as victim

Based on the Benchmarking Smart Metering Deployment report published by the European Commission [11], recently there is great progress in the use of smart meters. The PLC is used in more than 14 EU countries as one of the used protocols in the smart metering system. Consequently, the PLC-based smart meters were chosen as the victim in this thesis.
A lot of EU countries have already replaced most electrical meters with smart ones. As shown in Figure 1.2, countries like Italy, Spain, Finland, Estonia, and Sweden have already replaced more than 90 % of their old metering systems with smart ones prior to 2020. The other EU countries are working towards replacing all the meters by the end of 2030. In the meantime, there are 123 million electricity meters being read remotely using PLC transmission, which are estimated to be 43 percent of all meters installed in the EU states.

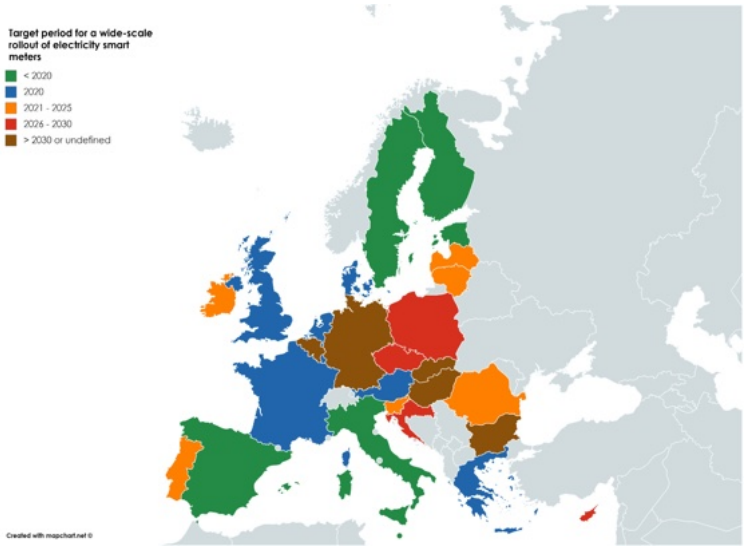

Figure 1.2: EU Countries progress in the smart meter deployment [11].

1.3. Objective

Based on the state-of-the-art, the thesis assumption is: It is possible to improve the reliability of Power Line Communication data transmission by control algorithms and modulation parameters of power electronic converters operating in nearby electromagnetic environment. For the sake of ease and clarity, the used converter in the setup is a basic buck converter in order to study the effect of the EMI generated from the least number of switches (one or two) on the PLC systems. The communication system behaviour varies depending upon several variables. In this thesis, the effect of the power converter Pulse Width Modulation (PWM) on the PLC systems' channel performance is considered. PWM could be divided into two main general types: Conventional modulation and Random modulation (Spread-Spectrum modulation) [12]. As such, this thesis considers both the techniques for analysis. Additionally, two approaches have been employed to evaluate the performance of the PLC channel in this thesis:

a) Calculating the Frame Error Rate (FER) in percentage.

b) Calculating the channel capacity in Kbit/sec using the Shannon Hartely equation.

The two approaches have been used in several operating scenarios to assure the robustness of the results [13, 14]. The FER calculation focuses on the quantity of the data transmitted through the communication channel in the presence of the EMI, while the channel capacity factor focuses on the quality of the communication channel in the presence of the EMI.
Simultaneously, other statistical tools like the correlation factor have also been used to measure the relation between the communication channel performance and the spread-spectrum design parameters. The purpose of this is to formulate a relationship between the communication system parameters and the power converter modulation parameters.

1.4. What's next?

Consequently, the results conducted from this thesis will guide the engineers in choosing the best applicable parameters for the utilised power converter modulation. Indeed, this study aims to reach a point where the behaviour of the PLC communication system can be improved by controlling the modulation parameters of the used converters around it. Thus, it will aid in achieving both the purpose of the EMC standards as well as the communication standards.

Chapter 2

Power converters in smart grid

The power converters are used in almost all types of renewable energy applications such as wind generation systems [2], PV systems [1], and electric vehicle systems [12]. However, the gross use of the power converters in most of the smart grid applications results in increasing the possibility of EMI between the grid elements.

In this chapter, we will discuss the implementation of several types of SSM techniques on the power converters while also considering the effect of changing the SSM setting on the shape of the generated EMI.

2.1. Power converters as a source of EMI

The high switching in the converter topology leads to an increase in the noise and harmonics in the electrical grid, in addition to the high possibility of electromagnetic interference with other devices. Usually, the switching frequency of the converters is in the range of kHz (less than 100 kHz) and could interfere with other devices operating in the same narrow-band frequency range, if a parasitic coupling exists. Consequently, many researchers have proposed the designing of filters as a hardware solution for the EMI problem to eliminate the high peak amplitude of EMI noises at a specific range of frequency to pass the EMC compliance tests [16, 17]. However, this solution could increase the size of the converter's units due to the additional passive components added to the circuit. Other researchers have looked at utilising the wide-band semiconductors like Silicon Carbide (SiC) [18, 19] and Gallium nitride (GaN); for the advantage of low switching losses and high switching frequency capability (over 100 kHz), which could be a possible solution to overcome the overlapping in the frequency band. However, the high switching frequency increases the level of EMI in the high-frequency ranges [20–22].
On the other hand, a plethora of research has proposed the use of spread-spectrum modulation techniques as a mitigation tool for the EMI generated from the converters. The SSM techniques work to distribute the power of the signal into a wider band of frequencies to significantly reduce the EMI amplitude at the harmonics of the switching frequency [23–25]. Arguably, the SSM techniques have offered a solution for the EMI problem without adding any additional passive components, however, it could lead to an increase in the switching losses and in some cases to an increase in the harmonics in the system.
In accordance, the next section will introduce how the PWM signal is implemented in the case of conventional modulation and in the case of spread-spectrum modulation

2.2. Conventional Pulse Width Modulation (PWM)

The PWM signal can be defined by four main parameters — (1) the period of the signal T (related to the signal frequency f); (2) the amplitude A; (3) the turn ON time of the signal ϕ and; (4) the phase shift of the signal λ as shown in Figure 2.1. As the PWM control signal is usually generated from a micro controller, the setting of the signal parameters is controlled by a certain counter timer inside the controller [26].
For a standard PWM with a constant switching frequency, the signal compares the reference

values for the duty cycle to the constant carrier frequency generated by the timer (the period T remains constant with the time). In the frequency domain, spectral lines occur at fixed frequencies related to the carrier frequency and its multiples, as shown in Figure 2.2.Generally speaking, the switching signal from the conventional PWM could be represented in terms of its Fourier series expansion as:

$$S(t) = \sum_{k=-\infty}^{\infty} A_k e^{j2\pi k f_c t}, \tag{2.1}$$

where k is the harmonic order, A_k is the amplitude of the kth harmonic and f_c is the fundamental frequency of the switching signal. Thus, the generated power spectral density of the rectangular signal could be written as $S(f)$:

$$S_{EMI}(f) = |H(f)|^2 \sum_{k=0}^{\infty} |A_k|^2 \cdot \gamma(f - kf_c), \tag{2.2}$$

where $H(f)$ is the transfer function of the EMI coupling and $\gamma(x)$ is the amplitude probability density function of the spread function.

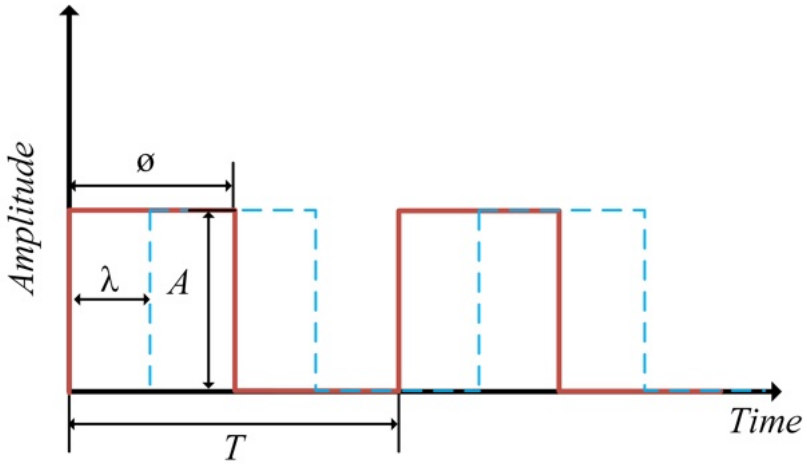

Figure 2.1: Conventional PWM in time domain.

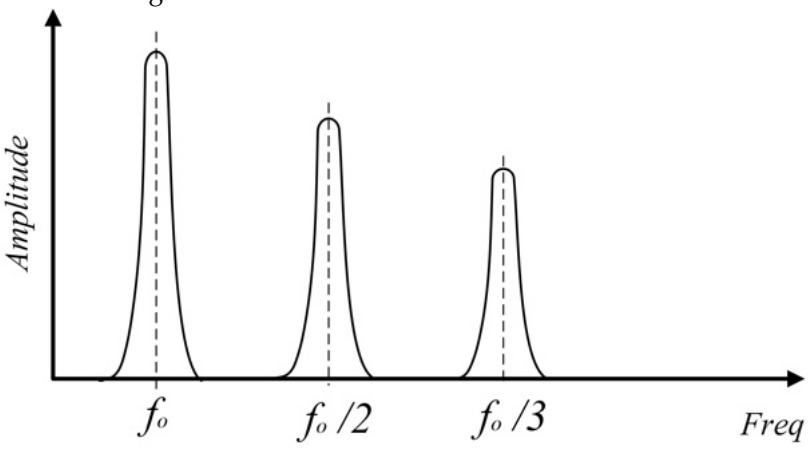

Figure 2.2: Conventional PWM in frequency domain.

2.3. Spread-spectrum modulation

In the spread-spectrum modulation techniques, the one or several parameter/s of the rectangular signal change simultaneously over time . The SSM approaches could randomise the switching frequency or the duty cycle, or the phase shift of the signal [26]. As a result, in all cases, the power of the signal is decreased (as shown in Figure 2.3) according to the modulation spreading depth settings to fulfil the standards. Based on [27], the SSM could be divided into two main types — Randomised techniques with randomised sampling frequency and Randomised techniques with constant sampling frequency.

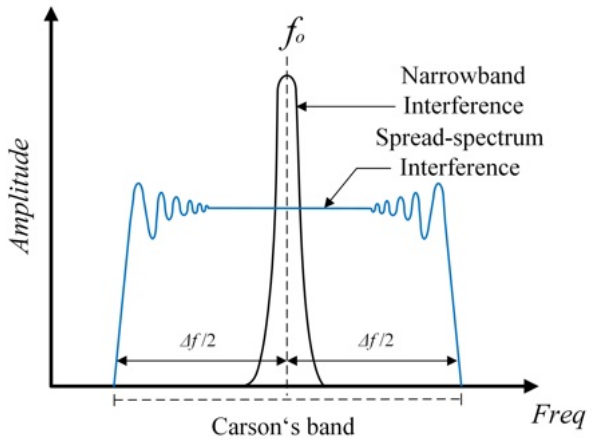

Figure 2.3: Sketch to show the difference between a conventional and a spread spectrum modulation.

2.3.1. Random Techniques with Randomised Sampling Frequency

The basic concept of these types of SSM is to spread the power of the spectrum to several frequencies, changes instantaneously with time within accepted range of frequency [25]. We can divide the SSM in this case into two types:

- Random Carrier Frequency Modulation with Constant Duty cycle (RCFMFD) [28–37].
- Random Carrier Frequency Modulation with Variable Duty cycle (RCFMVD) [10, 25].

- *Random Carrier Frequency Modulation with Constant Duty cycle (RCFMFD)*

For the RCFMFD, the frequency slope of the carrier signal generated by a controller timer changes rapidly with time while maintaining a constant peak value. Consequently, as the reference signal is in terms of the peak value of the carrier signal, the duty cycle remains fixed at the required value as shown in Figure 2.4. Also, the phase shift of the signal remains constant with time [38]. Due to the frequency randomization, the output voltage from the converter in this modulation case will include some voltage ripples. Nevertheless, the average current output of the converter remains constant.

- *Random Carrier Frequency Modulation with Variable Duty cycle (RCFMVD)*

In the case of RCFMVD, the signal frequency changes by means of changes in the peak value of the carrier signal generated by the timer counter. Therefore, the slope of the carrier signal remains constant, however, the peak value of the signal changes rapidly with time as shown in Figure 2.5. The duty cycle of the signal changes every time (T), as the duty cycle reference value is proportional to the carrier signal peak value. Besides, the phase shift of the signal remains constant with the time of the phase.
The change in the duty cycle is followed by the significant changes in the average current output from the converter. Consequently, this way of modulation causes a high voltage ripple in the out signal from the converter [25].

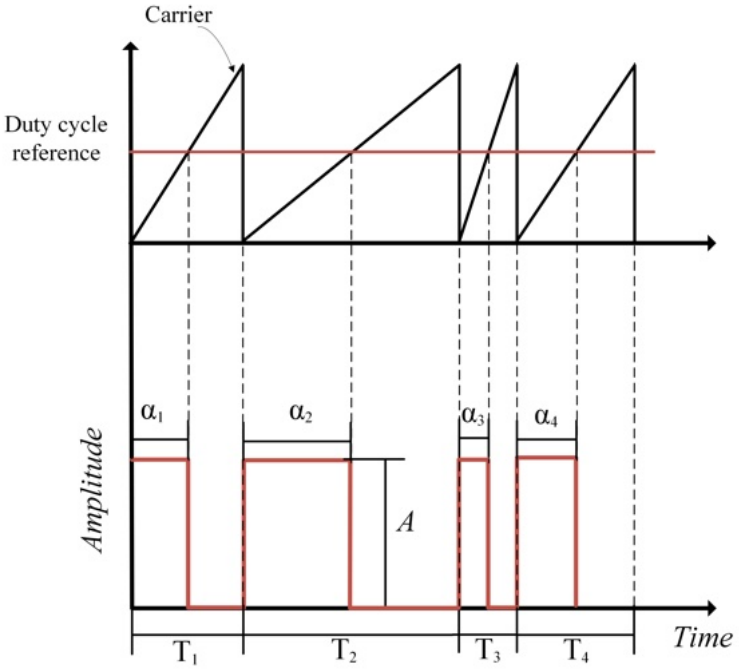

Figure 2.4: RCFMFD Technique operation.

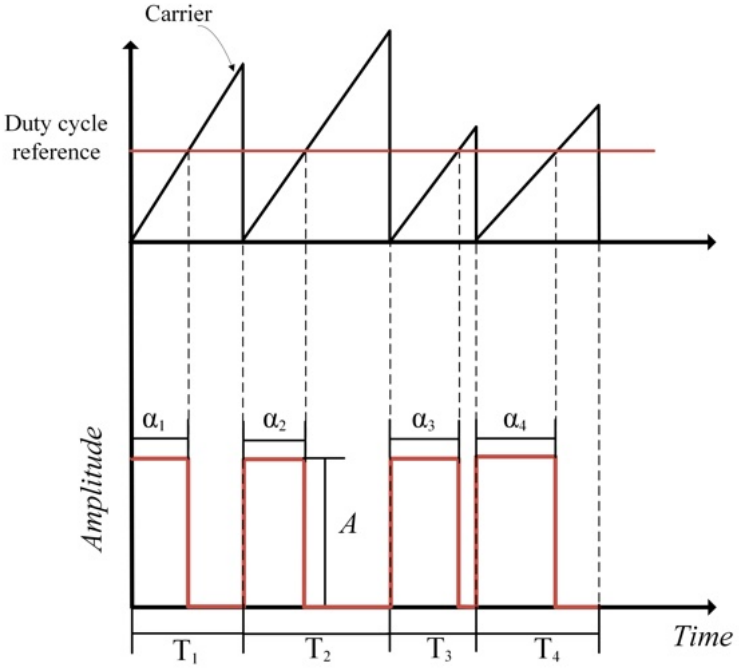

Figure 2.5: RCFMVD Technique operation.

2.3.2. Random Techniques with Constant Sampling Frequency

In these types of SSM techniques, the frequency of the carrier signal remains constant, however, the signal could be randomized by changing other parameters like the duty cycle reference or the phase shift of the signal. Two types of modulations could be considered in this approach: the first is the Randomized Pulse Width Modulation (RPWM) [39–41] and the second is the Randomized Pulse Position Modulation (RPPM) [42–49].
In the case of RPWM, the duty cycle reference of the modulation signal changes randomly within a definite range as shown in Figure 2.6. However, the voltage ripple in this approach is significantly high due to the rapid change in the output current caused by the duty cycle change. In contrast, the RPPM approach works based on changing the phase shift of the modulation signal within a constant duty cycle (with leading- or trailing-edge modulation) as shown in Figure 2.7. Nevertheless, the average converter current changes signifying for different phase shifts. Consequently, the output voltage ripple will be increased. Another approach for the RPPM modulation was presented in [50], to avoid the output voltage variation caused by random pulse position, which is called random symmetric-on symmetric-off modulation.

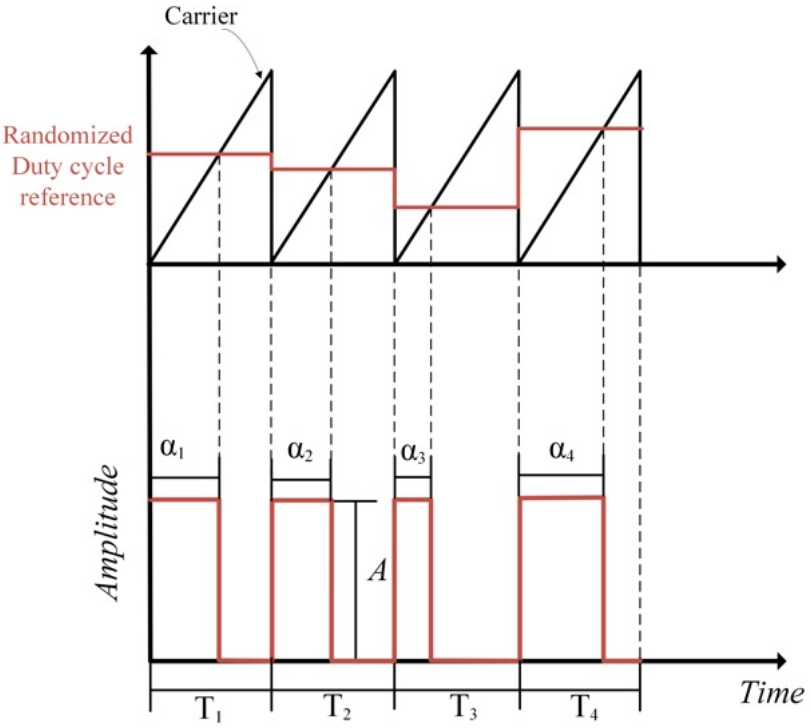

Figure 2.6: RPWM Technique operation.

Table 2.1: Spread-Spectrum techniques classifications.

Switching Scheme	Signal period T	ON time α	Phase shift λ	Duty cycle $d = \frac{\alpha}{T}$	Sampling frequency
Conventional PWM	Constant	Constant	Zero	Constant	Constant
RCFMFD	Randomised	Randomised	Zero	Constant	Randomised
RCFMVD	Randomised	Constant	Zero	Randomised	Randomised
RPWM	Constant	Randomised	Zero	Randomised	Constant
RPPM	Constant	Constant	Randomised	Constant	Constant

Table 2.1 shows the difference between the operation of each SSM technique and which parameter to be randomised under each scheme. The next section implements the RCFMFD technique on the converter control, as it is one of the most common frequency modulations used in many applications [51, 52].

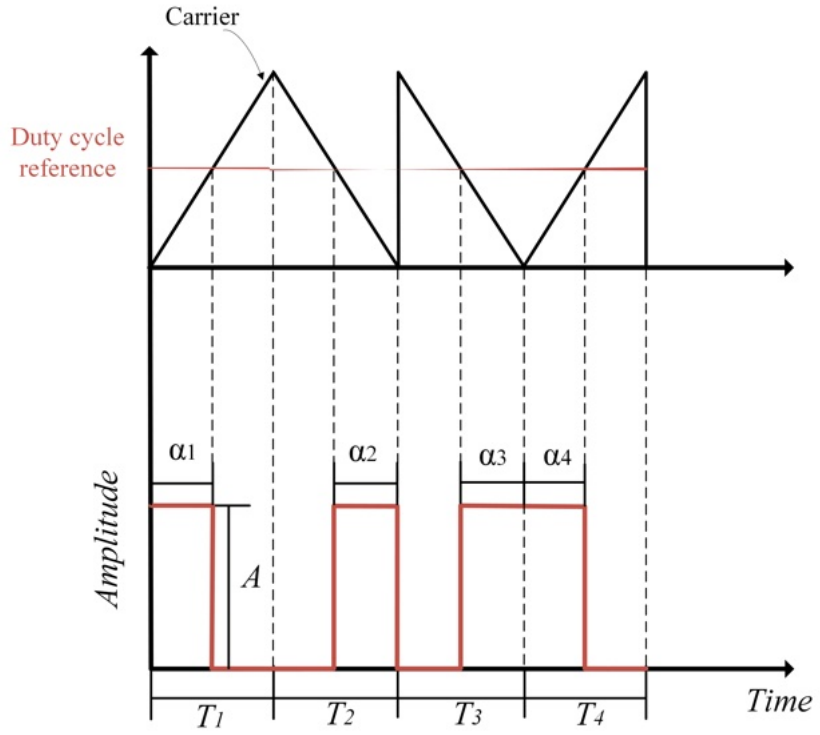

Figure 2.7: RPPM Technique operation.

2.4. Implementation of spread-spectrum modulation using RCFMFD

Let's consider the carrier frequency f_c varies for every nth impulse according to a driving signal $\varepsilon(t)$. The signal of the carrier signal could be represented in the time domain as [53]:

$$S(t) = A_c \cos(2\pi f_c t + 2\pi\Delta f \int_{-\infty}^{t} \varepsilon(t)dt) \tag{2.3}$$

$$\Delta f = \alpha f_c \tag{2.4}$$

where A_c is the amplitude of the carrier frequency, Δf is the frequency deviation around the main switching frequency, α is the spreading factor used to set the required frequency bandwidth, i.e. the Carson bandwidth of the switching signal $[f_c - \Delta f/2, f_c + \Delta f/2]$, as shown in Figure 2.3. The value of the spreading factor α could vary in practice from 0 % to 30 %, the increase of the α value increases signal bandwidth and decrease its spectral amplitude.
The frequency f_m of the modulating signal $\varepsilon(t)$ plays an important role in the shape of the generated EMI spectrum. The f_m could be calculated in terms of the modulating signal sampling frequency f_s and the number of points N considered to form its shape and is given as:

$$f_m = \frac{f_s}{N}, \tag{2.5}$$

Figure 2.8 shows how the modulating signal is built inside the controller using the parameters stated in equation (2.5). Indeed, the shape of the spectrum could be controlled in terms of the modulation index β, controlled by both Δf and f_m and equal to:

$$\beta = \frac{\Delta f}{f_m}, \tag{2.6}$$

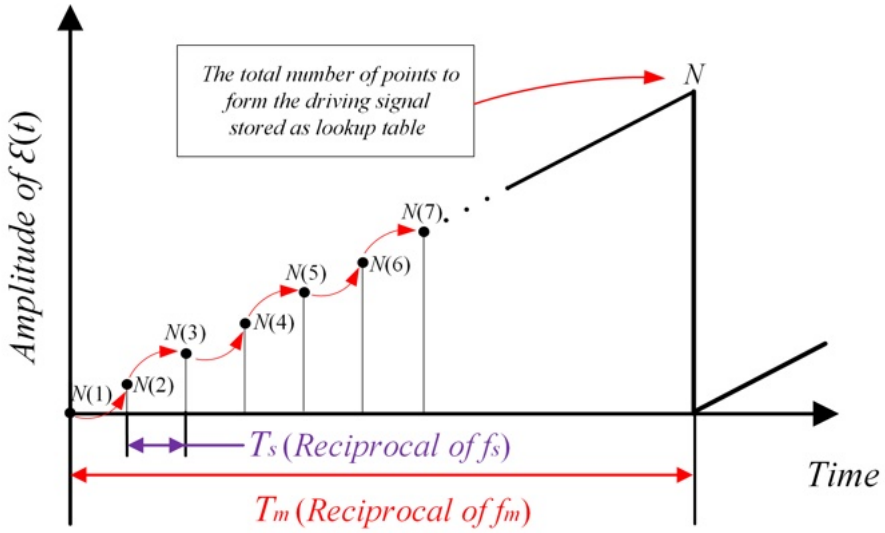

Figure 2.8: Sketch for explaining the modulating signal $\varepsilon(t)$ operation.

Based on Carson's rule, the estimated bandwidth of the SSM signal could be calculated as:

$$B_{ss} = \Delta f + f_m = f_m(\beta + 1), \tag{2.7}$$

Substituting in Equation 2.1, the SSM signal can be expressed in terms of its Fourier series as:

$$S_{ss}(t) = \sum_{k=-\infty}^{\infty} A_k e^{j2\pi k f_c t + j2\pi k \Delta f \int_{-\infty}^{t} \varepsilon(t)dt}, \tag{2.8}$$

Consequently, The power spectral density of the EMI of the signal $S_{ss}(t)$ will be expressed as [44]:

$$S_{ss}(f) = |H(f)|^2 \sum_{k=-\infty}^{\infty} |A_k|^2 \gamma\left(\frac{f - k f_c}{k\Delta f}\right), \tag{2.9}$$

Application of the above equations to the converter control result in a measured spectrum and spectrogram as shown in Figure 2.9 and could be summarised in the following points:

- The borders of the SSM are controlled by the Δf.
- The change in the frequency is controlled by the $\varepsilon(t)$, following a certain pattern like saw-tooth or sinewave or PAM.
- The rate of change in the frequency is controlled by the sampling frequency f_s, consequently, control the modulating signal frequency f_m.

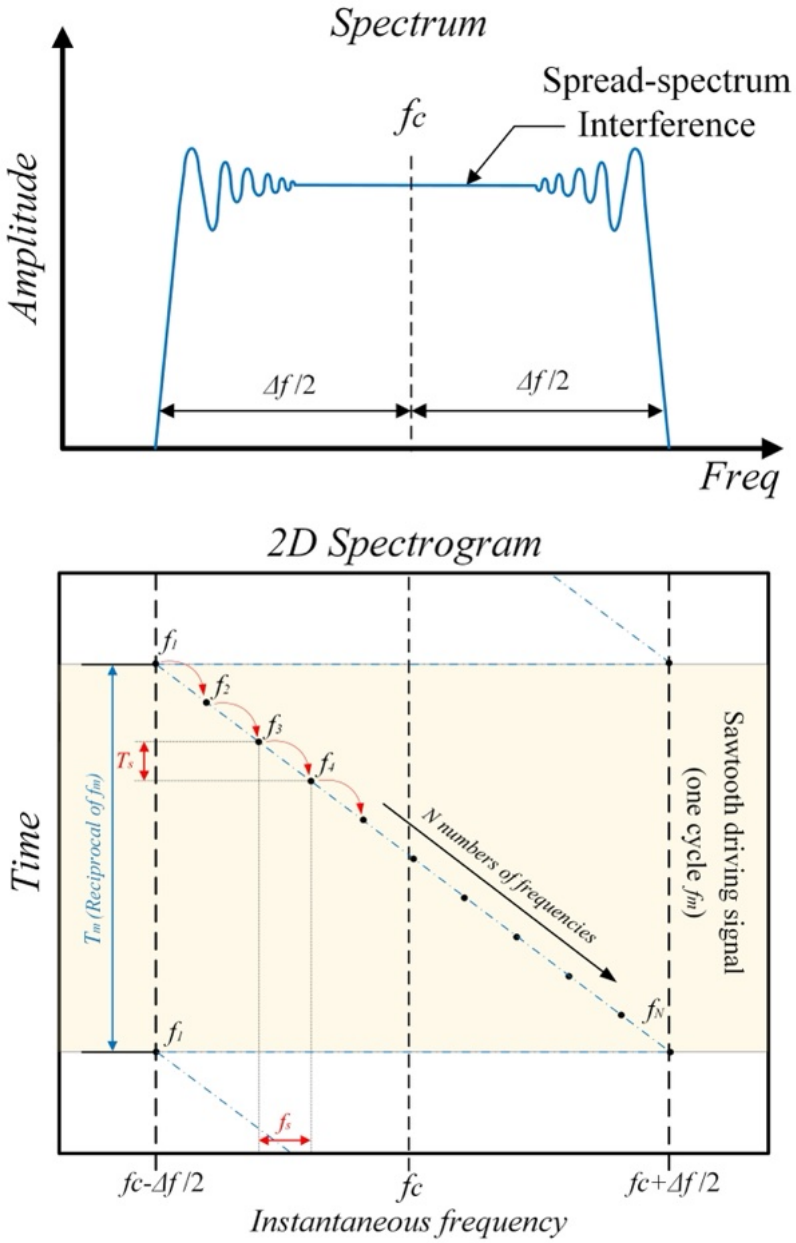

Figure 2.9: Sketch for the measured spectrum and 2D spectrogram results from the SSM.

2.4.1. Types of the driving signals

In order to change the switching frequency of the PWM used, the driving signal $\varepsilon(t)$ operate with variable amplitude with the time following a certain function. The function of the driving signal $\varepsilon(t)$ could be sinusoidal, triangular, or a random Pulse Amplitude Modulated (PAM) signal [49].

a) Pulse amplitude modulated (PAM) signal

The approach was established practically in [35], according to which the driving signal $\varepsilon(t)$ could be generated using a random sequence of numbers. The technique results in continuous EMI spectrum, independent from the measurements setting. Also, the frequency of the generated random numbers f_m is not obliged be outside the audible bandwidth, as the generated noise is white or colored noise.

The $\varepsilon(t)$ could be expressed as:

$$\varepsilon(t) = \sum_k \delta_k \, g\,(t - kT) \tag{2.10}$$

where δ_k is a uniformly distributed pseudo random number varying between -0.5 and +0.5, and $g\,(t - kT)$ is a rectangular function with duration time T. The mapping of random numbers sequence δ_k plays an important role in the shape of the measured spectrum. Figure 2.10a shows the spectrum resulting from the PAM spread-spectrum modulation.

b) Sawtooth signal

The sawtooth wave was commonly used as a driving signal due to its simplicity [36]. This technique provides a flat profile as well as small peaks generated by second order effects around the Carson's bandwidth ends as shown in Figure 2.10b. In this case, the driving signal $\varepsilon(t)$ could be represented as:

$$\varepsilon(t) = \sum_k g\left(\frac{t}{T} - k\right), g(\tau) = \frac{1}{2}(\tau \mod 1), \tag{2.11}$$

where $\frac{1}{T}$ represents the frequency f_m of the driving signal. The main disadvantage of this approach is the annoying whistles that can be noticed during circuit operation if the driving signal frequency is in the audible bandwidth.

c) Sinusoidal signal

It was the simplest driving signal established in [54]. At which the driving signal is a sinusoidal wave with a definite frequency f_m as shown in the equation:

$$\varepsilon(t) = \sum_k \sin(2\pi f_m t) \, g\,(t - kT) \tag{2.12}$$

The technique is simple and signal power is distributed throughout several frequencies, however,from the EMI reduction point view, the approach suffers from the presence of two peaks at both ends of Carson's bandwidth as shown in Figure 2.10c

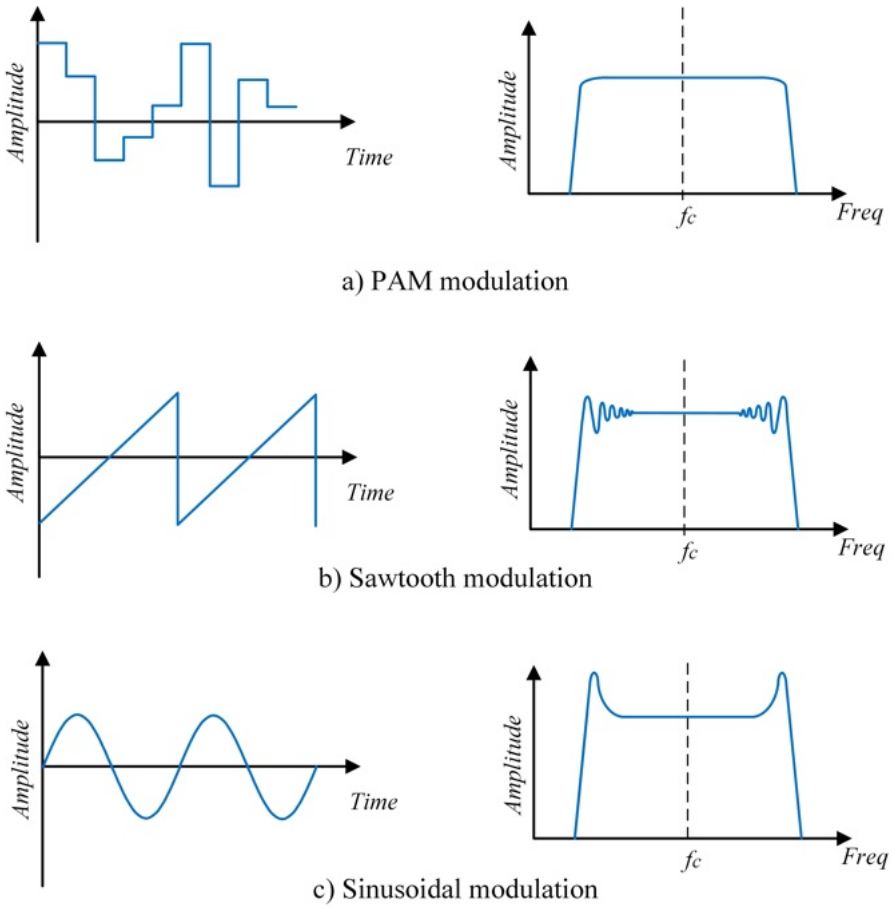

Figure 2.10: Sketch to show the comparison between power spectral density of the SSM for different driving signal $\varepsilon(t)$ [47].

2.4.2. The sampling frequency of the driving signal

One important parameter that effect the measurement of the SS modulated EMI is the sampling time T_s of the driving signal $\varepsilon(t)$. The duration time of the driving signal could be represented in terms of the modulation index (β); several values of β could have different affect on the performance of the victim device, according on the utilised device settings. In addition, it will affect the shape of the EMI measured by the receiver.

Usually, the EMI receivers follow the EMC standards and regulations, So, the Resolution Band Width (RBW) used by the receivers following the EMC standards is stated in Table 2.2. Consequently, the performance of the EMI receiver on measuring the SSM disturbance will changes based on the chosen β in the used SS technique. Generally speaking, if we consider the RBW of the EMI receiver to be R, the measured spectrum will appear as a continuous as the R is larger than the distance between two sequential spectral components, formed by the driving signal frequency f_m, i.e if $R > f_m$. The EMI receiver will be able to distinguish the measured signal better if the $R < f_m$ [31]. In order to connect the R of the utilised EMI receiver to the used SSM settings, a normalised frequency resolution ρ is calculated as:

$$\rho = \frac{R}{\Delta f}, \tag{2.13}$$

The ρ could be calculated in terms of the Δf used in the SSM settings and the chosen RBW in the EMI receiver. When connecting equation (2.13) with the previous condition of the RBW, the ρ should be less than the inverse of the modulation index β ($\rho < 1/\beta$).

Table 2.2: RBW for several frequency ranges from the EMC standards

Frequency	RBW	Measurement type
9 kHz – 150 kHz	200 Hz	Conducted
150 kHz – 30 MHz	9 kHz	Conducted
30 MHz – 1 GHz	120 kHz	Radiated
1 GHz – 18 GHz	1MHz	Radiated

2.5. Evaluation of spread-spectrum modulation techniques in terms of EMC

The evaluation of the spread spectrum modulation techniques depends mainly on two factors: the setting of the used SSM techniques and the behaviour of the EMI victims. Therefore, it is so hard to say that SSM techniques are good or bad approaches. We can say that we have two main parameters that control the shape and the power distribution of the SSM signal: The first is Δf derived by a spreading factor α and the second is the driving signal $\varepsilon(t)$. The question is: what are the perfect SSM parameters settings that provide an effective EMI reduction?

To answer this question, we should understand how the EMI victim's work, any EMI victim is sensitive to a definite few frequency range. Consequently, the probability of victim malfunction increases if a great energy of the EMI signal lies at the same sensitive frequency range of the victim. Besides, it is extremely hard to determine all the victims exposed to the EMI in the grid.

Based on [44], the authors recommends a general SSM three design considerations that will assure effective EMI reduction:

a) Increasing the Δf as much as possible.

b) Utilising as fast driving signal $\varepsilon(t)$ as much as possible.

c) Providing a flat power spectrum as much as possible (which could be achieved by the PAM SSM).

Considering the above three conditions, the SSM will work for most cases.

2.6. Summary

In this chapter the Spread-Spectrum (SS) modulated converters were discussed as a source of EMI. Firstly, the types of the SS modulation techniques were presented and the RCFMFD modulation technique was chosen as an example of a good EMI mitigation tool. Secondly, the parameters that affect the shape of the SS EMI were discussed as an important factor from the EMC perspective. Finally, the evaluation of the SS techniques was presented followed by some recommendations for providing a proper SSM technique design.

Chapter 3

Power line communication

The proper operation of the smart grid electrical network requires proper communication between the system components. Due to the variety of devices, different communication protocols are used between the smart grid elements, such as the CAN bus in traction applications [55], the RS-232 in solar farms and industrial applications [56], and a lot of wireless solutions, like, in Vehicle-to-Grid (V2G) [12]. Apart from the above mentioned communication technologies, the Power Line Communication (PLC) may be used in smart grids, for instantce in metering systems [1] and industrial systems [57]. The PLC uses the existing power cables for data transmission, which leads to reduced investment and maintenance costs. Nevertheless, the PLC communication system is prone to a lot of disturbances, especially with the PLC that works in the frequency band between 2-150 kHz.
In this chapter, we will discuss the operation of the PLC communication system as a considerable victim of the conducted EMI generated in the grid.

3.1. The effect of different loads

Typically, a lot of papers have divided the PLC disturbing signals into four types — (1) Background Noise; (2) Narrowband Noise; (3) Periodic Impulsive Noise, and; (4) Asynchronous Noise [58, 59]. However, the real signals are more complicated and are a composite of these basic types [60]. The PLC signal usually is exposed to a high level of conducted Electromagnetic Interference (EMI) due to the existence of parasitic coupling between the power electronic circuits and the communication circuits, mainly when the converter switching frequency or its harmonics lay in the same frequency bandwidth as that of the communication system. Thus, due to the level of interference, the bandpass filters installed in communication devices are not able to provide protection. Consequently, the Signal to Noise Ratio (SNR) decreases below the level of noise-free communication, leading to data transmission error and sometimes failure of communication [3].
A study in [61] that show the effect of loads in the smart meter system in Finland. According to the results, common causes of communication problems in the PLC systems have been frequency converters, energy saving lamps and certain single-phase devices (such as antenna amplifiers, teleoperator devices, digital set top boxes). These are typically equipped with single phase switch-mode power supplies. In the following paragraphs we will discuss the effect of non-linear and power converters based loads on the PLC systems.

3.1.1. Study the effect of lamps on PLC

In [62], the paper studies the effect of two groups of LED Lamps — with passive rectifier and with active rectifier. The interference level from passive rectifier LED lamps is significantly below the allowed maximum PLC signal levels in band 150 kHz – 30MHz. However, they produce noise in band 3 kHz – 150 kHz, the level of noise is between 60 dBuV and 70 dBuV, which is still below the PLC signal levels, therefore, there is no threat to the power-line communications. The second group of lamps shows the same results in band 3 kHz – 150 kHz, however, the interference appears in band 150 kHz – 30 MHz.
In [63], the effect of the Compact Fluorescent Lamp (CFL) on the PLC signal was studied and

the results show that while the noise levels of PLC and CFL are governed by the same EMC standard, the CFL Lamp can cause interference and effectively can weaken the communication signal. The same response is shown in [64] in the metal halide lamps. In the case of mercury vapor lamps [65], it has been shown that the level of noise in the CENELEC band (3 kHz – 150 kHz) is below the allowed PLC signal level and, therefore, it is "safe" to use the mercury-vapor lamp in this frequency range. In the case of fluorescent lamp [61], It has been demonstrated that fluorescent lamps do inject conductive noise in the PLC channel. Fluorescent lamps produce noise in the 3kHz- 150 kHz CENELEC bands, but this interference is 20 dB to 40 dB lower than the allowed PLC. In [67], a study was performed on the effect of a group of LEDs in the PLC signal.

3.1.2. Study the effect of power converters on PLC

As stated in Chapter 2, the application of using fast switching semiconductor devices such as IGBT or MOSFET provides a nearly square wave form, however, this rising and falling voltage times of few V/s have unwanted side effect on the EMC, the steep slope of the voltage waveforms cause the existence of parasitic capacitive coupling, forcing the EMI current to flow [60]. In [56], a study was implemented to see the influence of power converter on the communication data transmission errors, the communication protocol used was RS232, the study shows that there is no significant difference between the use of random modulation over the deterministic modulation in the context of data transition errors. However, the change of the switching frequency causes a significant change in the probability of data transmission errors. These phenomena of interference happen when the value check moment of the transmitted signal meets the modulated signal rising or falling edges at the same time . In [68], some results were obtained in addition to studying the effect of increasing the number of power converters in the data transmission error. According to [61], in the case of switch-mode power supplies, two different root causes of problems were detected. The first is the ageing of the power supply, especially the smoothing capacitor after the rectifier and the second is the lack of emission limits in the frequency range 3...150 kHz. The latter causes problems, especially, if the switching frequency of the power supply is close to the signaling frequencies of the PLC system.

3.1.3. Conducted EMI mitigation solutions in the PLC signal

The EMI mitigation could be achieved by two ways:

- Hardware solutions.
- Software solutions.

a) Hardware solutions

Commonly, hardware solution implies installing a passive filter in the series with the PLC signal. In [16], the work focused on the implementation of a filtering system for interference in the 120–150 kHz band that is introduced into the network by receivers. In [17], a feasibility study was conducted to see the effect of adding CM Choke coil in the Analog Front End (AFE) circuit of the PLC modem to reduce the CM noise coupling onto the power line, the study showed that adding a CM choke in the AFE circuit of a PLC modem is not a feasible solution to reduce the CM noise in the power line network.
Another way of hardware improvement is by improving the way of measurement as shown in [69],the advantage of this device is that it can easily measure the voltage in a specific smart meter and analyse the problem and since it is a light weight equipment, it can show the basic source of noise that affect the performance of PLC in the smart meter in question. However, it does not solve the problem and requires specific field measurements for each of the smart meter of the PLC. In [70, 71], the idea is based on collecting the network parameters and implementing an optimization technique to control the operation of the loads or minimising the data transmission rate to improve the performance of the PLC.

On the other hand, the solution for the EMI problems in the PLC systems could be from the power converters side, by implementing the right passive or active filters on the converter output terminals.

b) Software solutions

In the case of software solutions, the use of the active filters is one of the most commonly employed approaches. In [72], an innovative approach for information signal denoising in the time domain method based on Widrow's adaptive denoising filter, this filter is used in order to reduce the impulsive noise effect when it happens. In [73], The proposed algorithm uses a forward linear prediction error filter to remove the interferences from the incoming signal. Interference suppression is achieved through a zero-forcing algorithm in [74] that raise the multichannel reception and requires channel state estimates for the interference signal. Results indicate that the methods are successful, on average, in mitigating interference to enable recovery of the desired signal
Another way of solving conducted EMI problems in the PLC is by changing the way of modulation in the power converters as introduced in [75], this paper studied the influence of using the Pseudo-random PWM modulation technique on the PLC. The results show improvement in the performance of the PLC using the Pseudo-random PWM modulation over conventional space vector modulation. However, this test was implanted only on a PLC modem that uses the Frequency Shift Keying (FSK) modulation technique, therefore the results may be different in the case of Orthogonal Frequency Division Multiplexing (OFDM)- Phase Shift Keying (PSK). The same results were investigated in [76], the author uses the elimination of electromagnetic interference in communication channels by using the Spread Spectrum Technique(SSM).

The impact of the SSM on the communication systems performance is found to be variable according to the communication systems. Generally speaking, the communication systems could be divided into two main types: featuring forward error correction codes and un-coded communication systems. In the case of coded communication systems like in [53] and [77], the influence of SSM on I2C was studied and the results show that the SSM modulation results in more problems to digital communication channels than the normal non-SSM switching signals. In contrast, in the case of un-coded communication systems such as RS 232, the SSM EMI has almost the same effect on the communication system as the EMI generated from the conventional. In [78], a model is presented which illustrates that both the SSM and non-SSM have the same effect on the performance of the RS 232 protocol. Also, some studies confirm the lack of difference between the conventional PWM and SSM, Furthermore it has been shown that ostensible reduction of the EMI level generated by randomly modulated converters results from the methodology of the EMI spectrum measurement [79,80].

3.2. PLC Standards and Regulations

The PLC works by modulating the carrier signal and adding it to the main power signal. The PLC systems could operates in two main frequency bands: Narrowband (NB-PLC) and Broadband PLC (BB-PLC). The NB-PLC typically works at a range of 3 kHz to 500 kHz and BB-PLC works at a range of 1.8 MHz to 250 MHz [81]. The NB-PLC is used in smart metering application, traction, and battery charging systems; however, the BB-PLC is used in high-speed applications like the internet. There are three main standards are used, the first is the European Norm (EN) 50065, which was first established by CENELEC in 1992 [81], it allows the PLC operation in range between 3 kHz and 148.5 kHz. The second is the U.S. Federal Communications Commission (FCC), the PLC is used in the range between 9 and 490 kHz band, this regulation is not used for smart meter applications. The last regulation was established by the Japanese Association of Radio Industries and Businesses (ARIB) in the form of Standard T84, which allows the use of PLC in the 10–450 kHz band. Figure 3.1 shows all the standards and regulation frequency ranges.
Based on the EN 50065 standard, the highest limit of the intentional emissions generated by mains PLC communicating equipment is 120 dBuV, the unintentional emissions on the PLC channel should be below the maximum intentional power by (20-30 dB) to allow reliable PLC communication [82]. Many industries start developing PLC standards based on the regulation in Figure.3.1,the G3-PLC has been developed by the G3-PLC Alliance and the PRIME (Power line Related Intelligent Metering Evolution) has been developed by the PRIME Alliance. Both systems use the OFDM scheme for sending the data, the OFDM technique is commonly used

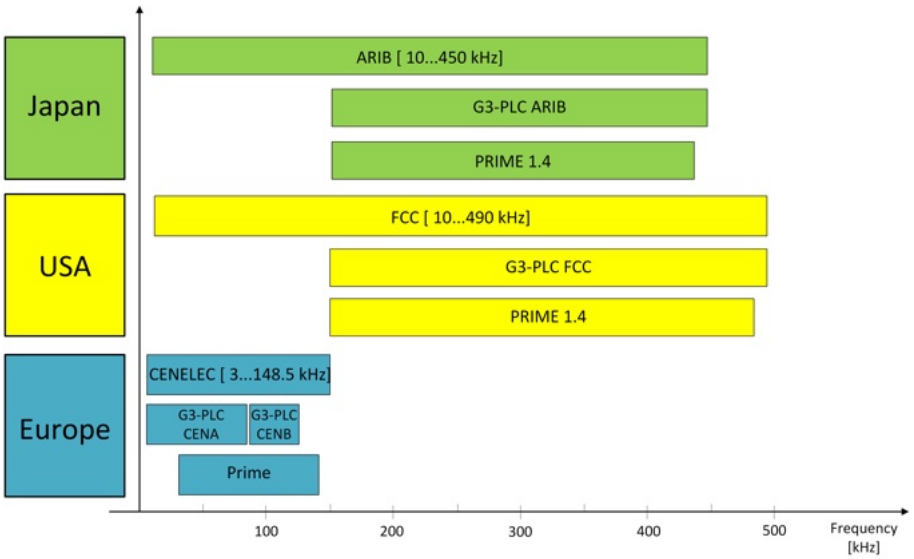

Figure 3.1: PLC Standards and Regulations.

in several communication protocols like Bluetooth and the Global Systems for Mobile (GSM). The OFDM provides robustness to the communication system as it distributes the transmitted data through several frequencies instead of one specific frequency. The steps to achieve the OFDM technique in both the PRIME and G3-PLC systems are the same, however, the technique parameters settings are different as we will discuss in the next section.

3.3. PLC system operation

3.3.1. PLC Transmitter

The PLC system is designed to work in the frequency range from 3 kHz to 150 kHz, the data comes from the Medium Access Control (MAC) and modulated using the Deferential Phase Shift Keying (DPSK). After that, the data is divided into symbols, each symbol consists of sub-carriers. Then, the Inverse Fast Fourier Transform (IFFT) is used to insert all the symbols in the required frequency range, the length of the IFFT samples, and the sampling frequency used set according to the type of standard used.

a) Signal modulation

The process starts by transmitting the digital information into the OFDM frame, this data should be modulated using a digital modulation scheme as stated before, this process is called mapping, and the end results is a list of the amplitudes and phases that are then to be transmitted at every frequency in the set. This data should be transformed to the time domain, the IFFT is the best option to implement this transformation. if the OFDM symbol x_n includes a certain numbers of sub-carriers , then the OFDM signal x_k is expressed as

$$x_k = \frac{1}{N} \sum_{n=0}^{N-1} x_n e^{j2\pi kn/N}, k = 0, 1, ..., N-1 \tag{3.1}$$

where N is the IFFT size, k is the sub-carrier index, n is the time index. In the case of the PRIME standard, the length of the IFFT is 512 samples and includes 97 sub-carriers, while in the case of G3-PLC, the length is 256 samples and includes 36 sub-carriers [76]. The frequency spacing ΔF_c between each sub-carrier is equal resulting from the division of the sampling frequency over the total numbers of IFFT samples used.

$$\Delta f_c = \frac{f_{ss}}{N} \tag{3.2}$$

In the case of PRIME, the sampling frequency is 250 kHz which yields a Δf_c = 488.281 Hz, on the other hand, the sampling frequency in the G3 is 400 kHz which yields Δf_c = 1562.5 Hz.

b) Adding Cyclic Prefix (CP)

Despite the rigidness of the OFDM technique on the data transmission, the OFDM system is more prone to the symbol carrier frequency and timing errors than in single carrier communications due to the Inter Symbol Interference (ISI), this is because the receiver sees multiple copies of the transmitted data, each arriving with different delay and amplitude. In order to eliminate this effect, a guard band is inserted between each data frame that is longer than the worst delay expected, this guard band is called Cyclic Prefix (CP) [83]. The CP usually repeats the last L samples of an OFDM block and then is arranged in front of the block as shown in Figure 3.2. The resulting symbol s_n can be represented as

$$s_k = \begin{cases} x_{N+k}, & -L < k < -1 \\ x_k, & 0 < k < N-1 \end{cases} \tag{3.3}$$

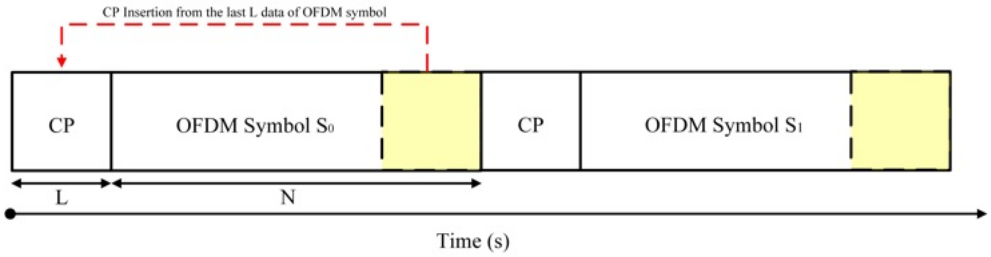

Figure 3.2: The OFDM symbol format.

After adding the CP, The time of each symbol T_{sym} can be calculated based on the given equation

$$T_{sym} = \frac{T_{signal}}{N + N_{cp}} \tag{3.4}$$

where N_{cp} is the number of cyclic prefixes used, T_{signal} is the sum of time taken for the IFFT (T_{IFFT}) and so the guard band cyclic prefix (T_{GB}), the T_{IFFT} and T_{GB} could be expressed as

$$T_{signal} = T_{IFFT} + T_{GB}, \tag{3.5}$$

where

$$T_{IFFT} = \frac{1}{\Delta F_c} \ , T_{GB} = \frac{T_{IFFT} \cdot N_{cp}}{N}, \tag{3.6}$$

In the case of PRIME, the CP is 48 samples equivalent to 192 μs, however, in the case of G3, the CP is 30 samples equivalent to 75 μs. The total time duration for each OFDM symbol after adding the CP will be 2240 μs in PRIME and 715 μs in G3 [83].

c) Adding Preamble Field

The first few frames consist of known data used for synchronising the data with the receiver, this frame is named as "Preamble Fields". It is divided into two parts: the (P) frames (preamble frames) and the (M) frames. The M frames are encoded differently from the P frames and are used as a synchronisation mark to identify the start of the user data field. After the preamble, some OFDM symbols are used as header. In the PRIME system, the header consists of 2 symbols equivalent to 4480 μs, while in the case of G3, the header consists of 13 symbols equivalent to 9295 μs. Respectively, the transmitted packet format is the sum of the preamble frame, header symbols, and data OFDM symbols as shown in Figure 3.3.

d) The up-conversion of the PLC signal

PLC Frame

	Preamble	Header	M OFDM Symbols
PRIME	2048 µs	4480 µs	M × 2240 µs
G3	6080 µs	9295 µs	M × 4 × 715 µs

Figure 3.3: The PRIME and G3 frame structure.

Digital Up-converter (DUC) provides the digital implementation from the complex signal to the real pass band signal, as shown in Figure 3.4. The input of the DUC is sampled at a relatively low sampling rate. Before converting the signals, they are filtered and up sampled using a Square Root Raised Cosine filter (SRRC).

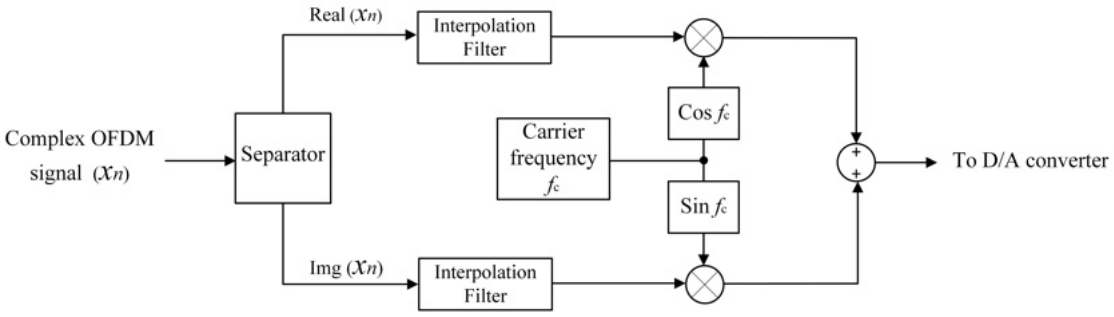

Figure 3.4: The up-conversion of the OFDM Signal.

The transmitted signal should be quantized using the digital to analog converter (D/A) of the controller, which quantizes the time domain signal to a specific quantize step size depending upon its own size [83]. In the same framework, the carrier frequency f_c is tuned to be equal to the Intermediate Frequency (IF) of the OFDM frequency band. Consequently, if the oscillator frequency is not precise, the carrier frequency offset may appear, in addition to the phase noise which appears due to the demodulation process of the transmitted signal.
Table 3.1 shows the difference between the PRIME and G3 transmitter settings.Figure 3.5 shows the whole block diagram of the transmitter in the case of the PRIME system and G3 PLC.

Table 3.1: PRIME vs. G3

Parameter	PRIME	G3
Frequency Range	42-89 kHz	35-91 kHz
Sampling Frequency f_{ss}	250 kHz	400 kHz
FFT size	512	256
Length of CP	48	30
Sub Carrier Spacing	488 Hz	1.5625 kHz
No. of Carriers Used	97	36
Max data Rate	128.6 kbps	33.4 kbps
Interleaving	Per OFDM symbol	Per data packet
Modulation	DBPSK, DQPSK, D8PSK in frequency	DBPSK, DQPSK in time

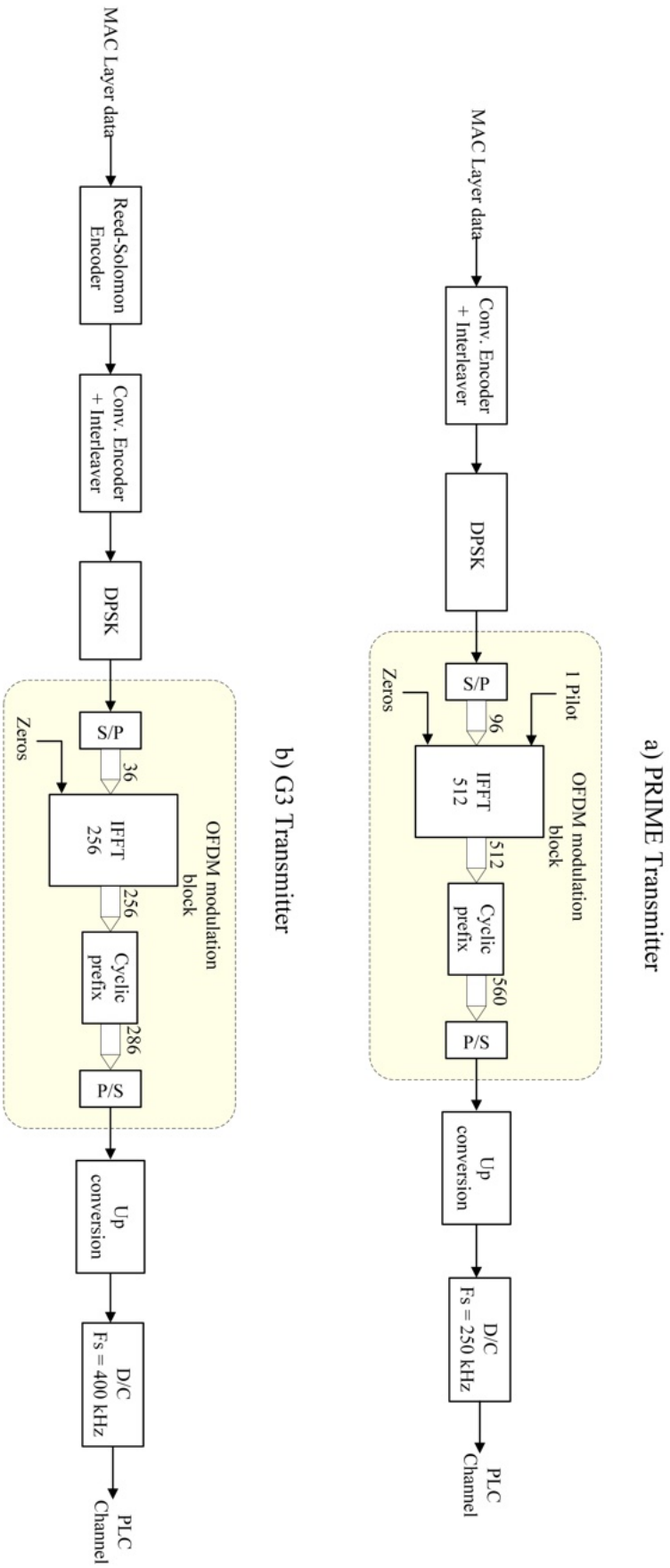

Figure 3.5: The block diagram for the transmitter in (a) PRIME and (b) G3.

3.3.2. PLC Channel

The PLC transmission channel practically represented in power cables. The signal attenuates with the increase in the length of the line according to the properties of copper wires and their insulation. The channel models are usually represented by their channel response function H(f). Based on [84], the channel could be a Flat channel, Frequency Selective channel, or Phase Shift Channel, depending upon the way the Finite Impulsive Response (FIR) filter in the receiver. Moreover, the presence of the background white noise and the periodical impulsive noise could interferes with the OFDM symbol, if a parasitic coupling exist between the noise source and the communication channel used as shown in Figure 3.6.
In the same context, the Shannon-Hartley equation could be used for evaluating the PLC channel capacity to confirm the behaviour of the PLC system in the presence of noise [53]. The Shannon-Hartley equation calculates the maximum allowable data transmission rate over a communication channel in the presence of noise, which is close to the rate achieved in practice by communication systems featuring advanced channel coding, like the Forword Error Correction (FEC) codes adopted in G3-PLC and PRIME [6]. The capacity of the PLC channel is expressed as:

$$C_{G3} = \int_{B_{\min}}^{B_{\max}} \log_2 \left(1 + \frac{S_{PLC}(f)}{N(f)}\right) df, \tag{3.7}$$

Here B_{min} and B_{max} are the frequencies limits of the PLC bandwidth channel, $S_{PLC}(f)$ is the power spectral density of the PLC signal and $N(f)$ is the total noise power spectral density (p.s.d) respectively. The total noise of the channel in our case is equal to:

$$N(f) = S_0 + S_{EMI}, \tag{3.8}$$

where S_0 is the power spectral density of the background noise, modelled as Additive White Gaussian Noise (AWGN), and S_{EMI} is the EMI power spectral density. Consequently, the capacity loss percentage C_{Loss} could be calculated as:

$$C_{Loss} = \frac{C_0 - C_{G3}}{C_0} \times 100\% \tag{3.9}$$

where C_0 is the calculated capacity of the PLC channel in the EMI-free case, i.e. only including the AWGN ($N(f) = S_0$).

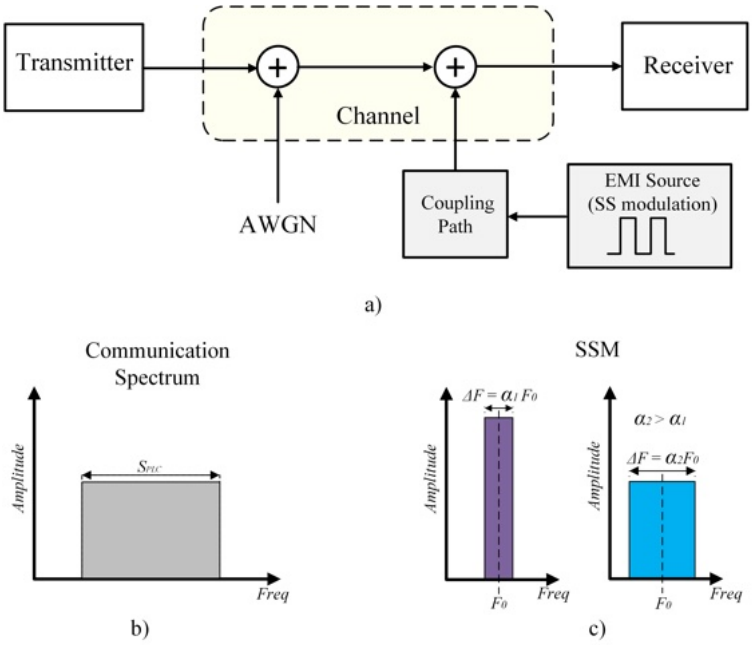

Figure 3.6: Block diagram representing the G3-PLC channel with the EMI noise.

3.3.3. PLC Receiver

The demodulation of the received signal starts with passing the carrier signal through a passive low pass filter to extract the PLC signal from the main grid power (220v- 50Hz). Following this, converting the analog signal into a digital signal using an Analog to Digital (A/D) converter

a) The PLC signal down-conversion

The Digital Down Converter (DDC) technique is used to extract the digital data from the carrier signal, a complex sinusoid wave at the Intermediate Frequency (IF) is multiplied with the input signal to restore the signal to its complex form. After that, a low pass filter is used to extract the original data signal from the received signal, consequently, the received data is ready to enter the OFDM demodulation as shown in Figure.3.7 [83] .

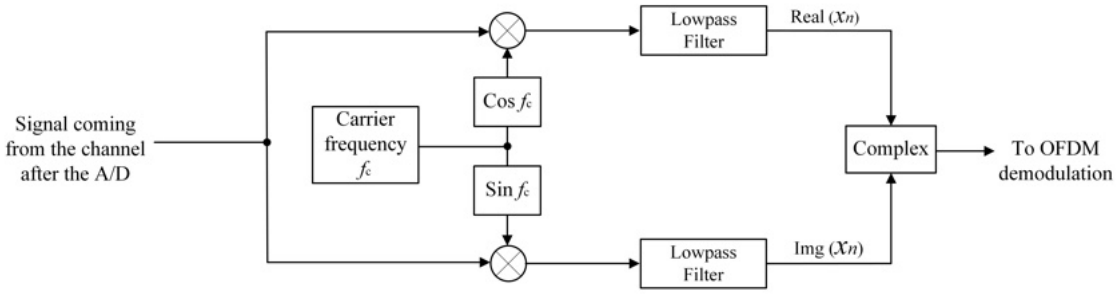

Figure 3.7: The down-conversion of the OFDM Signal.

b) The OFDM demodulation

The received signal is represented by the convolution of the transmitted time signal with the channel impulse response h(t) and an AWGN term

$$r_k(t) = s_k(t) \cdot h_k(t) + N_k(t) \tag{3.10}$$

The received time-domain signal is transformed back into the frequency domain utilizing Fast Fourier Transform (FFT) and contains data symbols given as:

$$R_n = \frac{1}{N} \sum_{k=0}^{N-1} r_k e^{j2\pi kn/N}, n = 0, 1, ..., N-1 \tag{3.11}$$

where R_n is the out signal after performing the FFT. Then, the signal sub carriers are extracted from the FFT signal by removing the added cyclic prefix and the zero pads samples [83].

c) Signal demodulation

The signal is demodulated using the DPSK to restore its digital form. In the PLC systems, the Differential Binary PSK (DBPSK), the Differential Quad PSK (DQPSK), or the Differential 8-bit PSK (D8PSK) could be used for the demodulation process according to the transmitter settings.

d) The synchronisation of the OFDM signal

Due to the communication channel clock differences, various synchronisation errors will appear in the front end of the OFDM receiver, so, the synchronisation process is very important for the OFDM signal. The synchronisation error appears due to the presence of two types of offsets: timing offset and carrier frequency offset.

3.4. Summary

In this chapter, the increasing developments in the PLC systems are introduced along with the operation of the PLC systems. The chapter also presents the standards and regulations for the PLC systems. Essentially, the operations of the PRIME and G3 PLC systems are addressed starting from the transmission point to the receiving point.

Chapter 4

Simulation Results and Discussion

In this chapter, the simulation of the communication system behavior in the presence of spread-spectrum modulated EMI is presented. The Matlab SIMULINK tool is used and the results were analyzed by the Shannon Hartley equation.

4.1. Building the system blocks

As stated in chapter 2 and chapter 3, the idea of simulation is to study the influence of the generated EMI from the power converters on the smart metering systems utilizing the G3-PLC or the PRIME communication protocols. The MATLAB/SIMULINK software was used as a good simulation tool.
The simulation consists of two main circuits: the communication circuit and a buck converter circuit as shown in Figure 4.1, both circuits are coupled together through a parasitic capacitance of 10 nF. The communication circuit consists of two G3-PLC modems, one act as the transmitter and the other act as receiver, and they are connected through a copper wire of length 42 m. The sampling frequency of the whole simulation was chosen to be 15 MHz to be suitable for the utilized SSM driving signal frequency rate of change (f_s).In the next subsections, we will discuss the implementation of both circuits in details.

4.1.1. Implementing the buck converter circuit

The converter is working in the synchronous mode utlizing two IGBT transistors. Besides, the proposed SSM technique is applied to the converter with various operating conditions. The buck converter was implemented without the output filter, in order to see the effect of generated first order oscillatory mode current on the communication channel behavior.Figure 4.2 shows the simulation block of the buck converter used. Table 4.1 shows the electrical parameters of the utilized converter. Figure 4.2 shows the simulation block of the buck converter used. Table 4.1 shows the electrical parameters of the utilized converter.

Table 4.1: Buck converter electrical parameters

Item	Value
Transistors type	IGBT
Input Voltage	50V
Input current	0.6
Output Voltage	25V
Output current	1.2A

In the same framework, the SSM was implemented in the Simulink environment with the ability to change all the SSM settings easily as shown in Figure 4.3. As stated in Chapter 2, the chosen technique is the RCFMFD. Based on equation (2.2), three parameters control the shape of the SSM output spectrum:(1) The spreading factor,(2)The driving signal profile, and (3)The driving signal frequency. Each parameter has its effect on the performance of the communication system as we will present later in section 4.3.

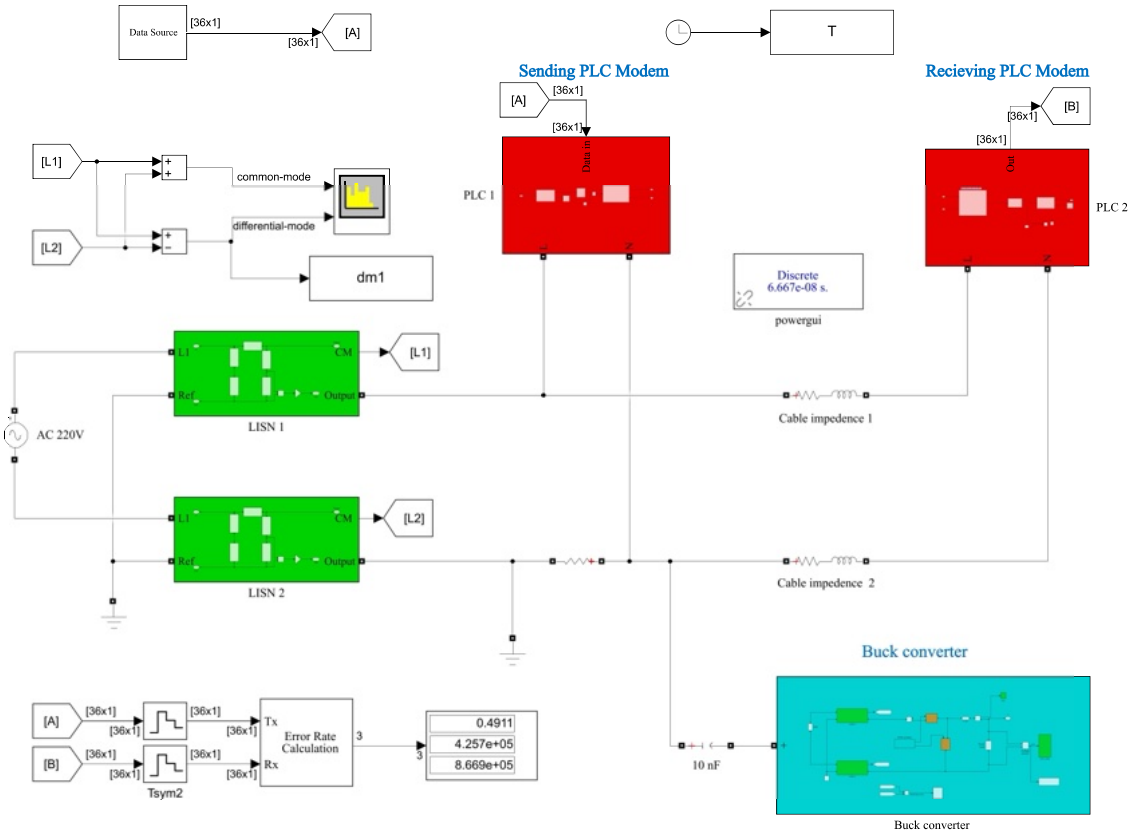

Figure 4.1: Simulink Simulation blocks.

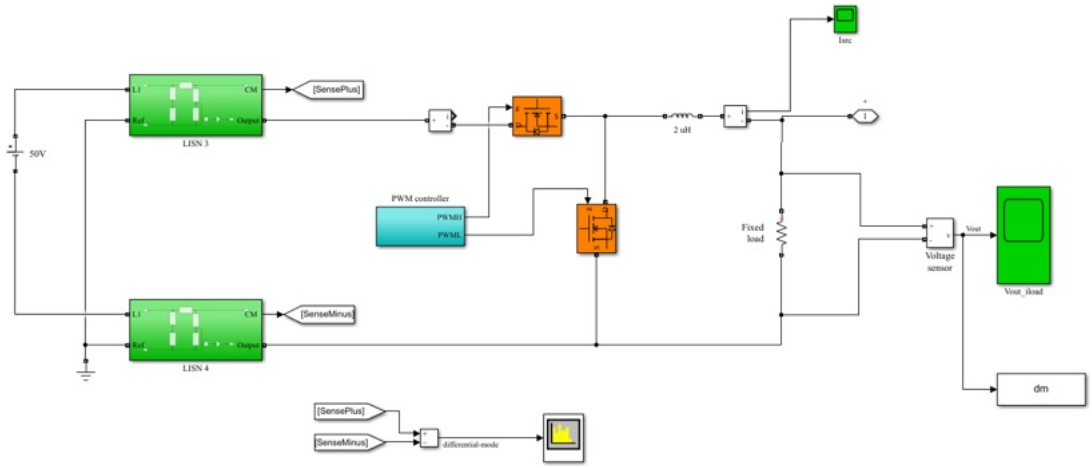

Figure 4.2: Buck converter Simulation block.

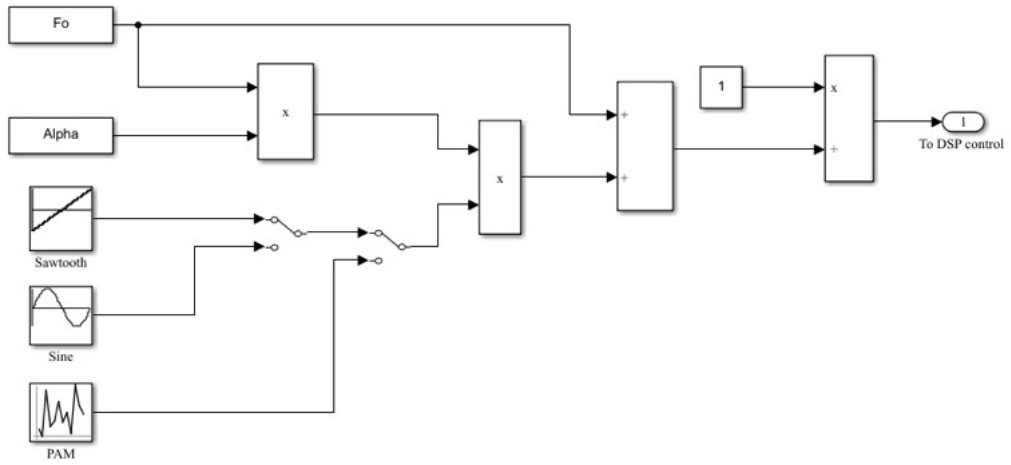

Figure 4.3: The SS modulation Simulation block.

The output from the SS modulation block goes to the PWM generator block as shown in Figure 4.4. The block mimics the operation of a a real micro-controller timer, at which a counter is working every raising step from a square wave generator. After that, the counter value is compared to a specific time value equivalent to the required duty cycle. In practical, the used micro-controller in this thesis is the TMS320F28335, manufactured by Texas Instrument (TI) company. For decreasing the simulation time, the sampling frequency f_{ss} chosen to be equivalent to 10% of the actual on-board crystal of the TI board (150 MHz).

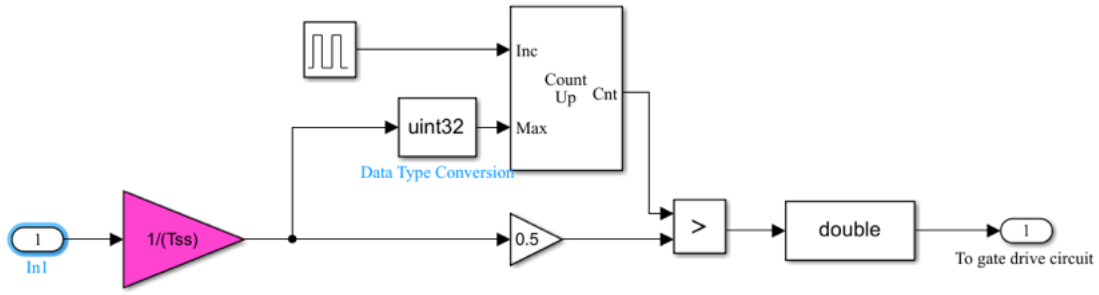

Figure 4.4: The PWM generator block.

4.1.2. Implementing the G3-PLC system

The implemented Simulink Simulation follows the procedures stated in Chapter 3. Hence, the communication system consists of three elements: the Transmitter Modem, Channel, and Receiving Modem as shown in Figure 4.1. In this simulation , the considered protocol is the G3-PLC. Thus, the OFDM system will follow the parameters stated in Table 3.1.

a) Transmitter modem

The transmitter modem consists of 4 blocks as shown in Figure 4.5. The first block is the binary data to be sent, the data should be distributed into 36 sub-carriers to be ready to enter the second block. The second block is the OFDM modulator, first the data is mapped using the BPSK, after that, it goes through the IFFT block to generate the OFDM output signal as a vector of 286 columns (256 Symbol output from the IFFT + 30 symbol for the cyclic prefix) as shown in Figure 4.6. Then, the data is converted to serial data to be ready for the third stage. The third block is the up-conversion at which the data is multiplied by a certain sinusoidal carrier signal of 2 V amplitude, its frequency is equivalent to the intermediate frequency of the OFDM bandwidth (63 kHz) as shown in Figure 4.7. Finally, the last block is for the coupling stage, usually, it consists of very high resistance for protection, in addition to a coupling circuit for adding the small communication signal to the power grid voltage (220 V).

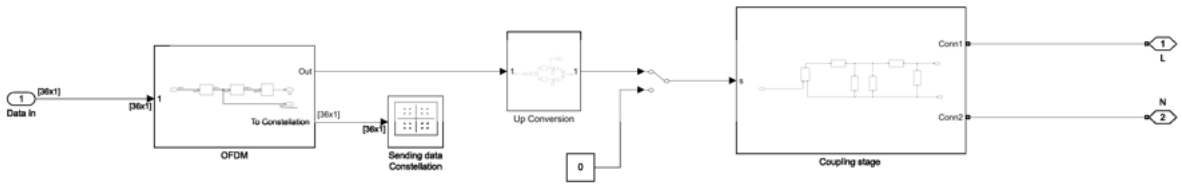

Figure 4.5: Transmitter modem simulation blocks.

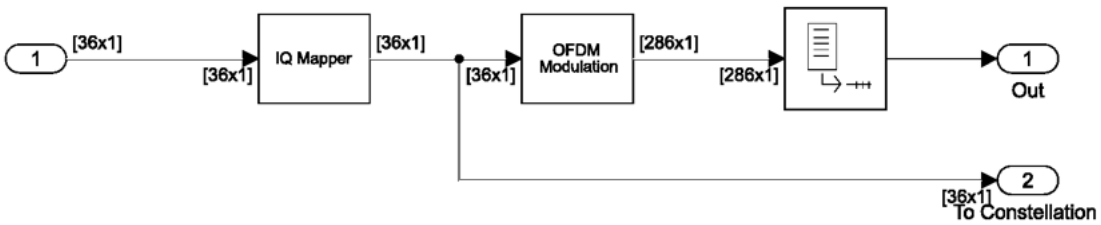

Figure 4.6: The PWM generator block.

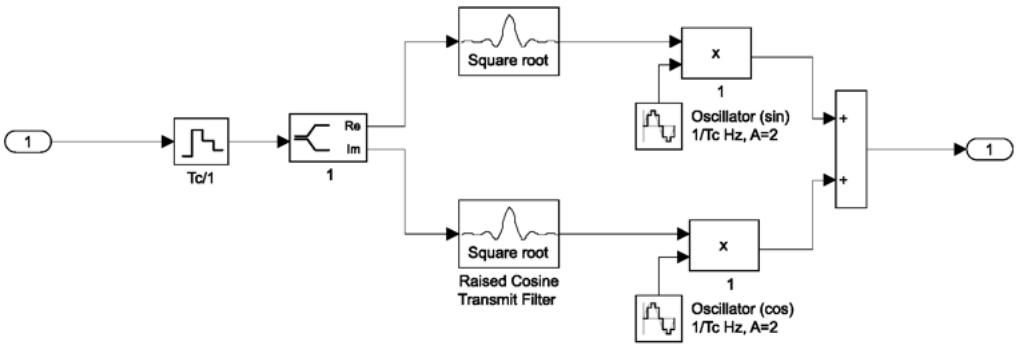

Figure 4.7: Up-converter block

b) Receiving modem

The receiving modem follows the opposite direction of the transmitter modem, it consists of three blocks as shown in Figure 4.8. The first block is the filtering stage, which consists of a passive band-pass filter to extract the communication signal from the AC grid voltage signal. The second block is the down-conversion stage that extracts the OFDM signal from the sinusoidal carrier signal by means of a digital low-pass filter as shown in Figure.4.9. The filter order is 8 and is tuned for a cut-off frequency of 40 kHz (70% of the carrier frequency used). Finally, the data is demodulated through an OFDM de-modulator as shown in Figure 4.10. Moreover,

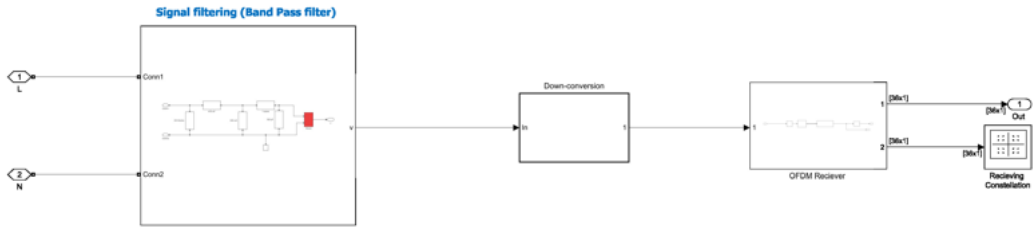

Figure 4.8: The receiver modem simulation blocks.

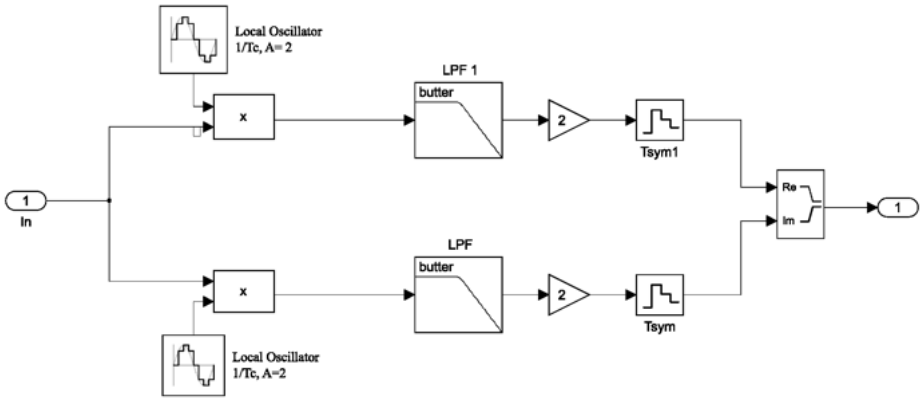

Figure 4.9: The down-conversion simulation block.

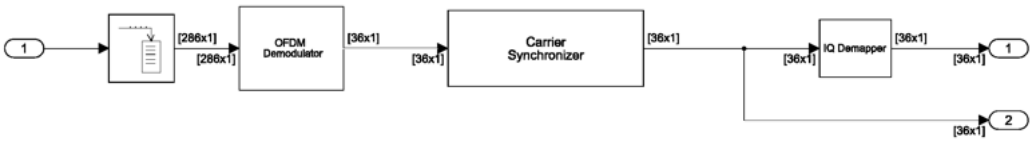

Figure 4.10: OFDM demodulator simulation block.

due to the delay that existed from several sources in the utilized circuit, a carrier synchronizer should be used to match the received data with the transmitted data.

c) G3-PLC Channel

The channel is presented as a normal copper wired cable of length 42m include to wires go and return, the cross-section area of each wire is 1.5 mm, and the total impedance per wire is equal to $0.5 + j0.028\Omega$. Also, the cable is connected to the AC grid through the Line Impedance Stabilization Network (LISN). Hence, the differential mode voltage spectrum of the PLC signal is measured at IFBW of 200Hz as shown in Figure 4.11. It was noticed that the spectrum of the PLC signal is between 32 kHz to 94 kHz which is almost the same as the original settings designed by the G3-PLC Alliance. The matlab code used for spectrum plotting is given on Appendix A.1

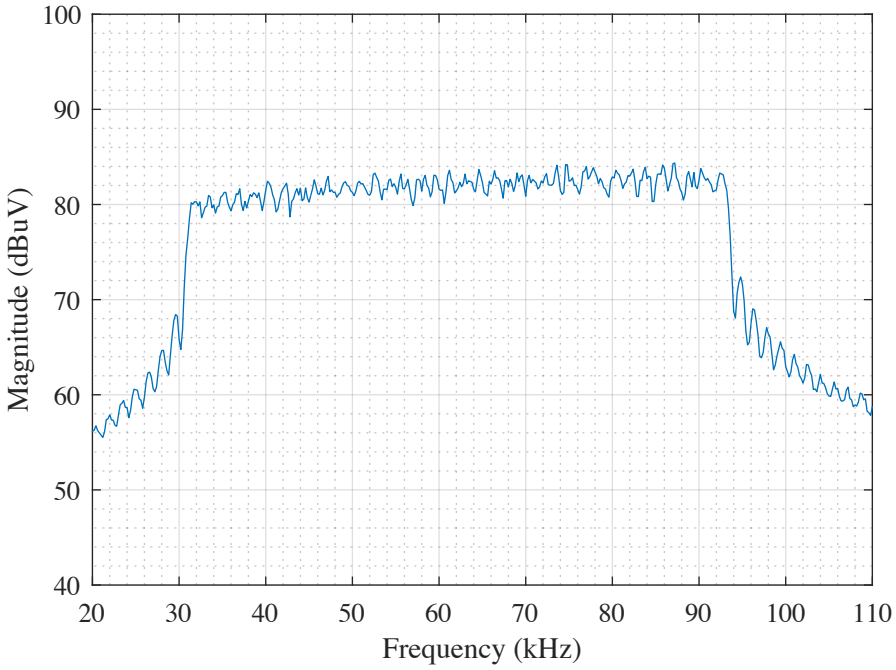

Figure 4.11: The PLC signal Voltage spectrum at IFBW = 200 Hz.

4.2. The influence of spread-spectrum modulated EMI on the G3-PLC performance

The SSM technique used in this simulation is the RCFMFD, so, the technique works to randomize the switching frequency of the PWM signal by changing several parameters simultaneously with the time. Figure.4.12 shows the difference between the output voltage of the simulated buck converter in the case of conventional PWM (Figure.4.12a) and SSM PWM (Figure.4.12b). The variation of the switching frequency around the main switching frequency of 63 kHz appears clearly in the output voltage as shown in Figure.4.12b. Moreover, the SSM parameters settings could vary and show different shapes of the generated EMI as presented later on in this section.

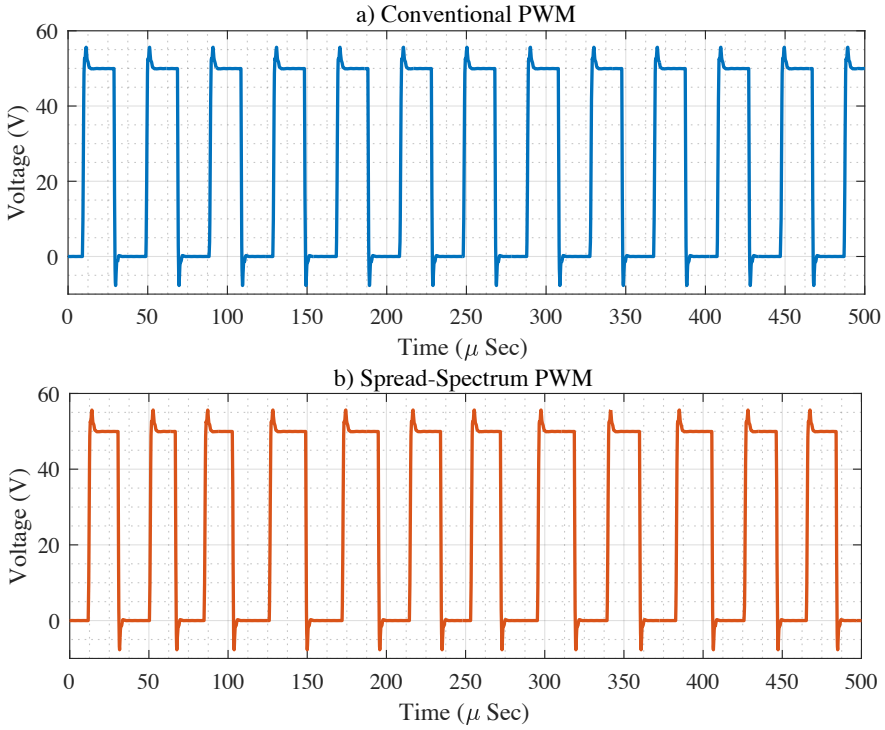

Figure 4.12: The time-domain signal of the generated output voltage from the buck converter in case of a) conventional modulation and b) SS modulation.

4.2.1. Changing the spreading factor

In this case, the spreading factor α of the SS signal is changeable at a PAM driving signal and with a constant driving signal frequency of 400 Hz. Table.4.2 shows the utilized SSM settings in this operating scenario. Figure 4.13 shows the deferential mode voltage frequency spectrum in the case of utilizing various values of α, measured from the LISN connected in the PLC circuit. It is noticed that the increase in the spreading factor value increases the SSM spectrum bandwidth, followed by a decrease in the peak amplitude of the generated EMI measurement.

Table 4.2: Buck converter electrical data.

Item	Value
The central switching frequency	63 kHz
Duty cycle	50%
Driving signal $\varepsilon(\tau)$	PAM
Driving signal frequency f_m	400 Hz
Spreading factor (α)	Varies between 0 to 30%

On the other hand, the Bit Error Rate (BER) shows the performance of the communication channel in the presence of the SS modulated EMI, in the case of using various spreading factor values. Figure 4.14 shows the BER percentage with the spreading factor in percentage. The results show an opposite behavior to the EMC standard hypothesis, that the more EMI mitigation provided, the fewer problems in the electrical grid. The highest BER percentage reaches 45% at $\alpha = 30\%$.
Figure 4.15 shows the channel capacity of the G3-PLC channel with the increase in the value of the spreading factor. As shown in the figure, the channel capacity reaches 780 kbit/sec at the EMI- free case, however, the value decreases gradually with the increase of the spreading factor, till it reaches its minimum value at a spreading factor equal to 30%. Figure.4.16 shows

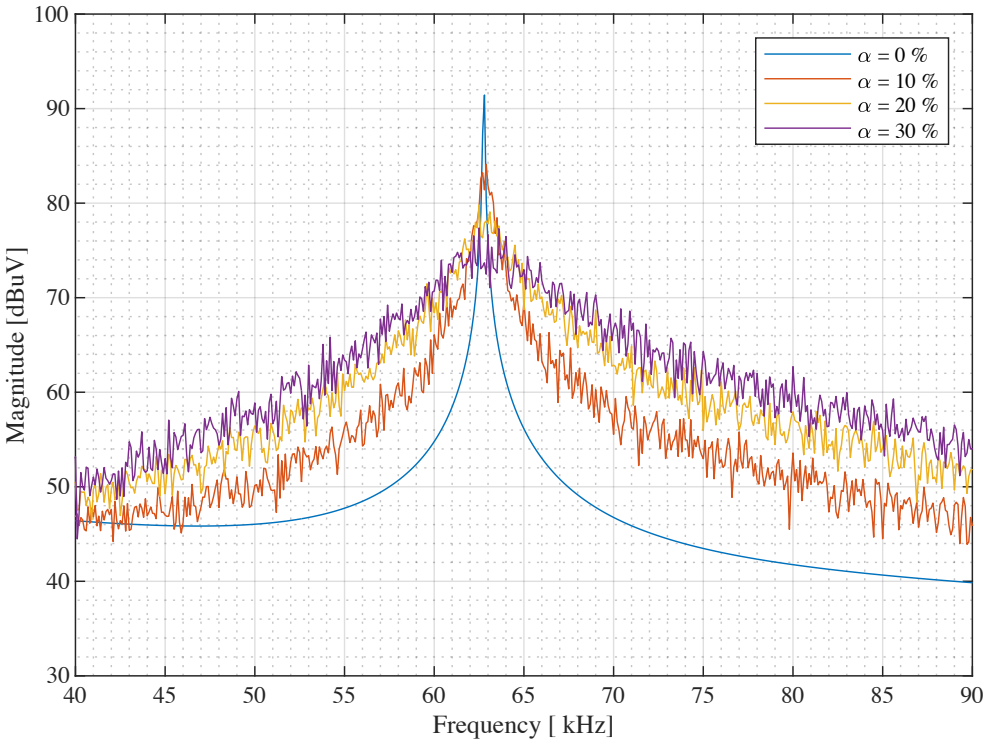

Figure 4.13: The differential mode voltage frequency spectrum at various values of spreading factor α at a constant driving signal frequency of 400 Hz.

the channel capacity loss in percentage with the increase of the spreading factor. Hence, the behavior of the channel loss percentage follows the behavior of the BER in Figure 4.14. Thus, the channel capacity succeeded to evaluate the behavior of the utilized SS technique efficiently, despite the EMI mitigation provided by the given technique. The matlab code used for the channel capacity calculation is given on Appendix A.2

4.2.2. Changing driving signal profile and frequency

The driving signal profile is the second parameter that affects the shape of the utilized SSM, consequently, it has an impact on the G3-PLC performance. In addition, the third parameter that could also affect the shape of the measured EMI is the frequency used by the driving signal to form its profile. In this simulation, we considered three driving signals $\varepsilon(\tau)$ profiles as mentioned in Chapter 2, which are the random PAM, the Saw-tooth, and Sinusoidal. Consequently, each profile could be formed by a certain number of points n , which could be built in a lookup table for each. Thus, the time between each cumulative point is equivalent to the inverse of the sampling frequency used. Furthermore, in this simulation, 100 points are considered to form the driving signal ranging from -0.5 to 0.5 in all the utilized profiles. Thus, in this operating scenario, the SSM follows the settings stated in Table 4.3.

Table 4.3: The spread-spectrum parameters at constant spreading factor.

Item	Value
The central switching frequency	63 kHz
Duty cycle	50%
Driving signal $\varepsilon(\tau)$	PAM, Sawtooth, and Sinewave
Driving signal frequency f_m	Varies from 0.3 to 3000 Hz
Spreading factor (α)	15%

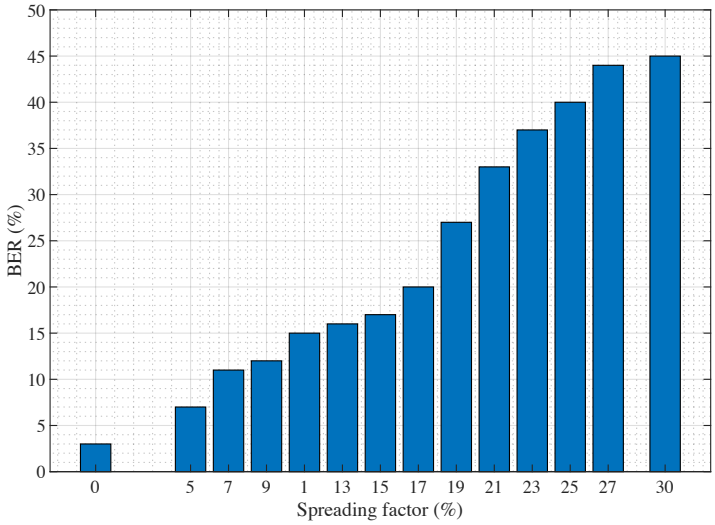

Figure 4.14: BER vs Spreading factor.

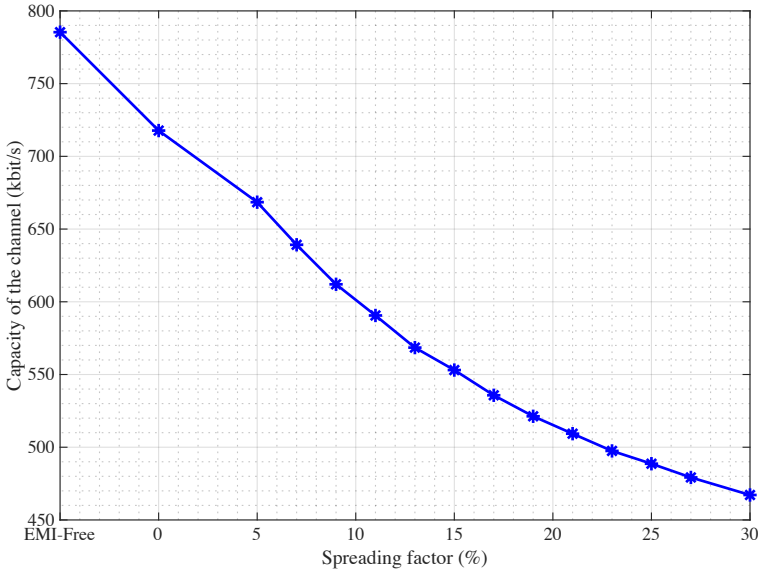

Figure 4.15: The capacity of the channel in the case of using different values of spreading factor.

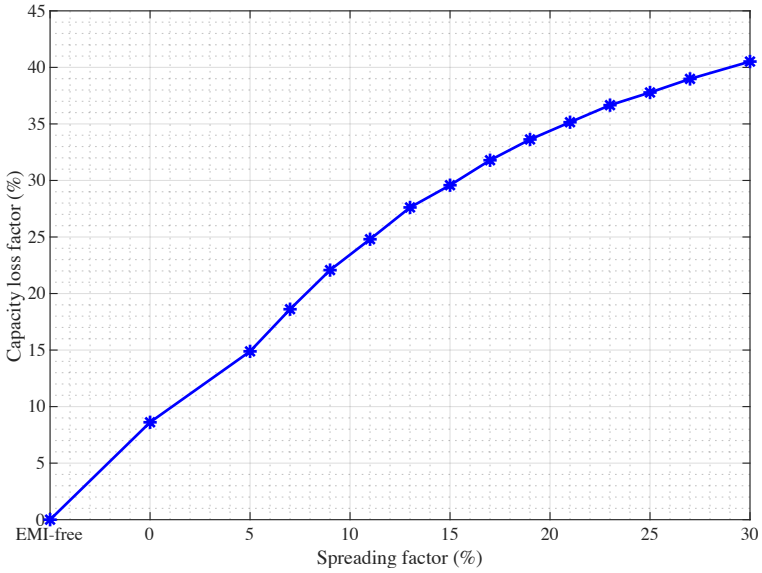

Figure 4.16: The channel capacity in percentage vs spreading factor.

b) EMI spectrum measurements

Figure. 4.17 shows the output voltage spectrum of the buck converter in the case of using the three used driving signals at a driving signal frequency of 300 Hz. The difference between the generated frequency spectrum from the three driving signals appears clearly in the figure. Following the EMC standards, the sinusoidal driving signal provides the worst EMI mitigation due to the presence of two peaks appearing in the SS bandwidth borders, while the Random PAM is the best approach as it provides the highest possible EMI mitigation. However, these shapes change dramatically with the driving signal frequency used as shown in the further figures.

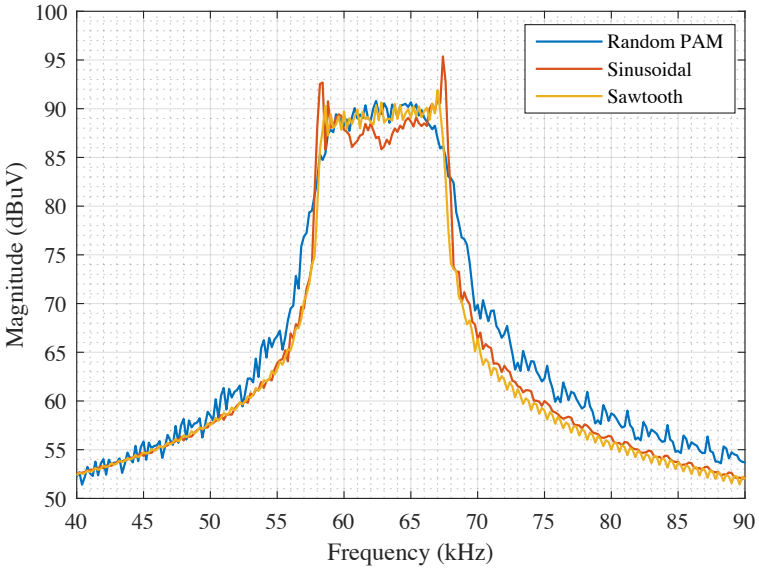

Figure 4.17: The buck converter output voltage frequency spectrum measured in the case of using three driving signal profiles.

Figures 4.18, 4.19, and 4.20 shows the differential mode voltage frequency spectrum, for the three utilized driving signals with various values of driving signal frequency f_m, respectively. The measured spectrum were taken from the communication circuit side. As shown in the figures, each driving signal profile provides different EMI shapes of the frequency spectrum with various values of driving signal frequency. The shape of the measured spectrum is hardly connected to the RBW of the used EMI receiver. In this simulation, the spectrum analyzer RBW was chosen to be equal to 200 Hz following CISPR A. It seems from the results that the relation between the peak amplitude of the measured EMI spectrum and the frequency of the driving signal is not linear as we will discuss in the next paragraph.

Following equations (2.7) and (2.14) in Chapter 2, the normalized frequency resolution ρ is calculated to be equal to 0.02 as the RBW used is 200 Hz and the bandwidth of the SSM Δf used is $63000 \times 0.15 = 9450$. On the other hand, the modulation index β is calculated based on the frequency of the driving signal f_m. Consequently, the peak value of the spectrum varies with the change of the modulation index at a normalized frequency resolution $\rho = 0.02$. Figure 4.21 shows the peak magnitude of the SS modulated noises measured from the PLC side in the case of using different driving signals with various values of β at $\rho = 0.02$ and $\alpha = 0.15$. It seems that the relation between the modulation index β various non-linearly with the peak magnitude of the EMI spectrum, there is an optimum value of β for which maximum EMI reduction is achieved as shown in Figure 4.21. In the lower values of ($\beta < 1000$), the peak magnitude of the EMI decreases gradually with the increase of β value following the decrease in the driving signal frequency f_m. In contrast, when the β value becomes more than 1000, the driving signal becomes very slow (f_s is very small) and the EMI receiver detector sees the SSM signal as a single tone moving within the SS modulation bandwidth. Thus, its magnitude appears similar to the conventional deterministic modulation.

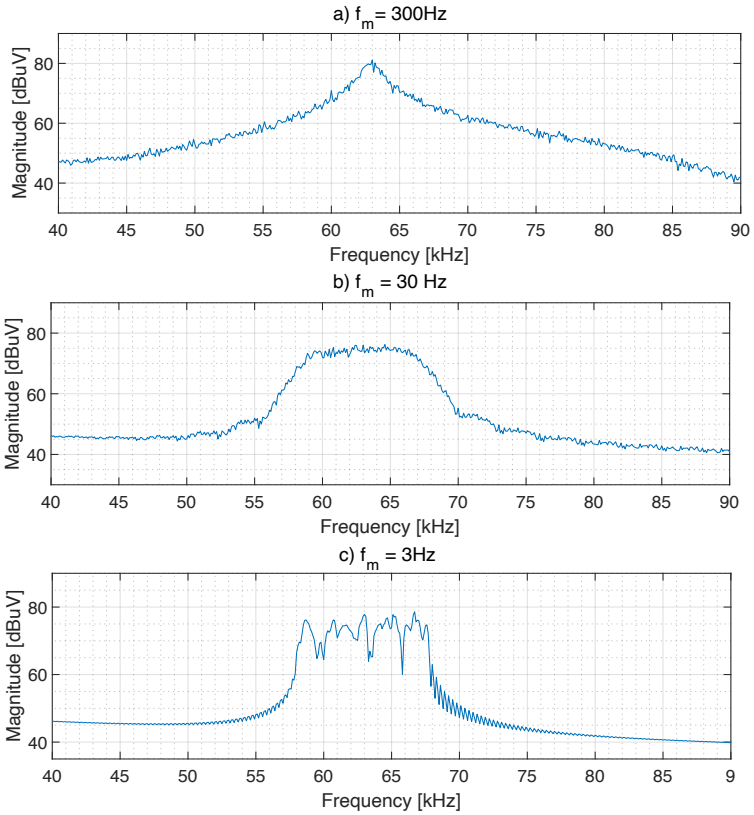

Figure 4.18: The EMI voltage frequency spectrum for PAM SS modulation utilizes various driving signal frequencies.

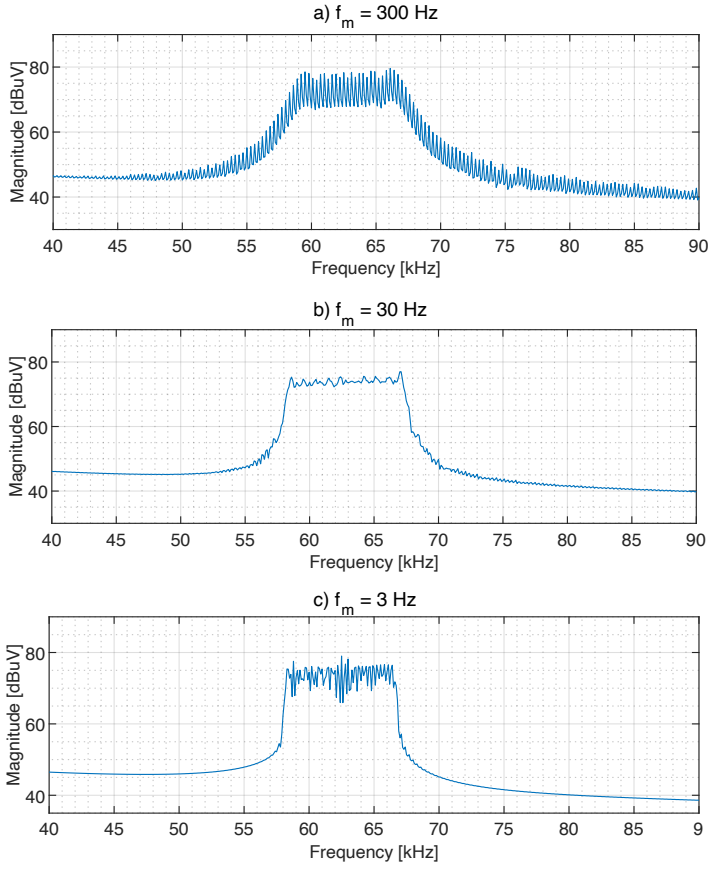

Figure 4.19: The EMI voltage frequency spectrum for saw-tooth SS modulation utilizes various driving signal frequencies.

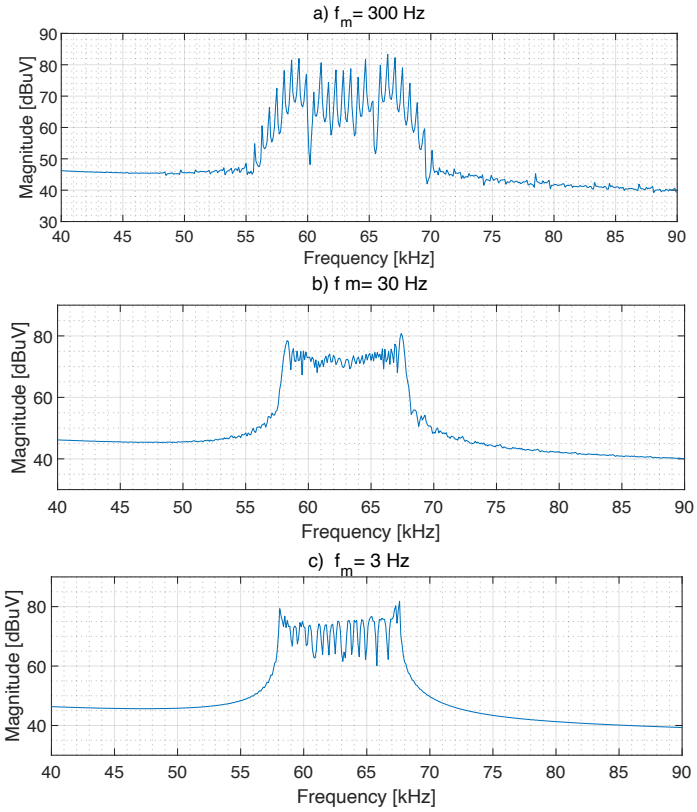

Figure 4.20: The EMI voltage frequency spectrum for sinusoidal SS modulation utilizes various driving signal frequencies.

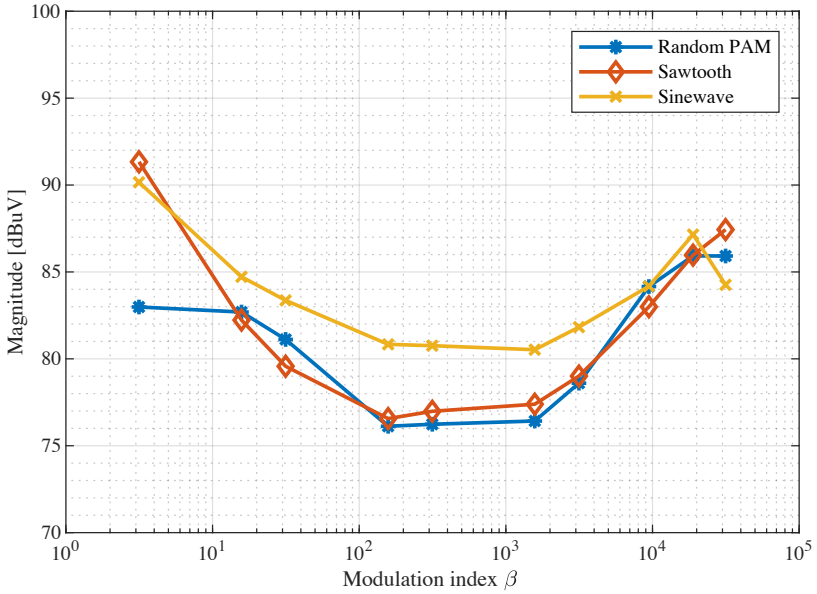

Figure 4.21: The spectrum peak amplitude of the SS modulation utilizes various driving signals with modulation index β values, using the AV detector with IFBW = 200 Hz.

b) The PLC performance in the presence of EMI

Figures 4.22, 4.23, and 4.24 show the BER percentage with the driving signal frequency values in case of using various spreading factor values for the three utilized driving signals in our setup, respectively. Basically, the BER percentage increase with the increase of driving signal frequency f_m in all cases of the used driving signals profiles, till the BER reaches the maximum value at f_m between 600 and 6000 Hz. In the case of $\alpha = 0.15$, the BER percentage reaches its maximum value of 73 % at $f_m = 60Hz$. Moreover, the same behavior is noticed in all the utilized values of spreading factor α , as shown in Figures 4.22, 4.23, and 4.24.
In the higher frequency rates (above 60 Hz), the G3-PLC channel behaves differently according to the utilized driving signal type, whether it was a non-periodical signal or a periodical one. In the case of a non-periodical signal like the random PAM one, the BER starts to decrease gradually with higher sampling frequencies. On the contrary, when the driving signal is periodical like in the case of the saw-tooth signal or the sinusoidal ones, the BER percentage maintain almost constant with the increase of the f_m as shown in Figures 4.23 and 4.24.

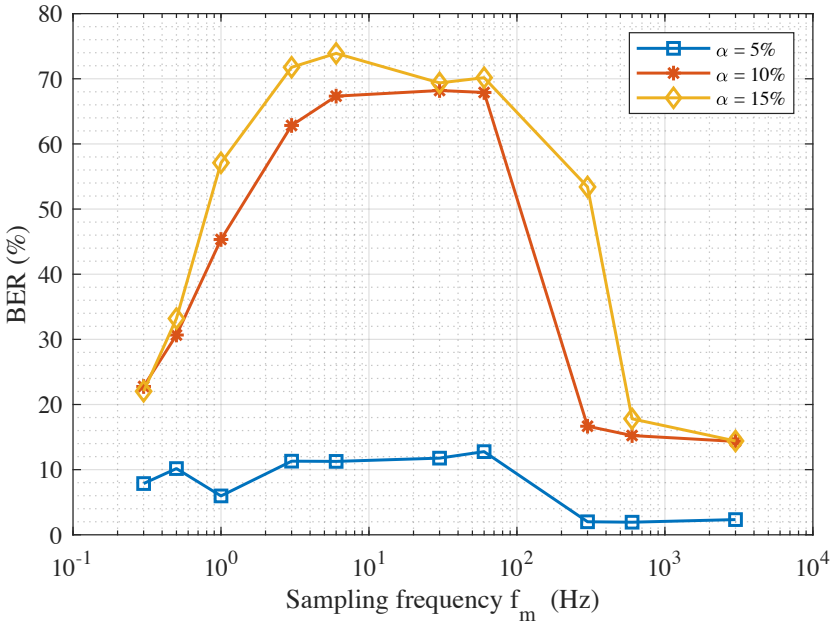

Figure 4.22: The BER vs the driving signal frequency f_m in case of using uniform pesdo-random signal with different spreading factor α values.

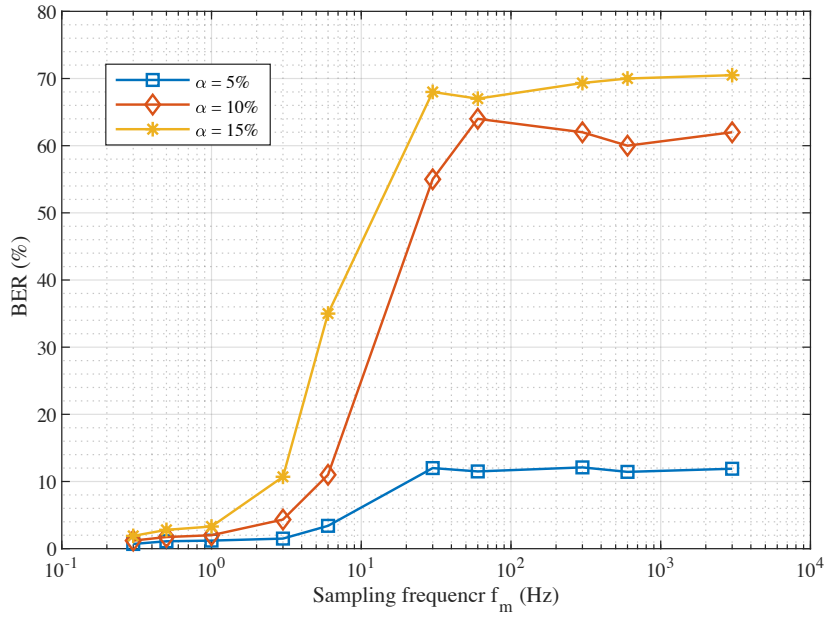

Figure 4.23: The BER vs the driving signal frequency f_m in case of using sawtooth signal with different spreading factor α values

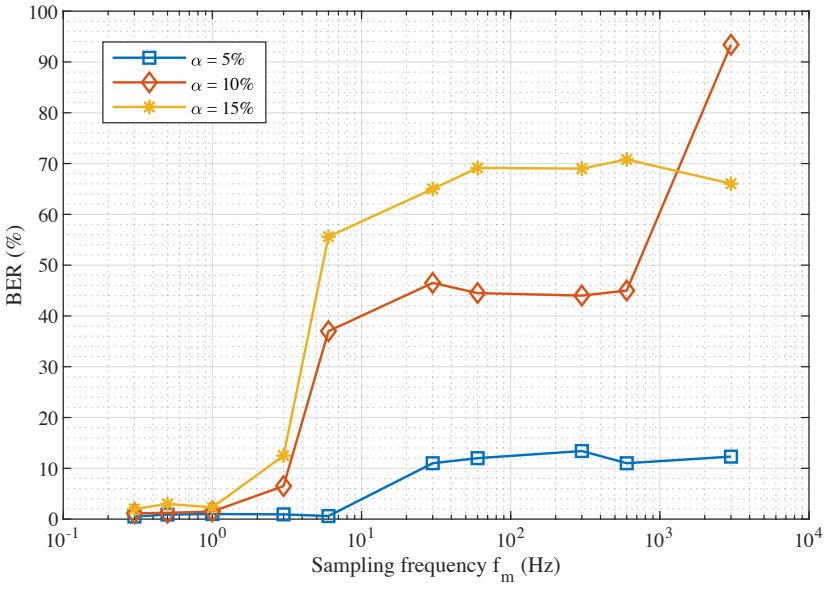

Figure 4.24: The BER vs the driving signal frequency f_m in case of using sinewave signal with different spreading factor α value.

b) The Shannon- Hartley equation evaluation

The above results were confirmed by the Shannon-Hartley equation. Figure 4.25 shows the channel capacity in kbits/sec for the three utilized driving signals at a constant spreading factor of 15%. The channel capacity decreases with the increase of the driving signal frequency in all cases of the three driving signals used. Thus, the Shannon-Hartley equation succeed to represent the behavior of the channel in the presence of SS modulated EMI with different driving signals, specifically in the lower values of frequency (less than 300 Hz). The Shannon Hartley equation depends on the power spectral density measured by the EMI receiver, as a result, at a lower driving signal frequency, the EMI receiver can see the frequency change of the utilized SS technique, and the measured spectrum appears similar to that in the case of the convention modulation signal moving slowly in the given SS bandwidth.

On the other hand, the Shannon Hartley equation failed to confirm the behavior of the channel in the case of the higher sampling rates (higher than 6 kHz), as the EMI receiver see the SS modulated EMI as a group of peaks separated from each other by constant frequency spaces equivalent to the frequency f_m of the utilized driving signal. Thus, the measured frequency spectrum area decrease, and the channel capacity increase. Figure 4.26 shows the channel capacity losses in percentage in all cases of the three driving signals used. The matlab code used for the channel capacity calculation is given on Appendix A.1.

4.3. Summary

In this chapter, the influence of the SS modulated EMI on the G3-PLC channel performance was simulated in various operating conditions. The simulation was implemented using the MATLAB SIMULINK environment. In all operating conditions, the voltage spectrum of the EMI was measured and the communication channel was evaluated by the BER calculation. Finally, the behavior of the channel was confirmed by calculating the channel capacity in the presence of noise at the given operating conditions.

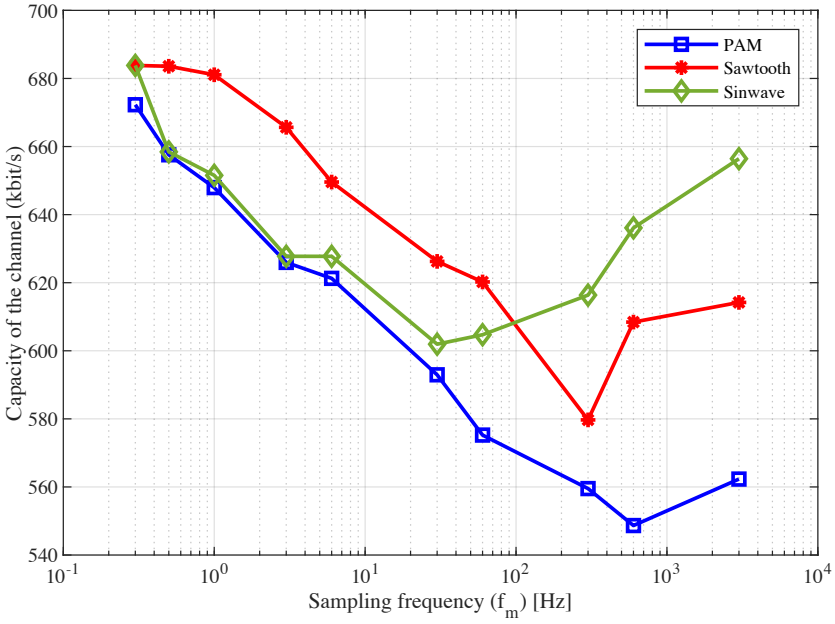

Figure 4.25: The channel capcity Vs the driving signal frequency.

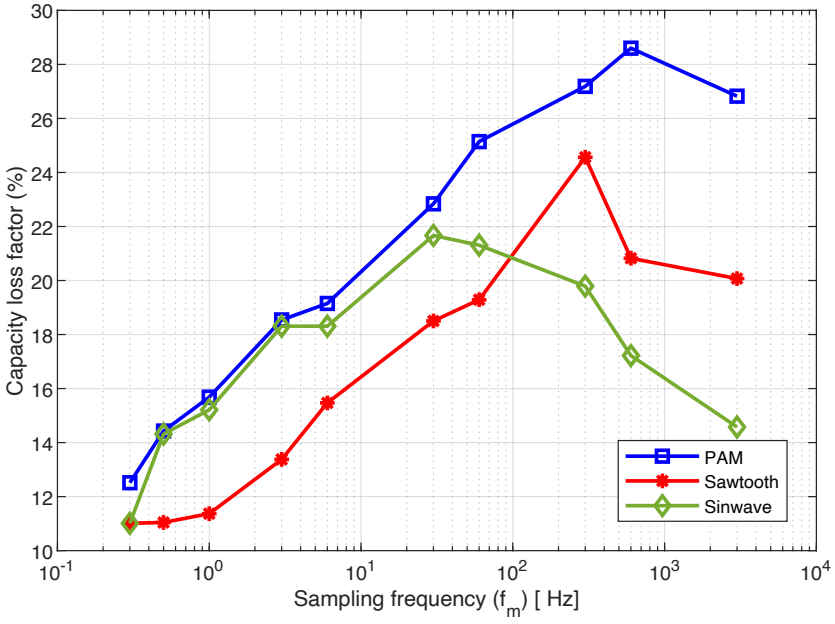

Figure 4.26: The channel loss Vs the driving signal frequency.

Chapter 5

Practical Implementation

The practical implementation is an important step in research, especially in the EMC field. Usually, the EMI is a parasitic relationship between the EMI sources and the victim/s, this relation happened due to the existence of an unwanted coupling path between both devices.In addition, the victims itself could act as a source of EMI due to the internal parasitic components in included on its circuit. In this chapter, we will study the effect of SS modulated EMI on the G3-PLC performance practically. The tests were carried in the University of Zielona Gora EMC lab. The performance of the communication was evaluated in terms of the change of several SS modulation settings like the SS bandwidth, the driving signal type, and the main switching frequency.

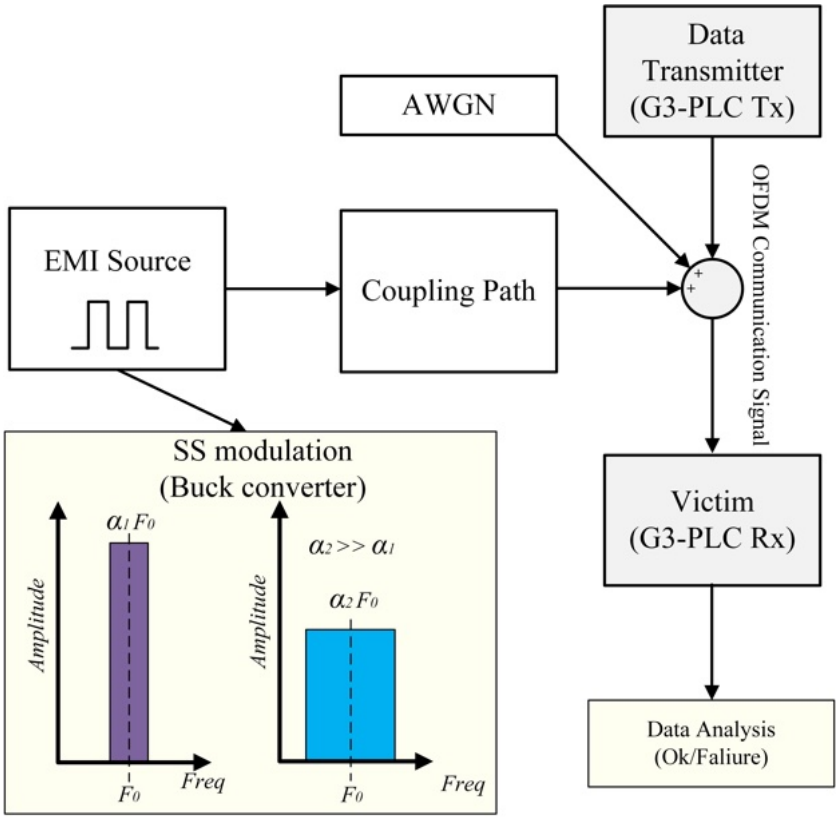

Figure 5.1: Block diagram for coupling between the SS modulated converter and the PLC channel.

5.1. Implementing the conventional and spread spectrum modulations

In this study, a DC buck converter is considered as the source of EMI, and the G3-PLC acts as the victim. Consequently, as the EMI is flowing in the electric cables (considering conducted emissions), the EMI could sneak into the PLC communication channel through several coupling paths as shown in Figure 5.1. The Texas Instruments (TI) TMS320f28335 DSP card is used for the buck converter switching control signal. The card is programmed by the Matlab Simulink software tool. The hardware setup was designed to able the operator to change the switching frequency using a simple potentiometer ranging from 0 to 92 kHz, hence, the Analog to Digital Converter (ADC) in the card is used for this purpose. The ADC in this card is 16-bit and the maximum input voltage is 3.6V. Figure 5.2 shows the ADC block used in the Simulink graphical interface, the input is multiplied by a gain to convert the output digital value from the ADC into the needed switching frequency. Also, the switching frequency could be set internally without the ADC input as shown in the figure. The duty cycle of the signal is set to 50% and could be changed according to the operator's needs.

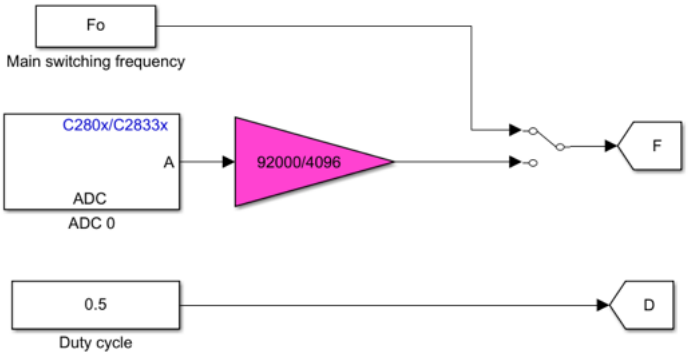

Figure 5.2: The ADC block used by Simulink to change the switching frequency.

After that, the switching frequency f_c is used in designing the SS technique, the designed SS technique is RCMFD. The operation of the utilized SS technique follows the given equations

$$f_{PWM} = f_c + \Delta f \cdot \varepsilon(\tau), \tag{5.1}$$

$$\Delta f = f_c \cdot \alpha, \alpha : 0.05 \; to \; 0.3, \tag{5.2}$$

where f_{PWM} is the output frequency of the spread signal, α represents the spreading factor of the signal and $\varepsilon(\tau)$ is the driving signal for the frequency change. The function of the driving signal $\varepsilon(\tau)$ could be sinusoidal, triangular, or a random Pulse Amplitude Modulated (PAM) signal [57]. Figure 5.3a shows the implemented SS technique equations. Moreover, the switching frequency f_c could be used directly to generate the conventional PWM as shown in Figure 5.3b. Finally, the outputs from the SSM block and the Conventional PWM block are connected to a switch for controlling the modulation technique used.

As the code works in the time-based frame, the switching frequency should be calculated to the TI on-board crystal frequency which is 150 MHz. Hence, the chosen switching frequency and duty cycle are connected to the PWM block as shown in Figure 5.4. The resulting spectrum is measured from the output of the buck converter as shown in Figure 5.5, the difference between both types of modulation appears clearly in the figure.

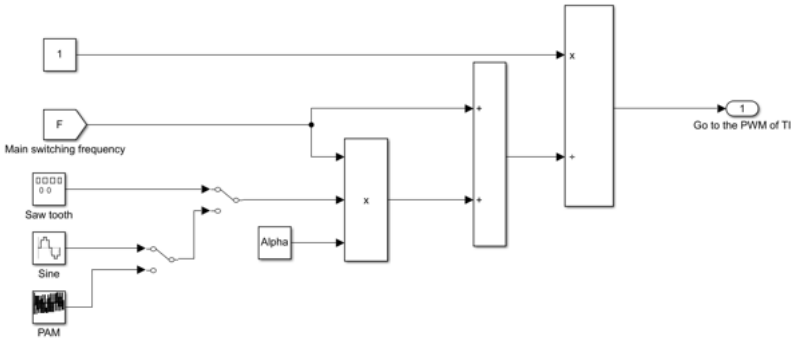

(a)

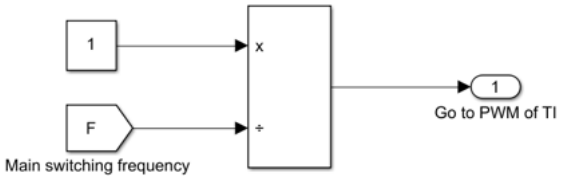

(b)

Figure 5.3: a) The designed SS technique inside the Simulink code, b) the conventional PWM .

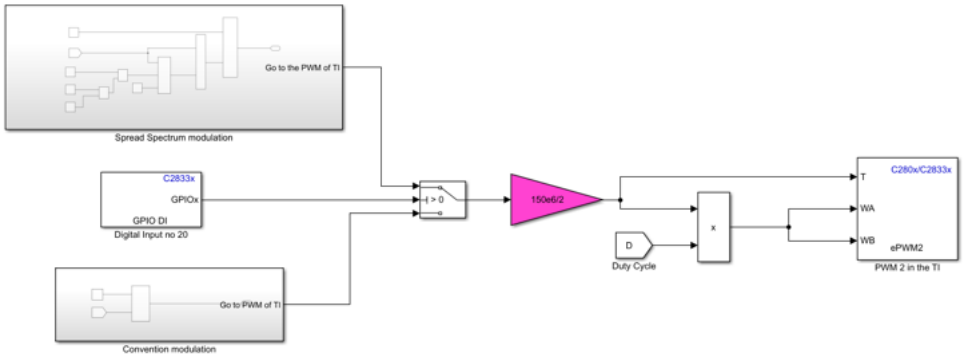

Figure 5.4: Connecting the SS and conventional modulations blocks to the PWM block in the Simulink Code.

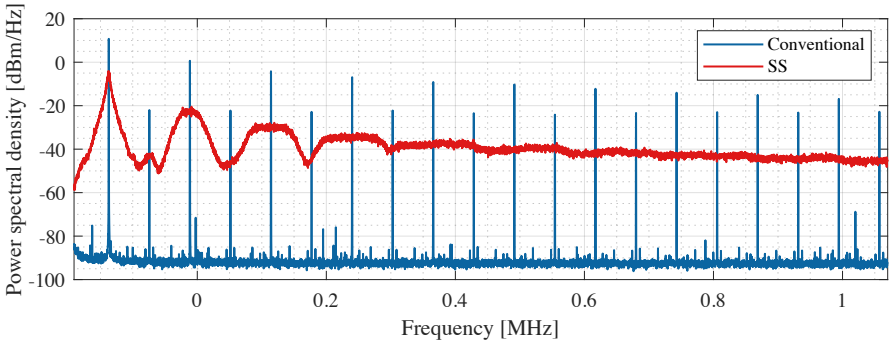

Figure 5.5: The PWM representation in the frequency domain.

5.2. The DC Buck converter

The power converter used in the experiment is the same power converter considered in the simulation (Chapter 4). The duty cycle is fixed to 50 % and the switching frequency is spread around a central frequency of 63 kHz, which coincides with the intermediate frequency of the PLC bandwidth. In order to see the difference between the Silicon and Silicon Carbide based converters, the type of the utilized switches were changed during the tests. Table 5.1 shows the electrical parameters of the used buck converter.
Usually, there is a type of filter on the output of the buck converter, but the purpose of the circuit is to show the influence of simple first-order oscillatory mode current on the G3-PLC performance. For this reason, the filter was not considered in our setup. As the test was implemented using laboratory equipment, the power of the applied load is not too high and a sliding resistor was used to set the required current. Figure 5.6 shows the used DC buck converter circuit test bed.

Table 5.1: Buck converter electrical parameters

Item	Value
Input Voltage	50V
Input current	0.6
Output Voltage	25V
Output current	1.2A

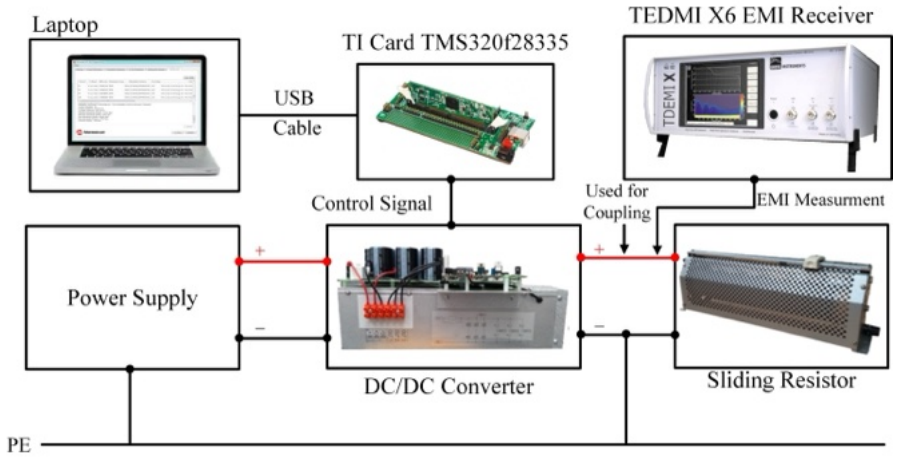

Figure 5.6: The DC buck converter circuit connection.

5.3. G3-PLC circuit

The communication works using two Microchip ATPL360 PLC modems representing the transmitting and the receiving points as shown in Figure 5.7, both modems are configured to work based on CENELEC-A standard frequency range and the G3-PLC mode. Besides, to isolate the outside EMI noise and to make certain of the robustness of the results, Isolating transformer and LISN are connected between the PLC circuit and the grid. The data sheet of the ATPL360 PLC modems is included in Appendix B.1

5.4. Implemented coupling circuits

Usually, there are several ways of parasitic coupling between EMI coupling between the power and communication circuits, in this research, we considered two types of coupling:

- Artificial EMI capacitive coupling
- Mutual coupling between cables

5.4.1. Artificial EMI capacitive coupling

The coupling was implemented between the buck converter circuit and the G3-PLC circuit through a parasitic capacitance, similar to that implemented in the simulation in Chapter 4. In addition,the parasitic capacitor is connected to the PLC circuit through a common resistance as shown in Figure 5.7. In the real system, the artificial circuit corresponds to a typical common mode path of interference for high-frequency EMI, the presented inductance can be associated with the inductance of the connected wire, the presented capacitance corresponds to parasitic couplings to the ground which could exist because of the load enclosures or any other reasons [84].
The setup in Figure 5.7 could be applied in the case of the residential DC Micro grid systems, at which there are a lot of DC and AC loads connected to the same grid with the presence of solar panels, batteries, and small-scale power wind turbines [85]. Figure 5.8 shows the setup test bed with both circuits coupled together.

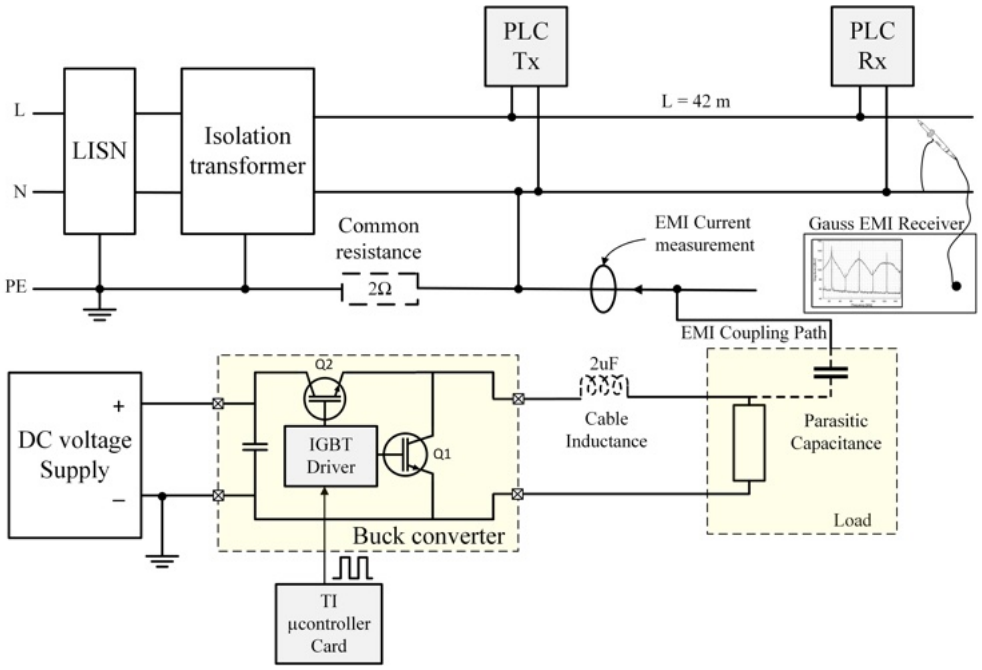

Figure 5.7: Connection diagram of the coupling circuit 1.

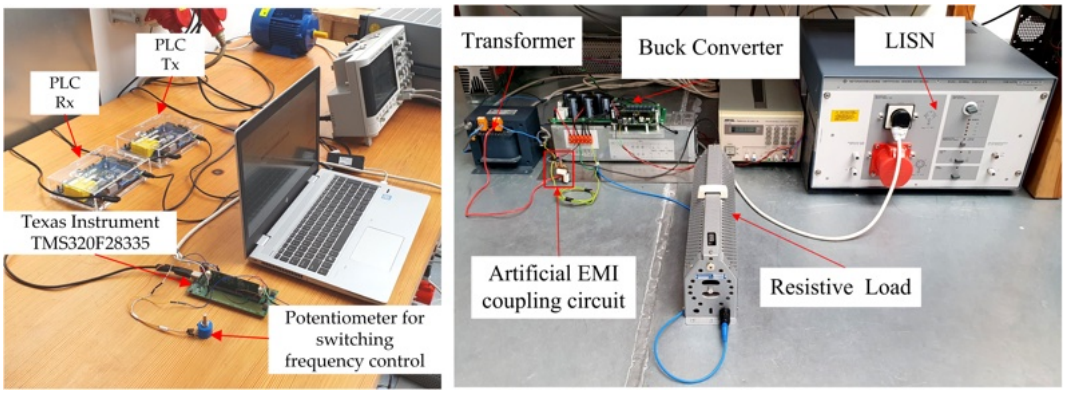

Figure 5.8: Setup test-bed for coupling circuit 1.

5.4.2. Mutual coupling

In this circuit, interference between the power circuit and the communication circuit is transferred through the mutual coupling between the cables. The PLC circuit is the same as in the previous one, however, at this time the power circuit cables were placed so close to the communication circuit cables so that the interference affects the communication performance through the mutual coupling. Figure 5.9 shows the proposed connection for this coupling circuit operating scenario.

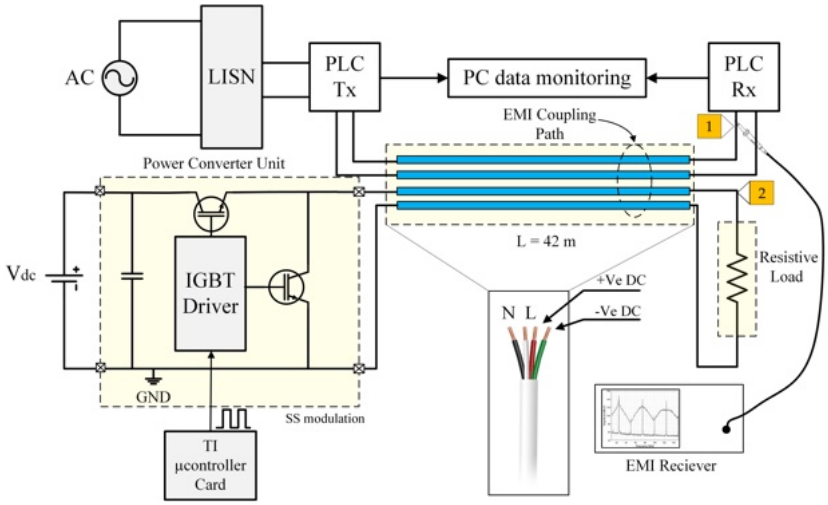

Figure 5.9: Connection diagram of mutual coupling circuit.

5.5. The G3-PLC modems settings and measurements

The performance of the PLC channel could be evaluated by the mean of Bit Error Rate (BER) or the Frame Error Rate (FER), the FER is chosen for the evaluation of the PLC performance as there are a lot of Physical (PHY) layer components such as equalization, header decoding, and Viterbi decoder are included per frame. In addition, the FER is more connected to the final evaluation of the Medium Access Control (MAC) from the PLC system [74]. The FER percentage represents the ratio between the broken frames to the total sent frames in percentage, as expressed in equation (5.3).

$$FER = \frac{Sent\ \ Frames - \ Recieved\ frames}{Sent\ \ Frames} \cdot 100\% \tag{5.3}$$

The numbers of the sent frames and the time between each frame were chosen after several tests to assure the rigidness of the FER results. Figure 5.10 shows the FER results come out from the G3-PLC modem when the PLC channel was under SS modulated EMI at certain SS settings. The test carried out ten trials for different numbers of total sent frames, the time between each frame, in this case, was set to 100 ms. The variation on the FER percentage decreases with the increase of the total number of sent frames till we reach 3000 frames. After that, the variation on the FER percentage remains almost constant, the standard deviation of the FER after ten trials was equal to 1.25 in the case of 3000 frames and was equal to 1.4 at 5000 as shown in Figure 5.11.
Another parameter that could affect the results is the time between each frame. Figure 5.12 shows the FER in case of using several times between each frame for a total sent frame of 3000. The FER value remains almost constant whatever the value of the time used between frames.
Figure 5.13 shows the frequency spectrum of the G3-PLC transmitted signal measured from the grid terminals. The output spectrum of the PLC modems follows the G3-PLC standard parameters,at which the OFDM range should be between 35 kHz to 91 kHz. Also, the measured spectrum is similar to the one measured from the simulation presented in Chapter 4. Consequently, the The transmitter modem chosen settings are stated in Table 5.2.

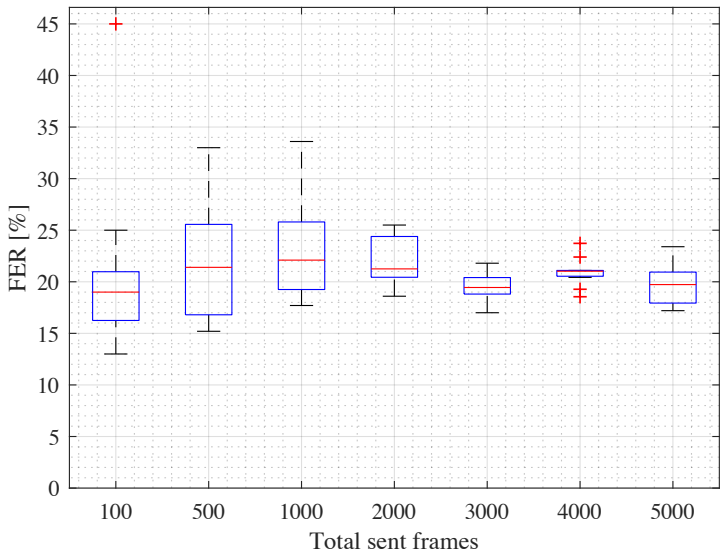

Figure 5.10: Box and whiskers for ten trials using different numbers of sent frames.

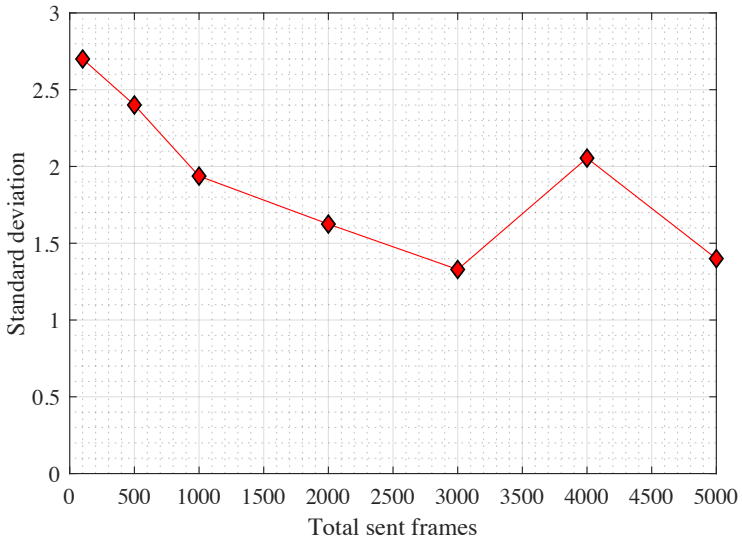

Figure 5.11: The calculated standard deviation is based on the ten trials for different numbers of sent frames.

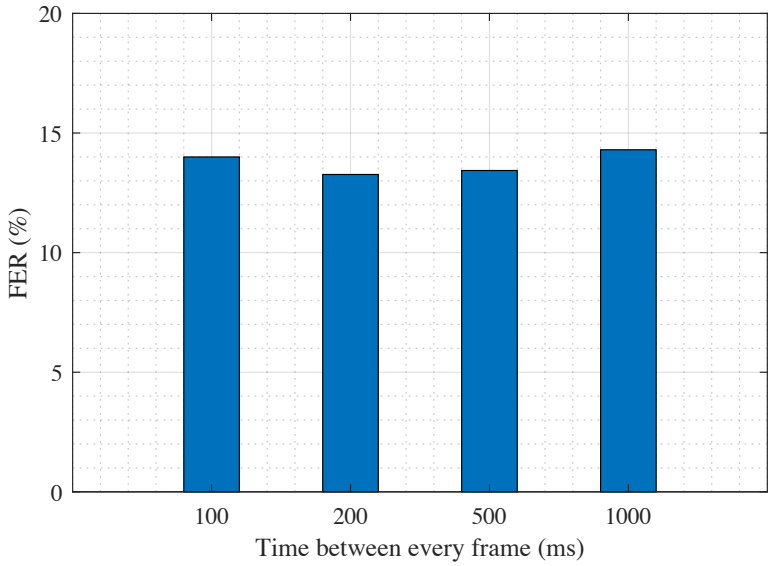

Figure 5.12: The FER in case of different time between frames when the total sent frames were 3000.

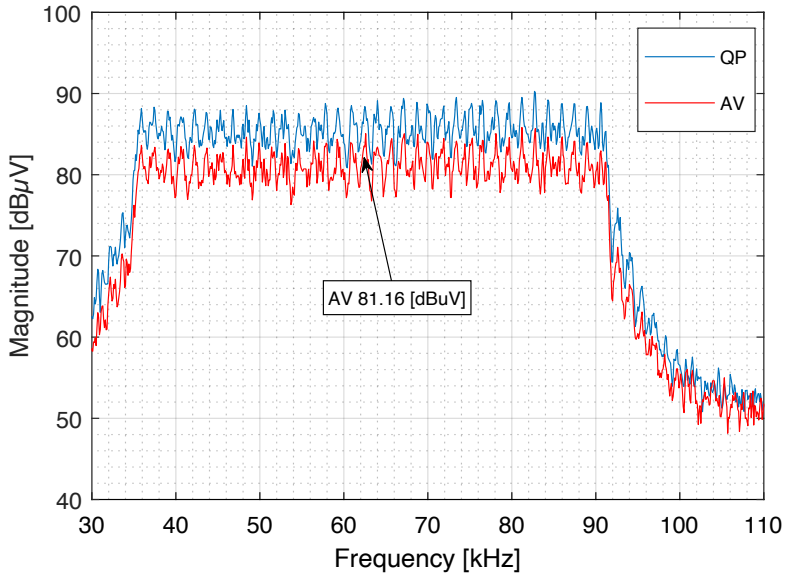

Figure 5.13: The Spectrum of the G3-PLC signal using the Average and Quasi-Peak detectors and IFBW = 200 Hz.

Table 5.2: G3-PLC communication setting.

Type of PLC communication standard	G3-PLC
Data size	65 bytes
Physical Layer	OFDM
Modulation	DBPSK- DQPSK -D8PSK
Total Frames data should be sent	3000
The time between each packet	100 ms
The Medium Single-phase cable of Length	42m

5.6. The influence of the conventional modulation on the G3-PLC performance

In this section, the impact of the conventional switching modulated EMI on the G3-PLC performance will be introduced. The tests consider three parameters:

1) The type of the utilized transistor (Silicon (Si) Vs Silicon Carbide (SiC))
2) The utilized supply voltage.
3) The utilized switching frequency.

The tests consider using two buck converters, one Si-based and the other is SiC-based as shown in Figure 5.14. The SiC transistors have the advantage of working on the high frequency-based applications; also, it sustains the high-temperature operation. The purpose of the test is to study the effect of using the SiC-based converters on communication, especially in this narrow band from 3 to 150 kHz.The SiC based converter used is CREE Silicon Carbide MOSFET Evaluation Kit(the data sheet is shown in Appendix B.2). Both converters were configured to work 62 kHz switching frequency, which is near to the intermediate frequency of the G3-PLC band (63 kHz). The duty cycle was chosen to be equal to 50%, and the sampling time used was 40 μs. The coupling circuit with the PLC circuit was through mutual coupling between cables (Section 5.4.2) and the PLC modems follow the settings in Section 5.4.3.
Figure.5.15 shows the measured frequency spectrum for the DC output in the case of both Si and SiC-based converters, the measurements were taken using the Average detector (AV) at an input supply voltage of 100 V. It was noticed that the peak amplitude of the output frequency spectrum of the SiC based converter is less than that in case of the Si-based one by 4 dB. Consequently, the SiC-based one should provide lower problems on the G3-PLC performance. However, the results show different behaviour.

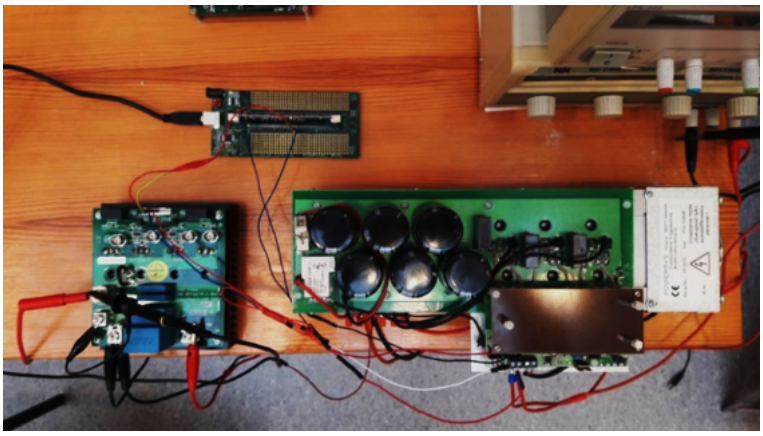

Figure 5.14: The used buck converters as EMI Sources.

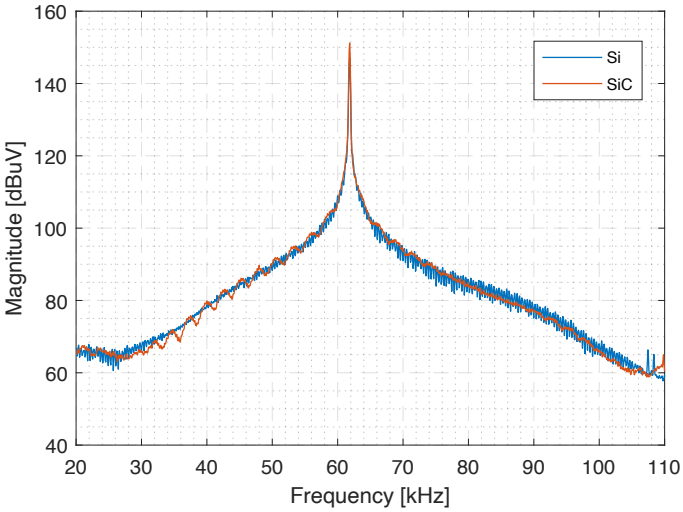

Figure 5.15: The frequency spectrum of buck converter output.

Figure 5.16, Figure 5.17, and Figure 5.18 show the percentage FER with the increase in the voltage supply ranging from 100 V to 200 V for the buck converter circuit in the case of Si-based and SiC-based converters, along with the change in the PLC modulation. The results show that the data transmission FER increases with the increasing signal magnitude. Moreover, both converters have almost the same effect on the data transmission error in all cases, and the maximum difference reaches 5%.

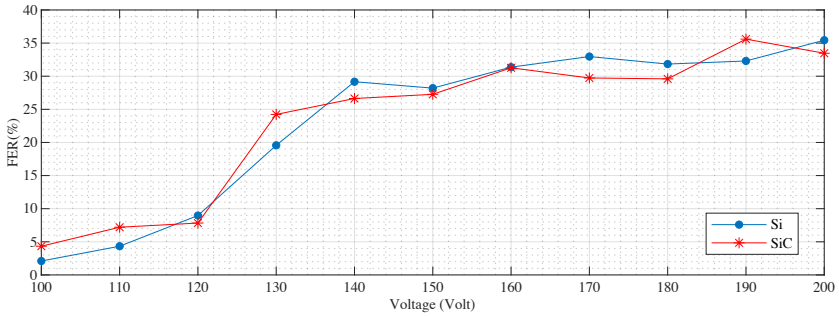

Figure 5.16: FER Vs Supply voltage in case of using DBPSK PLC modulation technique.

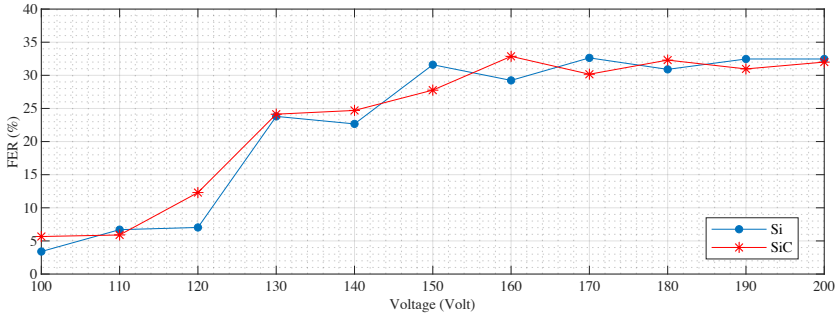

Figure 5.17: FER Vs Supply voltage in case of using DQPSK PLC modulation technique.

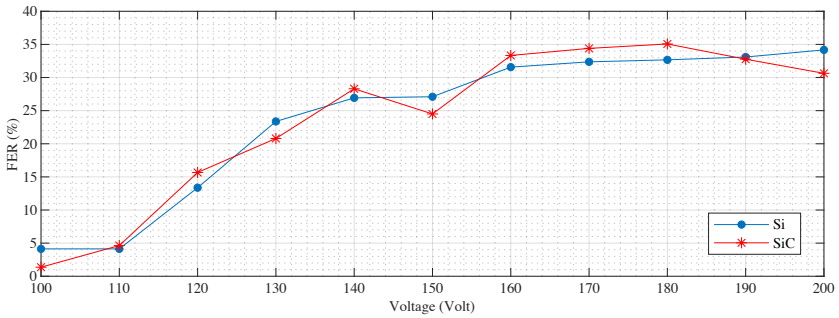

Figure 5.18: FER Vs Supply voltage in case of using D8PSK PLC modulation technique.

5.7. The influence of spread-spectrum modulation on the G3-PLC performance

As we considered the RCFMFD as the SSM technique used, the test target the change of its parameters settings. General speaking, three parameters control the shape of the SSM output spectrum:

1) The spreading factor.

2) The driving signal profile.

3) The driving signal frequency.

5.7.1. Changing the spreading factor

In this scenario, we assume the change only on the spreading factor and keep the other two parameters (driving signal profile and frequency) constant. In this case, the parameters of the used SSM are stated in Table 5.3.

Table 5.3: Buck converter electrical data 1.

Item	Value
The central switching frequency	63 kHz
Duty cycle	50%
Driving signal $\varepsilon(\tau)$	PAM
Driving signal frequency f_m	400 Hz
Spreading factor (α)	Varies between 0 to 30%

a) Coupling through the artificial EMI parasitic capacitance

In this case the used coupling circuit is the capactive one. Figure 5.19 shows the voltage spectrum of the SSM in case of changing the spreading factor from 0% (the conventional PWM) to 30% at a central switching frequency of 63 kHz and converter supply voltage of 50 V, measured from the PLC side using the AV detector and IFBW = 200 Hz. From the EMC standards point of view, the increase of the α decreases the EMI noise in the channel. Thus, the SSM signal in the case of $\alpha = 30\%$ is better than in the case of 10%. In contrast, the results show an opposite conclusion to this hypothesis. Figure 5.20 shows the FER percentage in case of changing the SSM spreading factor at a central switching frequency of 63 kHz, in three operating input voltage cases:10 V, 20 V, and 50 V. Obviously, the increase in the amplitude of the input voltage will increase the FER in the PLC channel as shown clearly in the figure. However, the decrease in the amplitude provided by the SSM delivers more problems to the communication signal. The FER reaches its maximum value at a spreading factor of 25% in the three cases of input voltages.

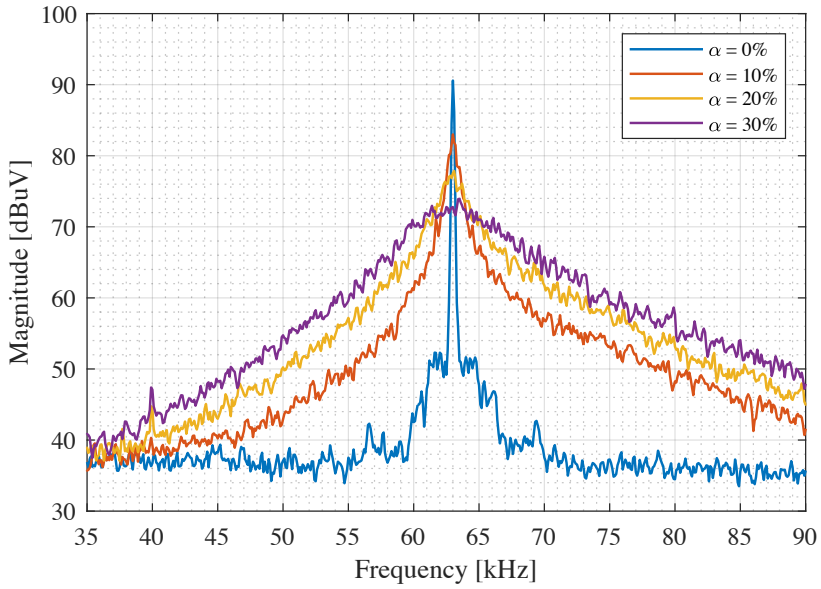

Figure 5.19: The spectrum of SSM EMI is measured from the PLC side.

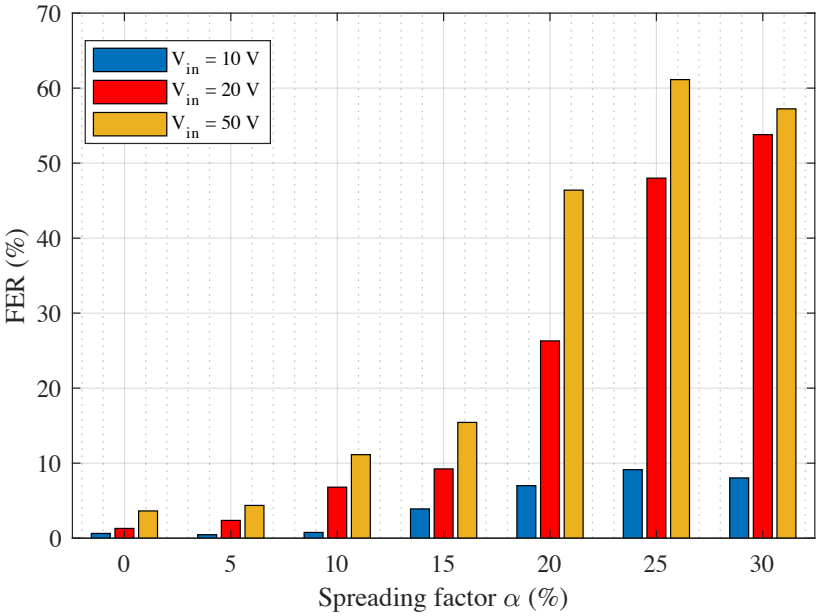

Figure 5.20: The PLC channel FER evaluation in case of SSM EMI with several amplitudes and spreading factor α.

Figure 5.21 shows the channel capacity evaluation based on equation (3.7) in all cases of input voltages. It seems clear that the channel capacity is decreased with the increase of the spreading factor of the signal, respectively, the capacity loss in the channel increase with the increase of the spreading factor as shown in Figure 5.22. The channel capacity calculation confirms the behavior of the FER of the PLC channel with the spreading factor of the SSM, knowing that the channel capacity represents the maximum allowable data that can be transmitted through the communication channel (the maximum bit rate for the G3-PLC is 33 kbit/ sec). Consequently, these results showed an opposite hypothesis to that used in the EMC standards. The matlab code used for the channel capacity analysis in this operating scenario is presented in Appendix A.2.

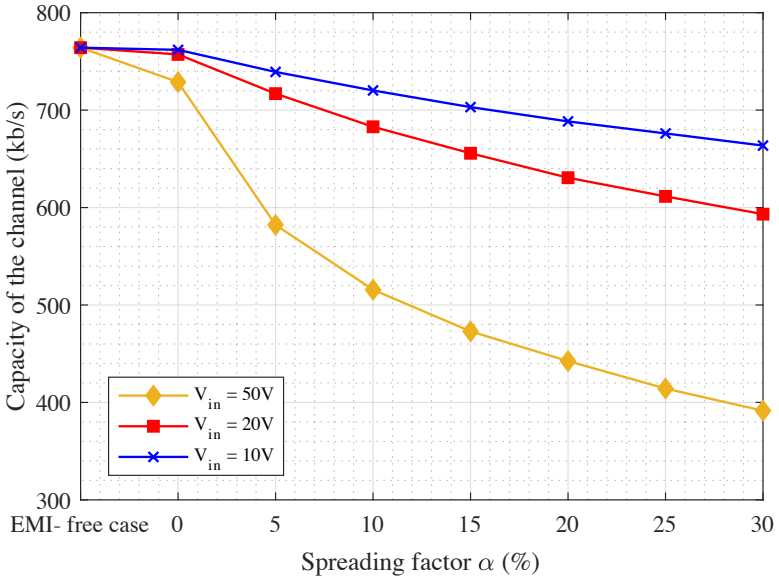

Figure 5.21: The PLC channel capacity in case of several values of spreading factor with the change of input voltage amplitude of the converter.

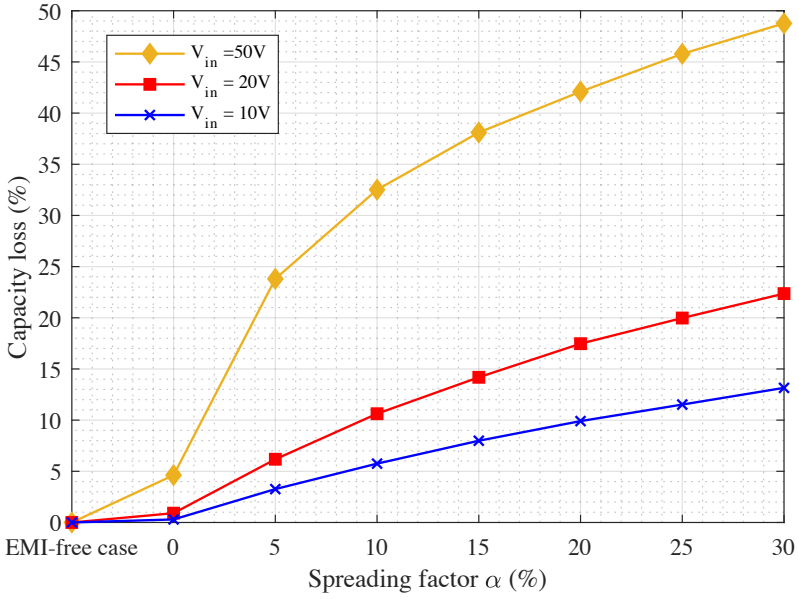

Figure 5.22: The PLC channel capacity loss in case of several values of spreading factor with the change of input voltage amplitude of the converter.

Figure 5.23 shows the FER percentage in the presence of EMI in the case of operating SSM with different central switching frequencies at a constant input voltage of 50 V. The results showed that at any value of SSM of central frequency ranging from 50 kHz to 75 kHz, the FER increases with the increase of the spreading factor α from 0% to 30%. Besides, the highest values of FER appear around the intermediate frequency of the communication bandwidth, between 56 kHz and 69 kHz. The variation of the central frequency of the SSM signal creates two situations in terms of EMI noise: Fully overlapped with the intentional bandwidth of the PLC signal or Partially overlapped with the intentional bandwidth of the PLC signal. The first case could appear as well as the value of the central switching frequency of the SSM is near to the intermediate frequency of the PLC signal, which is 63 kHz. On the other hand, the second case appears when part of the signal is out of the PLC bandwidth, as the switching frequency starts to go away from the intermediate frequency of the PLC bandwidth.

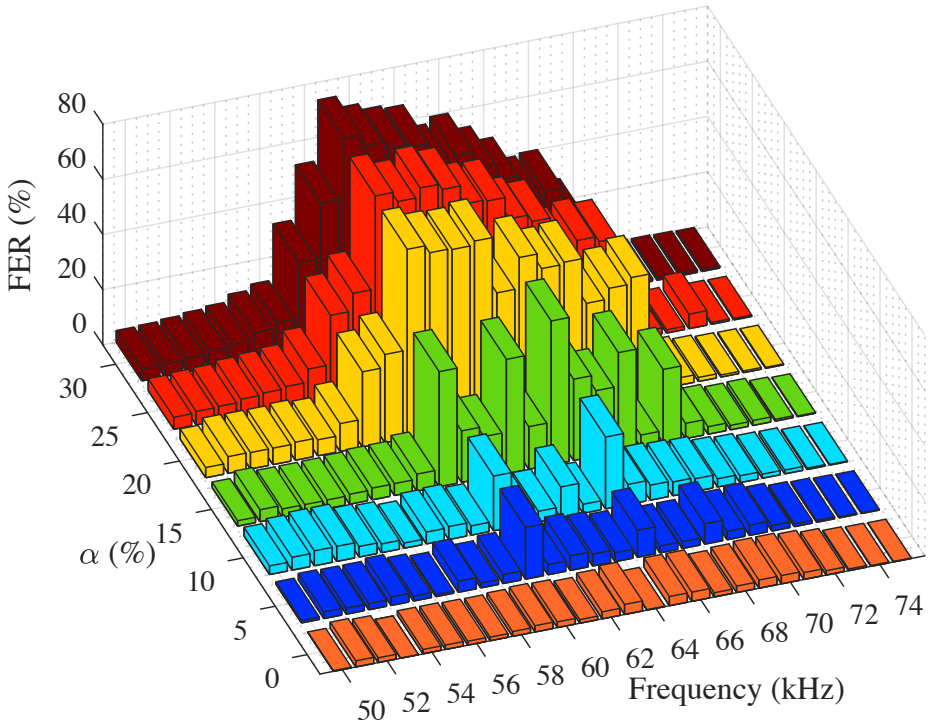

Figure 5.23: The PLC channel FER evaluation in case of SSM EMI with several switching frequencies and spreading factor α.

Figure 5.24 shows channel capacity calculation for the G3-PLC channel in case of SSM utilized three central switching frequencies, the first one is equal to the intermediate frequency of the PLC (63 kHz), the second is less than it by 13 kHz (50 kHz) and the third is greater than it by 12 kHz (75 kHz). It is noticed that that the channel capacity in case of the frequency equal to 50 kHz is less than that in the case of 63 kHz. However, in the case of 75 kHz, the channel capacity values are near that in the case of the intermediate frequency due to the nature of the EMI noise amplitude with the increase of the SSM central switching frequency. Also, the channel capacity decreases with the same slope in all switching frequency cases as shown in the figure. Figure 5.25 shows channel capacity loss due to the variation of the spreading factor in the three utilized central switching frequencies.

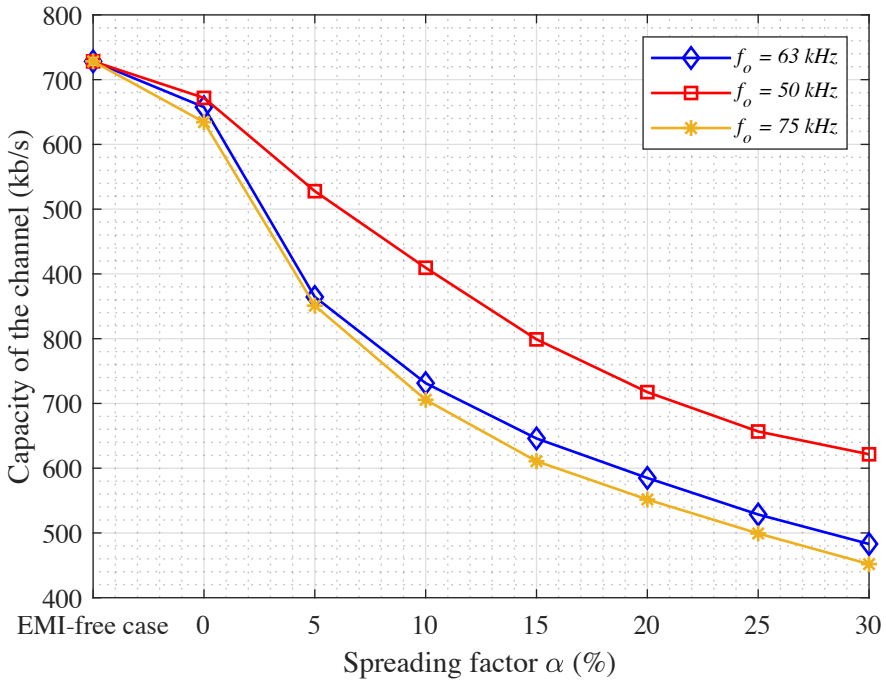

Figure 5.24: The PLC channel capacity in case of several values of spreading factor with the change of the central switching frequency of SSM.

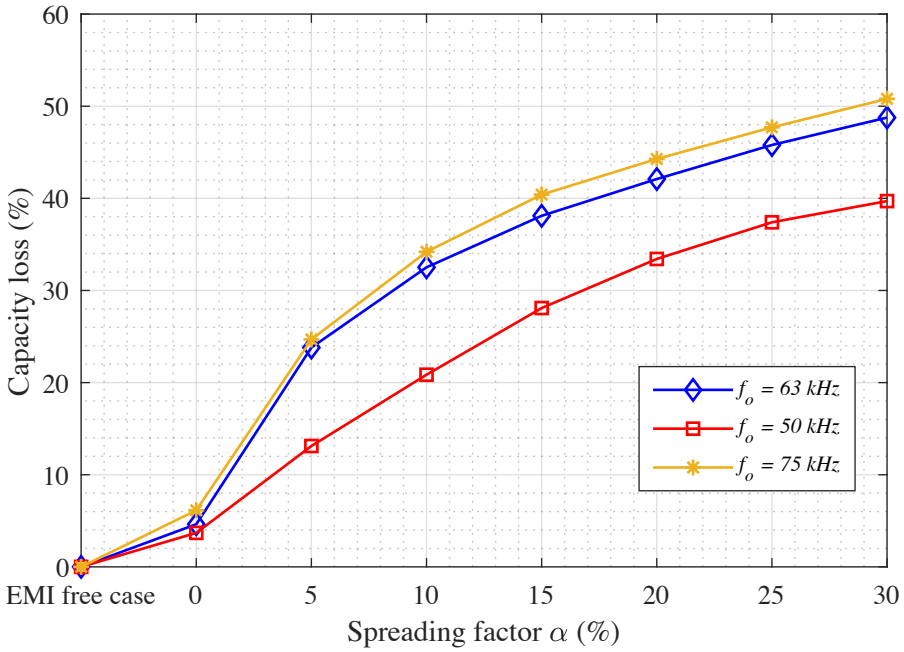

Figure 5.25: The PLC channel capacity loss in case of several values of spreading factor with the change of the central switching frequency of SSM

a) Coupling through Mutual coupling between cables

Due to the mutual coupling path between both circuits, the effect of the converter appears in the PLC system performance. In this case, the SSM setting follows the parameters in Table 5.3 The measured spectra for different values of α are shown in Figure 5.26. These were measured at the PLC side, i.e. at point 1 in Figure 5.9. It can be seen that increasing values of α give lower peak amplitudes and an increased spreading effect for the signal power.
The highest probability of erroneous data transmission appears in the case of α = 25 %. This effect is contradictory to the conventional assumption: "when applying spread spectrum techniques EMI is being mitigated". Figure 5.27 shows the impact of the converter modulation on the PLC signal and it reveals that the FER percentage increase with increasing α.

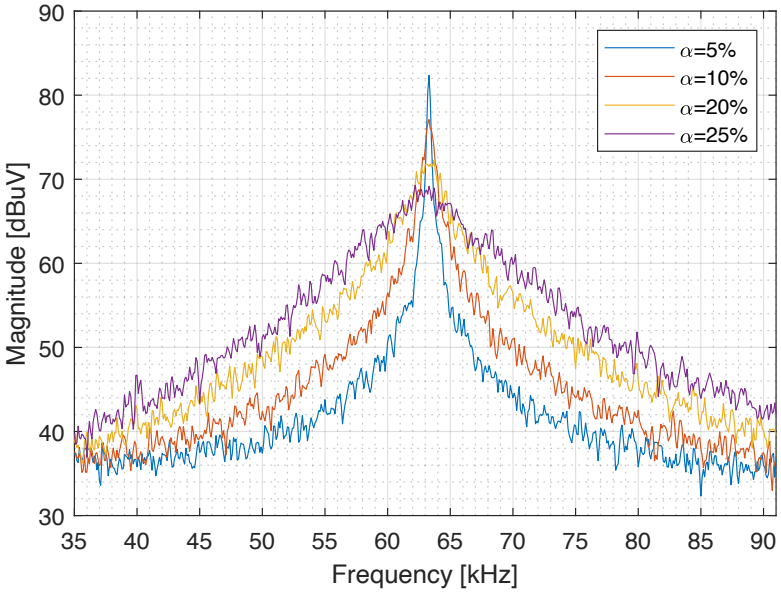

Figure 5.26: The spectrum of the measured voltage at the PLC circuit side in case of different spreading factor α values and no PLC signal.

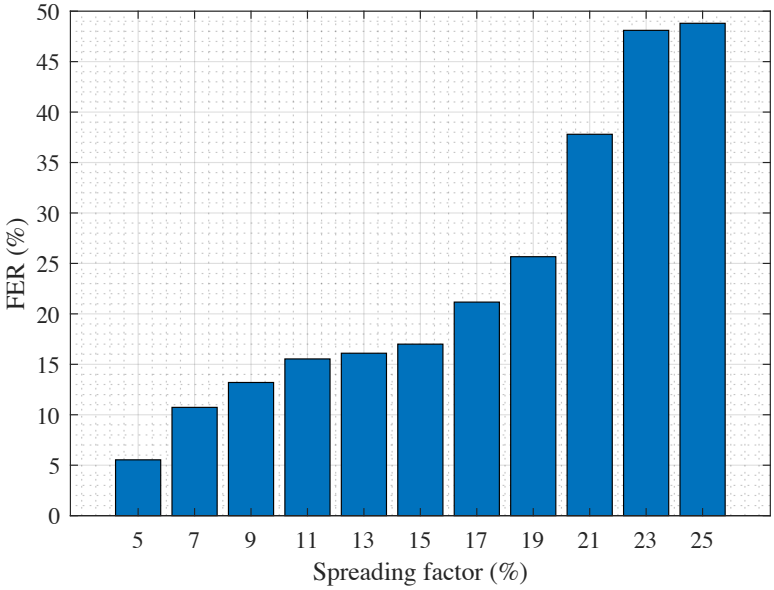

Figure 5.27: FER vs Spreading factor

Figure 5.28 shows the capacity of the PLC channel after applying equation (3.7) for the measured power spectral density of each spreading factor ranging from 0 % to 25 %, the results show that the channel capacity value decreases with increasing α in the randomized signal. The channel data loss percentage can be calculated as shown in Figure 5.28 based on equation (3.9).
Even if the channel capacity (in the 700 kbps range) is just an upper bound of the achievable bit rate and the actual G3-PLC and PRIME rate is significantly lower (in the order of 100 kbs), thus revealing a clear correlation between theoretical capacity loss and empirical error rate related to the adoption of SSM.

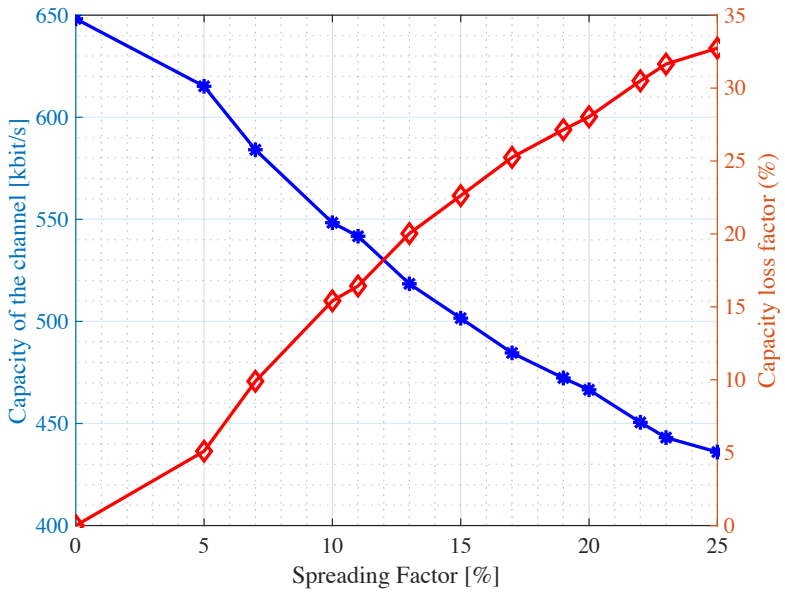

Figure 5.28: The capacity of the channel and capacity loss percentage.

Also, the same test of changing the central switching frequency was implemented to several frequencies and shows the same behavior as in the other coupling circuit. Figure 5.29 shows the FER with the variation of the central main frequency ranging from 50 kHz to 75 kHz, in case of spreading factor equal to 17%. The highest probability of FER appears around the intermediate frequency of the G3-PLC (63 kHz) and it decreases as the frequency goes far away from the intermediate frequency of the G3-PLC. Moreover, the same behavior was noticed on the other spreading factor values.

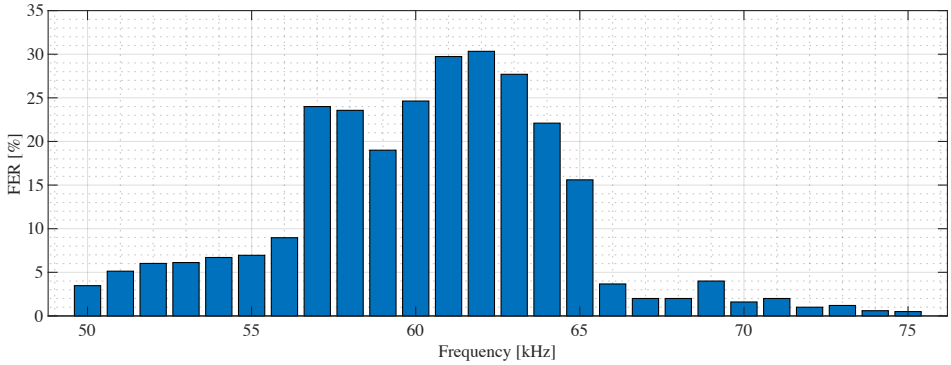

Figure 5.29: The FER percentage vs the variation in the main switching frequency values around the intermediate frequency of the G3-PLC bandwidth.

For higher values of spreading factor α over the 0.25, the FER percentage start to decrease gradually till it reach the lowest values at α=0.6. Figure 5.30 shows the FER (%) with the change of the spreading factor (α).The FER increases with increasing values of α, until α is equal to 0.25, in which case it reaches the maxim value of 62%. In contrast, in the case of $\alpha > 0.25$, the FER decreases gradually till it reaches almost 1% for α values greater than 0.45. This emphasizes that not only the amplitude of the noise affects the communication system performance but also there are other factors like the EMI modulation depth and the EMI main frequency selectivity.

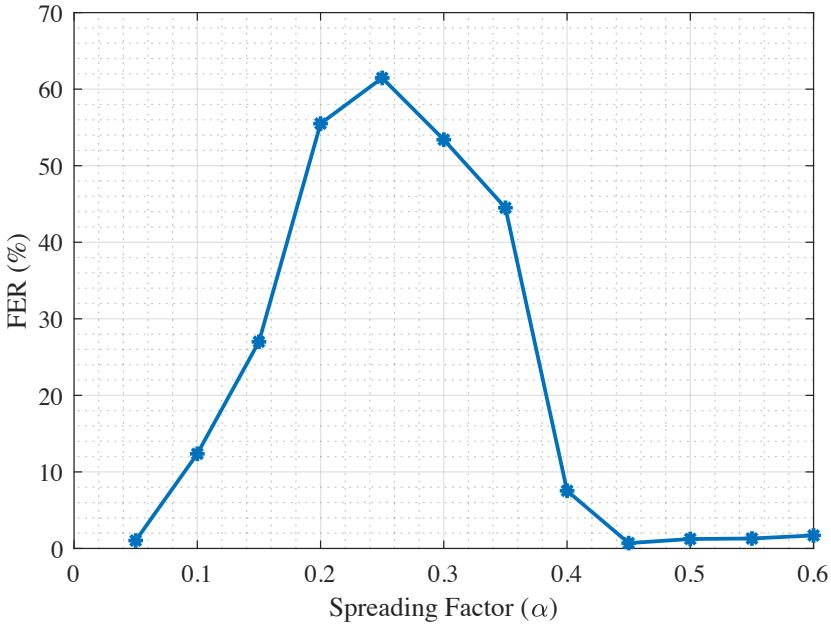

Figure 5.30: The FER Vs Spreading Factor at the intermediate frequency of the PLC channel.

The explanation for the results can be expressed based on the shape of the EMI noise signal [53]. Assuming a communication signal of bandwidth B_T and interfere with an EMI noise signal work with spread spectrum modulation of bandwidth B_{ss}. Moreover, the noise signal's main frequency is equal to the intermediate frequency of the communication channel. Similar to the case happens in the case of changing the central switching frequency in the previous coupling circuit, we have two operating scenarios: the noise signal spectrum is Fully overlapped or Partially overlapped with the communication spectrum.

In the case of a fully overlapped signal with the communication band, the ratio between the EMI noise bandwidth and the communication channel bandwidth is greater than one ($B_T/B_{ss} > 1$) as shown in Figure 5.31a, the spreading factor α was still less than 0.25. Consequently, the FER percentage increase as the distance between $B_{T_{min}}$ and $B_{SS_{min}}$ decrease, as well as the distance between $B_{T_{max}}$ and $B_{SS_{max}}$. The FER percentage reaches its maximum value when $B_T = B_{ss}$. Otherwise, when the spreading factor (α) is greater than 0.25, the bandwidth of the SS modulation signal B_{ss} was greater than the communication bandwidth B_T, the ratio between them was less than 1 ($B_T/B_{ss} < 1$), in this case, the noise signal was partially overlapped with the communication band spectrum. Respectively, with the increase of the value of α, the distance between the $B_{T_{min}}$ and $B_{SS_{min}}$ starts to increase again, as well as, the distance between the $B_{T_{max}}$ and $B_{SS_{max}}$, the FER percentage starts to decrease gradually with the increase of modulation depth as shown in Figure 5.31b.

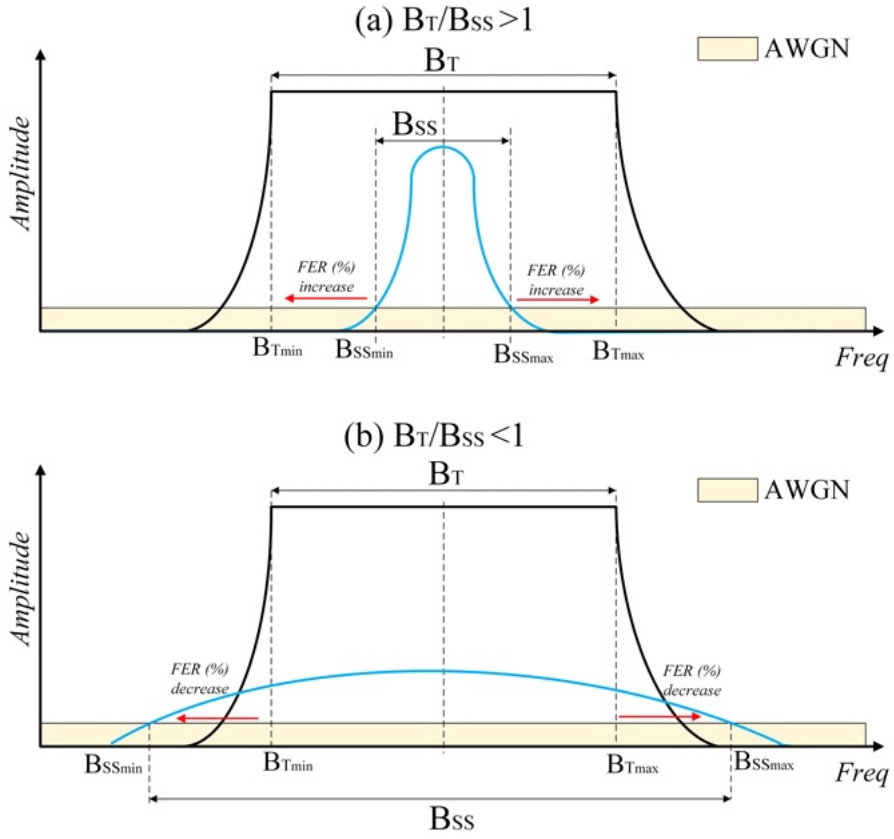

Figure 5.31: Sketch describes the overlapping between the EMI noise generated from the SS modulation with the G3-PLC spectrum in the case of a) full overlapping and b) partial overlapping.

5.7.2. Changing driving signal profile and frequency

Another factor that affects the shape of the SSM is the driving signal profile, consequently, it has an impact on the G3-PLC. Moreover, the frequency of the driving signal (f_m) has its effect on the SSM shape and can be adjusted by changing the sampling frequency (f_s) of the utilized driving signal. Generally speaking, the driving signal $\varepsilon(\tau)$ consist of a certain number of points k that form their shape, which could be represented in the form of a lookup table for the utilized driving signal. In our setup, we considered 100 points to create the driving signal ranging from -0.5 to 0.5 with a sampling time T_s between every two consecutive points. Thus, in this operating scenario, the SSM follows the settings stated in Table 5.5. The coupling circuit is through the artificial EMI parasitic capacitance discussed in Section 5.3.1.

Table 5.4: Buck converter electrical data 2.

Item	Value
The central switching frequency	63 kHz
Duty cycle	50%
Driving signal $\varepsilon(\tau)$	PAM, Sawtooth, and Sinewave
Driving signal frequency f_m	Varies from 0.3 to 600 Hz
Spreading factor (α)	15%

a) The EMI spectrum measurements

Figure 5.32 shows the voltage spectrum of the spread spectrum modulated EMI measured from the PLC side in Figure 5.6. The measurements show the spectrum of the SSM in case of using three types of driving signal patterns used in the setup at a frequency f_m of 30 Hz.

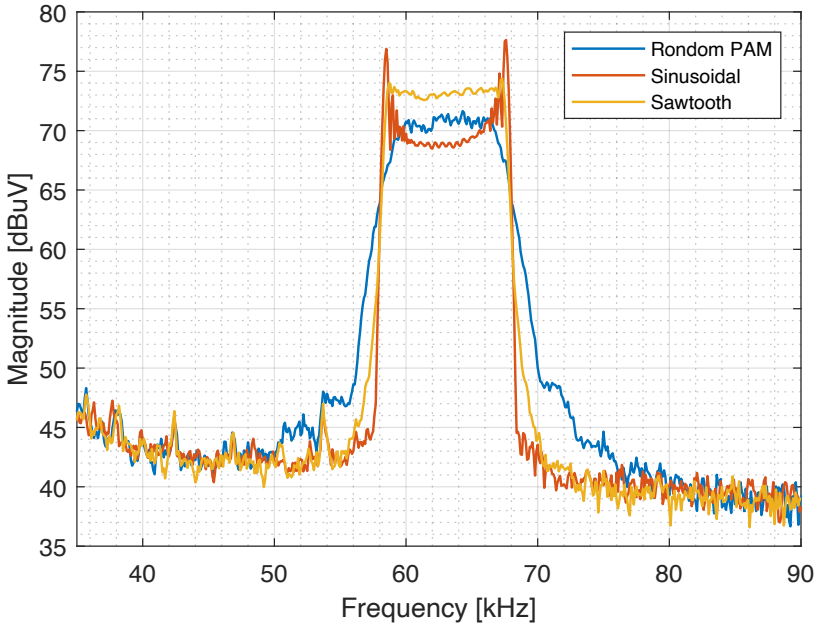

Figure 5.32: The voltage spectrum for SSM EMI utilizing various shapes of driving signal.

To see the difference between each pattern, Figure 5.33 shows the 2D spectrogram of the three driving signals types utilized in the test at spreading factor of 15% and driving signal frequency of 0.3 Hz. consequently, the switching frequency will change with very slow rate and the signal will appears similar to the normal conventional modulation. Similar to the results from the simulation in Section 4.2.2, the random PAM modulation had a lower impact on the performance of the G3-PLC, as the amplitude of the EMI is the lowest. However, the results will show different behavior. Figures 5.34, 5.35, and 5.36 show the voltage spectrum of the SSM EMI utilizing the PAM, sawtooth, and sine wave driving signals respectively, in the case of using different driving signal frequencies. The QP detector was used with IFBW = 200 Hz.

Following equations (2.7) and (2.14) in Chapter 2, the normalized frequency resolution ρ is calculated to be equal to 0.02 as the RBW used is 200 Hz and the bandwidth of the SSM Δf used is 63000 $\times$ 0.15 = 9450. On the other hand, the modulation index β is calculated based on the frequency of the driving signal f_m. Consequently, the peak value of the spectrum varies with the change of the modulation index at a normalized frequency resolution ρ = 0.02.
Figure 5.37 shows the peak magnitude of the SSM noises measured from the PLC side in the case of using different driving signals with various values of β at ρ = 0.02 and α = 0.15. The results confirms the results presented in simulation results on Figure 4.21, at which there is an optimum value of β for which maximum EMI reduction is achieved.

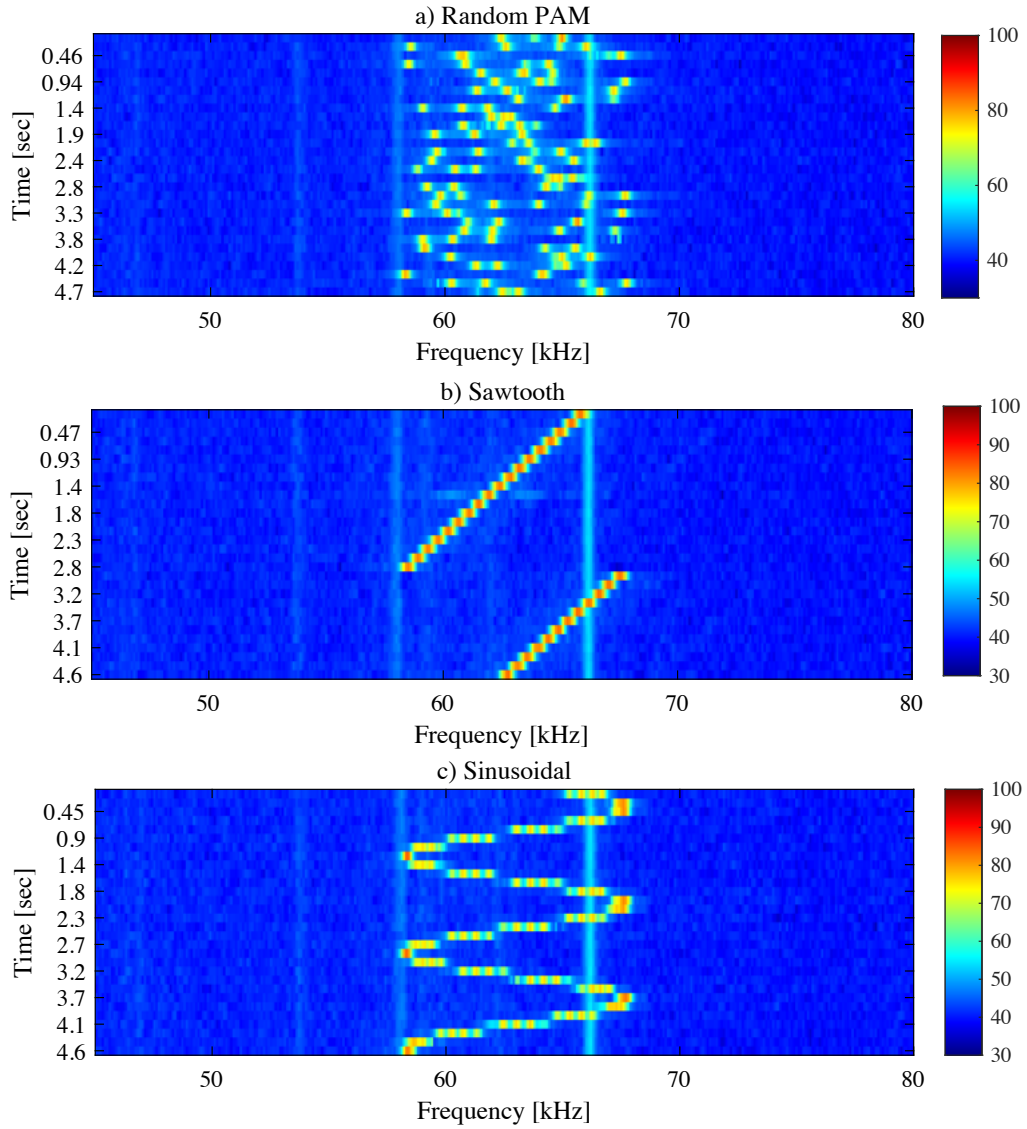

Figure 5.33: The voltage spectrogram for SSM EMI utilizing various shapes of driving signal.

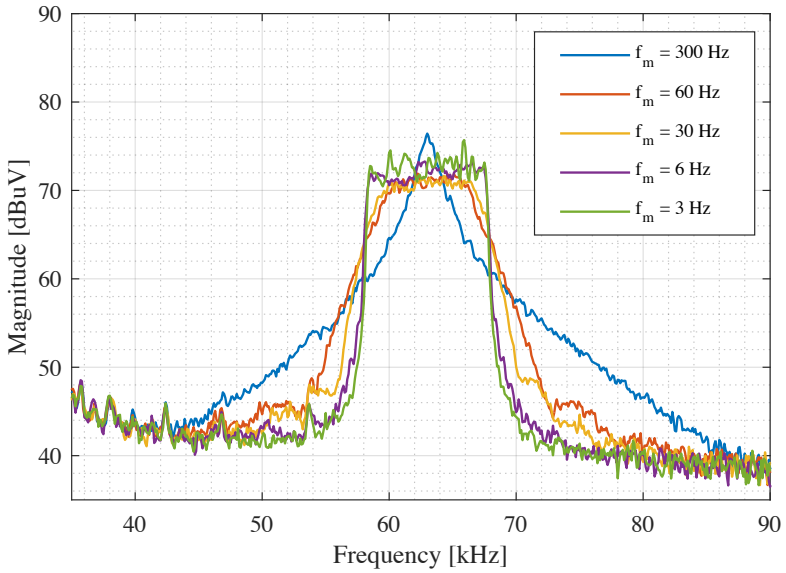

Figure 5.34: The voltage spectrum for PAM SSM utilizes various driving signal frequencies.

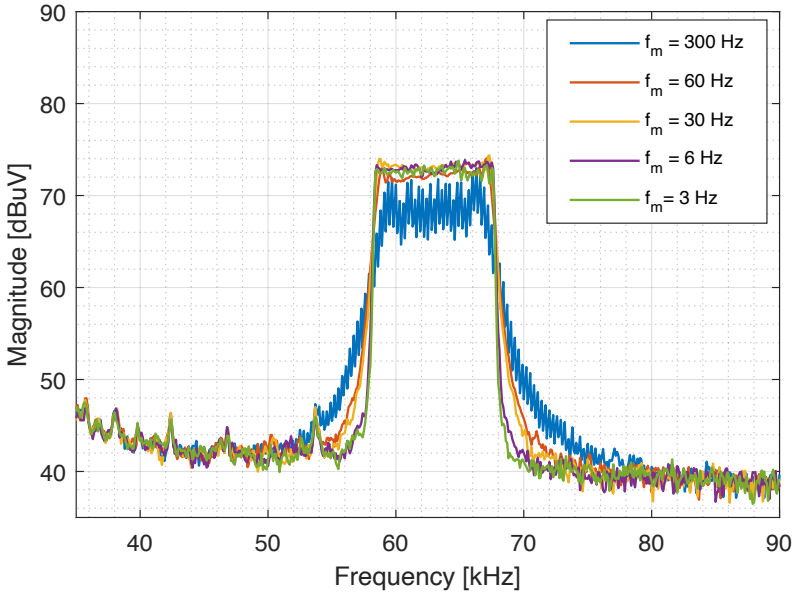

Figure 5.35: The voltage spectrum for sawtooth SSM utilizes various driving signal frequencies.

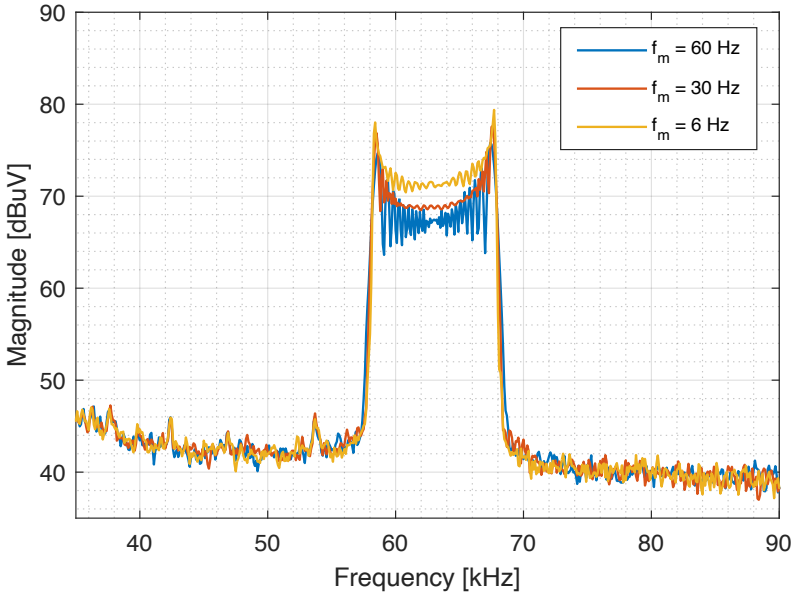

Figure 5.36: The voltage spectrum for sine wave SSM utilizes various driving signal frequencies.

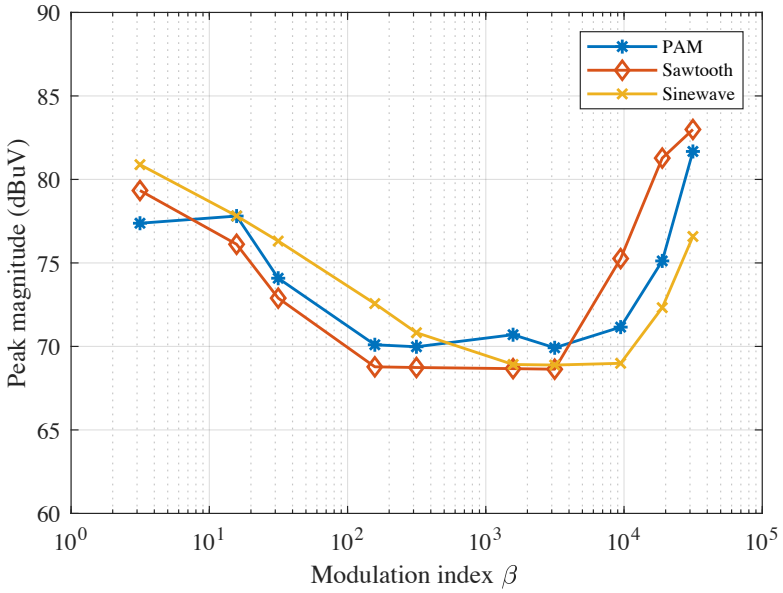

Figure 5.37: The spectrum peak amplitude of the SSM utilizes various modulation index β values , using the AV detector with IFBW = 200 Hz.

b) The PLC performance in the presence of EMI

In this section, the G3-PLC channel performance is evaluated in terms of the FER percentage. Figure 5.38, 5.39, 5.40, 5.41, 5.42, and 5.43 show the FER percentage using various spreading factors and driving signal frequency values in the case of the three utilized driving signals in our setup, respectively. Figure 5.38 shows a 3D surf plot for the FER percentage in case of varying both the spreading factor and the driving signal frequency for the random PAM signal. Moreover, a Heat map is added to show the worst cases of FER percentage in the given conditions as shown in Figure 5.39. It was noticed that the highest values of FER percentage appear when the spreading factor is in the range of 10% to 35% and the driving signal frequency is between 1Hz and 300 Hz. So, the FER percentage increase exponentially with f_m, till FER reaches the maximum value at f_m between 6 and 60 Hz, after that, the FER starts to decrease gradually with the increase of f_m as shown in Figure 5.38 and Figure 5.39.

Figure 5.40 shows a 3D surf plot for the FER percentage in case of varying both the spreading factor and the driving signal frequency for the Sawtooth signal. Moreover, a Heat map is added to show the worst cases of FER percentage in the given conditions as shown in Figure 5.41. In the case of $\alpha < 30\%$, the FER increases gradually with the increase of the driving signal frequency used till the FER reaches a maximum value at $f_m = 30Hz$ and maintain at this level till 600 Hz. In the case of $\alpha > 30\%$, the FER increases gradually with the increase of the driving signal frequency used till the FER reaches a maximum value at $f_m = 30Hz$, after that, it decreases dramatically to the lowest values as shown in Figure 5.40 and Figure 5.41. It was noticed that the highest values of FER percentage appear when the spreading factor is in the range of 10% to 35% and the driving signal frequency is between 30 Hz and 600 Hz.

Figure 5.42 shows a 3D surf plot for the FER percentage in case of varying both the spreading factor and the driving signal frequency for the Sinusoidal signal. Moreover, a Heat map is added to show the worst cases of FER percentage in the given conditions as shown in Figure 5.43. In the case of $\alpha < 25\%$, the FER increases gradually with the increase of the driving signal frequency used till the FER reaches a maximum value at $f_m = 6Hz$ and maintain at this level till 600 Hz. In the case of $\alpha > 25\%$, the FER increases gradually with the increase of the driving signal frequency used till the FER reaches a maximum value at $f_m = 6Hz$, after that, it decreases dramatically to the lowest values as shown in Figure 5.42 and Figure 5.43. Furthermore, the FER percentage values in the case of the sinusoidal signal are lower than that in the sawtooth and the random PAM ones.

Generally speaking, we can divide the driving signals into two types: non-periodical (uniform pseudo-random) and periodical (Sawtooth and sinusoidal). The relation between the FER percentage and the f_m is not linear as well as the relation with the spreading factor α. The reason for this high FER in this region is that the frequency f_m of the driving signal used is near to the sub carrier frequency used by the OFDM in the PLC channel. In addition, the FER percentage in the case of the PAM signal is higher than that in the other two cases.

In conclusion, these results are contradictory to the conventional assumption: "when applying spread spectrum techniques EMI is being mitigated". From the EMC standards point of view, the best performance for the PLC channel should be when the f_m is between 6 Hz and 60 Hz (β is in the range of 100 and 3000 at $\alpha = 0.15$ as indicated in Figure 5.34). However, the higher percentage of FER excites specifically in this range of driving signal frequency f_m.

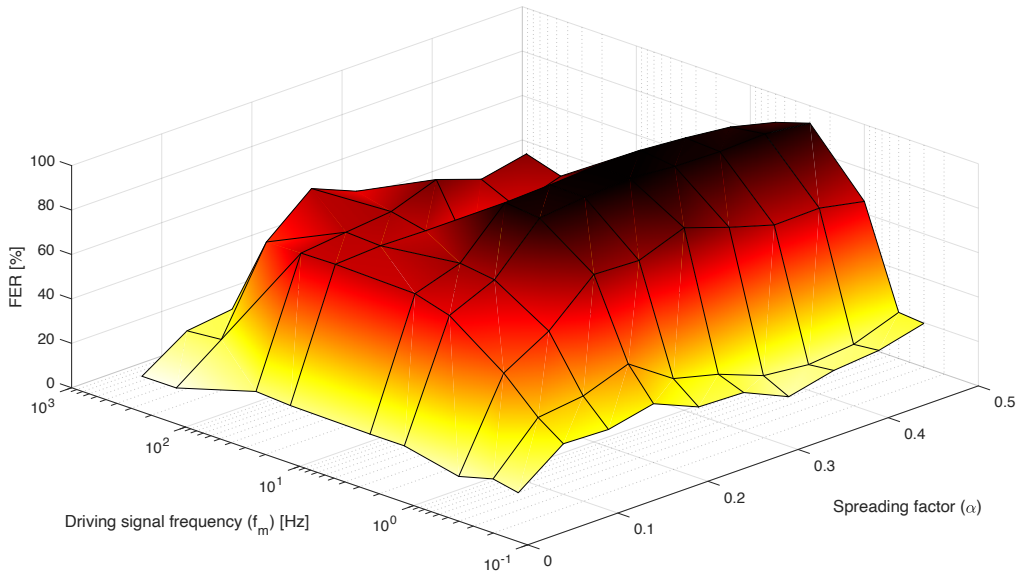

Figure 5.38: A 3D surf plot shows the FER percentage with various values of spreading factor α and driving signal frequency f_m in the case of using the random PAM signal.

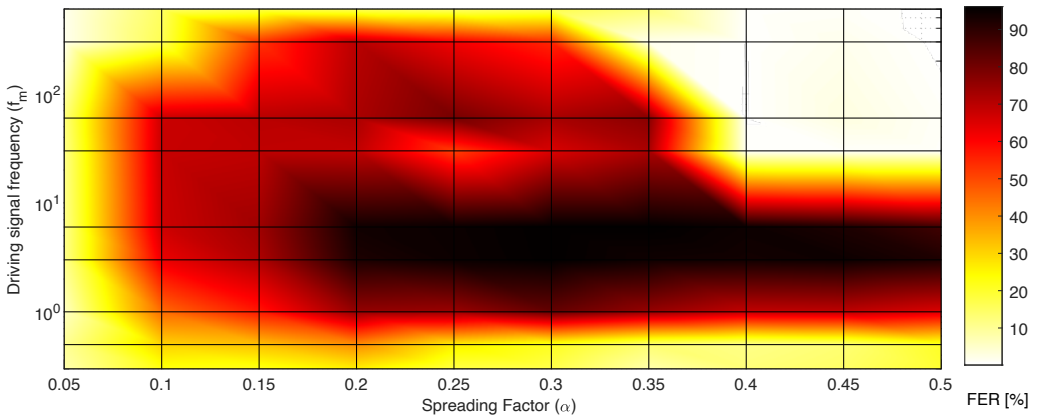

Figure 5.39: A heat map shows the FER percentage with various values of spreading factor α and driving signal frequency f_m in the case of using the random PAM signal.

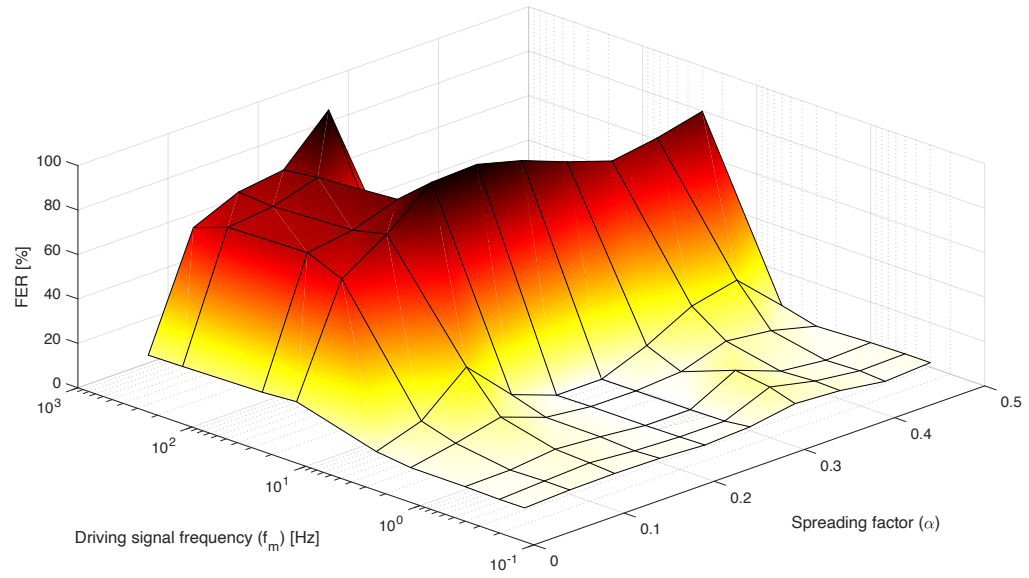

Figure 5.40: A 3D surf plot shows the FER percentage with various values of spreading factor α and driving signal frequency f_m in the case of using the sawtooth signal.

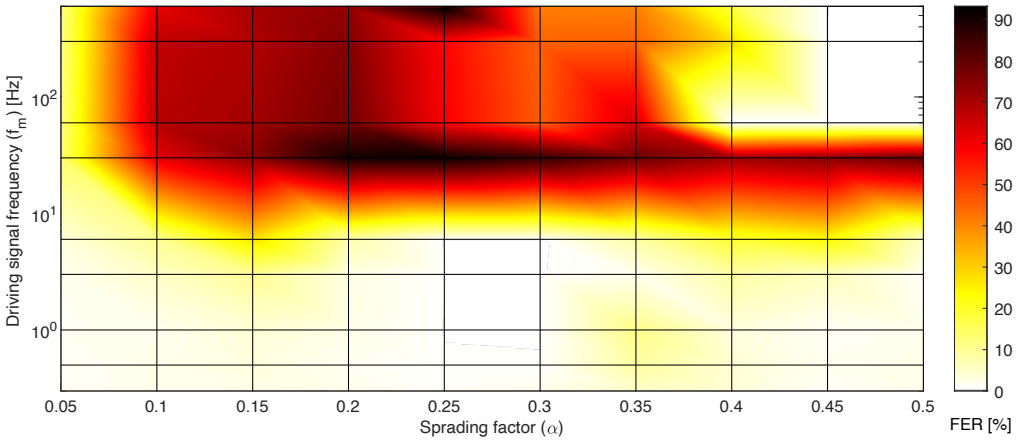

Figure 5.41: A heat map shows the FER percentage with various values of spreading factor α and driving signal frequency f_m in the case of using the sawtooth signal.

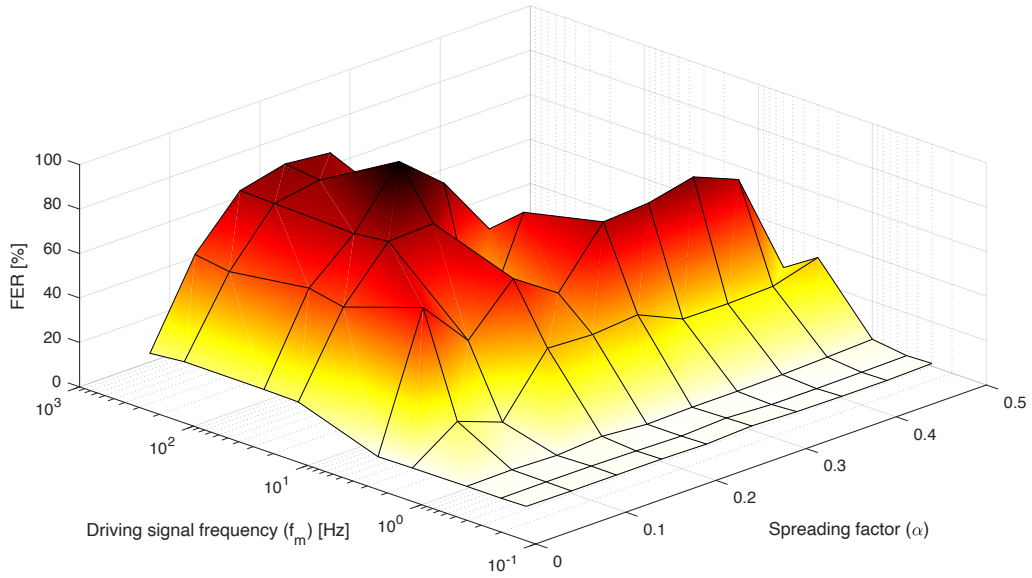

Figure 5.42: A 3D surf plot shows the FER percentage with various values of spreading factor α and driving signal frequency f_m in the case of using the sinusoidal signal.

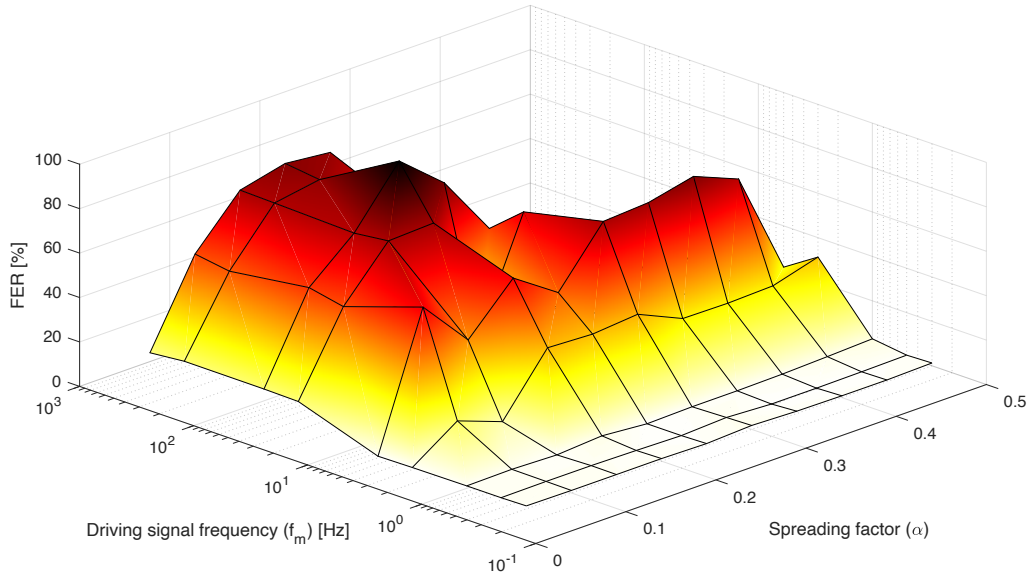

Figure 5.43: A heat map shows the FER percentage with various values of spreading factor α and driving signal frequency f_m in the case of using the sinusoidal signal.

c) Statistical analysis

To describe the relationship between the FER percentage and the parameters of the SS modulations, another interesting analysis could be done which is calculating the correlation coefficient between the collected data from the setup. The Pearson's correlation coefficient is the most common tool used to analyze the linearity between the parameters. Given that we need to calculate the correlation between two variables, the Pearson's correlation coefficient could be represented as:

$$r_{x,y} = \frac{\sum_{i=1}^{n}(x_i - \hat{x})(y_i - \hat{y})}{\sqrt{\sum_{i=1}^{n}(x_i - \hat{x})^2}\sqrt{\sum_{i=1}^{n}(y_i - \hat{y})^2}}, \tag{5.4}$$

where: n is the total sample size.
x_i and y_i are the individual sample point index with i.
$\hat{x}$ and $\hat{y}$ are the sample's mean values.

Based on the above equation, we can calculate the correlation factor between the results we have. The first correlation calculations were implemented between the output FER percentage measured in every driving signal profile, consequently, there are three sets of data: the first for the random PAM, the second is for the sawtooth signal and the third is for the sinusoidal signal. Table 5.6 show the correlation matrix results from the IBM SPSS software. The results show that there is a big correlation between the FER data measured in the case of using a sinusoidal signal and the sawtooth one, the correlation is significant at almost 0.6. This high correlation existed between these two data sets as both driving signals are periodical signals, so, they have a comparable impact on the communication channel performance. Thus, this means that any other periodical shape will have a close impact on the case of the sawtooth and sinewave.

On the other hand, the correlation between the FER results from using the PAM signal and the other two periodical signals is very low, the correlation between the FER in the case of PAM and the FER in the case of the sawtooth is 0.009, which is not significant. Moreover, the correlation between the FER in the case of PAM and the FER in the case of the sinusoidal signal is significant at 0.306, which is still also a small value of correlation. This confirms that the effect of the non-periodical driving signals on the communication channel performance differs from the periodical ones.

Another correlation could be calculated between the driving signal frequency and the output FER per each spreading factor in the chosen driving signal profile as shown in Table 5.6. In the case of using the random PAM, the relationship between the driving signal frequency and the FER at a given spreading factor show negative correlation values, which decreases gradually with the increase of the spreading factor. On the contrary, the situation is different in the case of sawtooth and sinewave signals, the correlation factor is positively high in the case of spreading factor less than 25%. However, it becomes negatively low in the case of a spreading factor more than 25%. This means that in the case of $\alpha < 25\%$, the probability of high FER increases linearly with the increases in the driving signal frequency f_m. Indeed, this explains numerically what is shown in Figures 5.40 and 5.42.

Table 5.5: Correlation matrix between the data set measured in the three used driving signals

		FER in PAM	FER in Saw	FER in Sin
FER in PAM	Pearson Correlation	1	.009	.306
FER in Saw	Pearson Correlation	.009	1	.306
FER in Sin	Pearson Correlation	.306	.597	1

Table 5.6: Correlation matrix between FER measured in the three used driving signals

Signal Frequency	Correlations in the case of the random PAM signal									
	Spreading factor	5	10	15	20	25	30	35	40	45	50
	Pearson Correlation	-.77	-.60	-.49	-.51	-.43	-.45	-.51	-.43	-.44	-.48
	Correlations in the case of the Sawtooth signal									
	Pearson Correlation	.55	.60	.59	.55	.66	.36	.31	.09	-.23	-.17
	Correlations in the case of the Sinusoidal signal									
	Pearson Correlation	.58	.53	.53	.48	.65	-.38	-.30	-.25	-.11	-.30

d) The Shannon Hartley channel capacity evaluation

The above results were confirmed by the Shannon-Hartley equation. Figure 5.44 shows the behavior of the channel capacity with the increase of the driving signal frequency at a constant spreading factor of 15%. It is noticed that the channel capacity decreases with the increase of the driving signal frequency, following the same behavior of the FER analysis, especially in the lower values of driving signal frequency. Moreover, the channel capacity equation represents efficiently the behavior of the channel in the case of the periodical and non-periodical signals. In contrast, it fails to represent the behavior of the channel in the case of the high sampling frequency non-periodical random PAM signal (f_m higher than 60 Hz). Figure 5.45 shows the channel capacity loss percentage with the sampling frequency of the driving signal.

5.8. Summary

In this chapter, the influence of the spread-spectrum modulated EMI on the G3-PLC performance was addressed in different operating conditions and spread-spectrum settings. In addition, two coupling circuits are considered in these tests. Finally , the results were analyzed by the Shannon-Hartley equation to show the PLC channel capacity in the presence of EMI generated from different SSM settings.

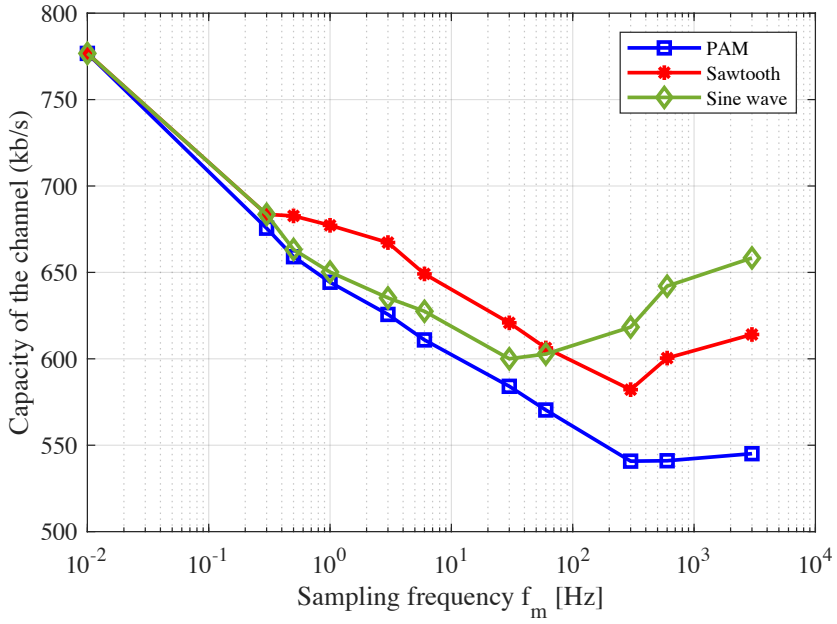

Figure 5.44: The channel capacity vs the driving signal frequency at constant $\alpha = 15\%$.

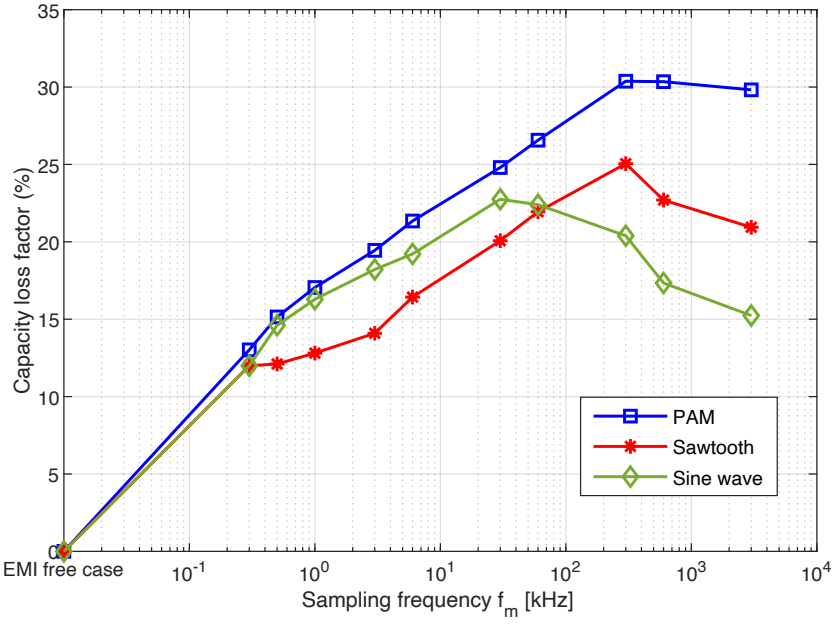

Figure 5.45: The channel capacity loss vs the driving signal frequency at constant$\alpha = 15\%$.

Chapter 6

Conclusions and directions for further research

6.1. Conclusions

6.1.1. Chapter 2

The different types of spread-spectrum modulation (SSM) techniques were discussed in this chapter. The purpose of these techniques is to mitigate the generated power converter's EMI. There are four main basic types of SSM in total — RCFMFD, RCFMVD, RPWM, and RPPM. Consequently, each technique works to randomise a certain or several parameter/s in the utilised PWM. The SSM technique could randomise the switching frequency or the duty cycle, or the phase shift of the signal. As a result, in all cases, the power of the signal is decreased according to the modulation spreading depth settings to fulfil the standards.
The RCFMFD was chosen for implementation in this thesis as it is widely used in several applications. As a result, the shape of the measured spectrum from the converter could be controlled by changing the used switching frequency and sampling time at a constant duty cycle. To be precise, three parameters control the switching frequency change — (1) the spreading factor; (2) the driving signal profile, and; (3) the driving signal frequency. The higher values of the spreading factor decrease the amplitude of the emissions, however, it could cause a lot of voltage ripple on the output voltage. Thus, there is an optimum value for the spreading factor at which the required mitigation will be achieved with an acceptable value voltage ripple. The increase in the driving signal frequency will make the signal appear smoother, especially in the case of using the PAM signal. On the other hand, the setting of the EMI receiver in the measurements plays an important role in the output measurements. To put in perspective, the shape of the spectrum will depend on the chosen RBW of the EMI receiver and the chosen SSM bandwidth (Carson's band).

6.1.2. Chapter 3

In this chapter, the operation of the PLC system in the presence of EMI was discussed. Like any other communication system, the PLC system requires a transmitter, channel, and receiver. Most of the PLC systems utilised in the smart grid systems work with the OFDM modulation to provide more robustness to the system. As the PLC systems channel the existing power cables, the PLC signal could be distorted by the interference generated from the residential loads connected to the grid, or from the power converters utilised in renewable energy sources and battery charger systems. Thus, a lot of studies were conducted to show the influence of the nonlinear loads such as lamps and switched-mode power supplies on the PLC systems. On the other hand, some research shows the influence of power converters' modulation on the performance of several PLC systems. From these studies, we concluded that:

- The EMI mitigation solutions to enhance the communication performance could be divided into hardware and software approaches.

- The influence of the converter modulation on the communication systems is not the same throughout all the communication protocols.
- There are several protocols used in the PLC systems. The most commonly used in smart metering are the PRIME and G3 PLC systems, which is why they selected and discussed in detail in this chapter.

6.1.3. Chapter 4

In this chapter, the influence of the SS modulated EMI on the performance of the G3-PLC systems was simulated in several operating conditions. The Matlab/Simulink software was used. Two circuits were considered in the simulation, the first is the DC buck converter as the source of the EMI, and the second circuit is the G3-PLC circuit which is considered the EMI victim. Moreover, both circuits were linked to each other by parasitic capacitance to mimic a real parasitic EMI coupling.

The SS modulation used here is the RCFMCFD, which is the one discussed in detail in Chapter 2. Thus, the influence of SS parameter settings on the PLC channel performance was considered in the simulation. The first parameter was the spreading factor that controls the bandwidth of the given SSM used. The results show that the increase in the SSM bandwidth lowers the performance of the communication channel, despite the EMI mitigation provided by the used SSM technique. The second parameter is the driving signal used to change the switching frequency with time. Hence, three driving signal profiles were considered. As a result, the G3-PLC channel performance was better when using non-periodic signals than in the case of the periodic ones. In addition, the G3-PLC channel performance was entirely analysed by the BER calculation of all the considered operating scenarios. Moreover, the behaviour of the channel in the presence of the EMI was confirmed by the Shannon Hartley equation in all the operating scenarios.

6.1.4. Chapter 5

The practical implementation of the thesis is introduced in this chapter. The results confirm the simulation results introduced in chapter 4. In general, the increase in the amplitude of the circuit EMI delivers more problems to the PLC channel. Also, the main switching frequency of the converter plays an important role in the results. The tests show that more problems appear in the G3-PLC systems when the power converter's main switching frequency is near to the intermediate frequency of the communication system utilised.

On the other hand, the shape of the spread-spectrum modulation used could be changed using three parameters. The first parameter that hardly affects the G3-PLC performance is the spreading factor of the EMI noise, the results show that despite the common interpretation of SS techniques in mitigating EMI, SS may interfere more severely with a communication system. The highest probability of FER appears when the communication bandwidth is equal to the SS noise signal bandwidth; in this case, the spreading factor α is equal to 0.25. Moreover, the FER percentage decreases as the borders of the SS noise signal drive turn away from the communication bandwidth borders.

The second parameter that affects the G3-PLC performance is the driving signal profile type, whether it is periodical or non-periodical. In this case, the results are hardly connected to the third parameter, which is the sampling rate of the driving signal. Thus, the results compared the behaviour of the PLC channel in terms of both (second and third) parameters together. Moreover, two analyses were used to evaluate the behaviour of the PLC communication system in the presence of SS modulated — statistical analysis and the Shannon Hartley equation. The statistical analysis is implemented using IBM SPSS software for calculating the correlation factor between the data set taken in various operating conditions. The study revealed that the random PAM in general (which is a non-periodic signal), provides the communication systems with higher FER in all the operating conditions than in the periodical ones like sawtooth and sinusoidal signals. In addition, the FER data set generated in the case of the Sawtooth signal is analogous to that of the sinusoidal signal, the correlation coefficient reaches 0.6. On the other hand, the correlation between the FER results from using the PAM signal and the other two

periodic signals is very low. This confirms that the effect of the non-periodic driving signals on the communication channel performance differs from the periodic ones.

Also, the statistical results show that the linearity between the FER results and the driving signal frequency is very high in the case of α lower than 25%. However, the linearity decreases as the α becomes higher than 25%. Finally, the behaviour of the channel in the presence of the EMI was confirmed by the Shannon Hartley equation.
Conclusively, the study revealed that the spread-spectrum technique is not usually a good choice for mitigating the EMI in the used circuit, however, it is a trade-off between the maximum allowable amplitude provided by the SSM and the FER results from the communication channel. General speaking, we can use the SSM to provide an acceptable EMI mitigation, as well as, provide an acceptable communication channel performance under certain conditions. These conditions could be summarised as follows:

- Choose a switching frequency far from the intermediate frequency of the communication system.
- Choosing a driving signal sampling frequency (f_s) far from the subcarrier frequency of the communication system.

Based on the presented theoretical analyses as well as experimental results the thesis has been proved.

6.2. Directions for further research

The results from this thesis point to several interesting directions for future work.
Firstly, address the effect of utilising different types of spread-spectrum techniques on the communication system performance rather than the one considered in this research work. As stated in the literature in Chapter 2, spread-spectrum modulation approaches like the RPPM, RPWM, or RCFMVD could be considered in the future. Consequently, every technique could have a different influence on the communication systems. As a result, an optimization technique could be implemented as a guide for engineers to choose the best spread-spectrum technique settings, which would not influence the communication systems and provide the required mitigation for the EMC standards compliance tests. Moreover, in this thesis we only considered the effect of the buck converter as the simplest EMI noise signal, however, different types of DC converters or AC converters could be placed under study to evaluate their effect on the communication systems in various applications.

Secondly, consider different types of communication systems and study their performance in the presence of noise. In general, any communication system utilising the OFDM like the G3-PLC should behave in the same way. However, there are different considerable configurations in every communication system that could change the behaviour of the channel in the presence of EMI disturbances as shown in Chapter 3.

Third, the thesis has focused on the influence of the conducted EMI on the communication systems in the low frequency ranges between 9 - 150 kHz, notably, the communication systems could behave differently in the high-frequency ranges.

Finally, the study could be applied to a real practical smart metering system already installed. In this case, the complexity of the system will be high and the effect of aggregated conducted emissions should be considered, as several EMI sources will influence the communication systems in general.

Bibliography

[1] D. Roggo et al., “Electromagnetic interferences in smart grid applications: A case study with power line communication smart meters and PV energy generation,” *CIRED - Open Access Proc. J.*, vol. 2017, no. 1, pp. 607–611, 2017.

[2] A. Hebala, W. Wafik, Walid.M.A.Ghoneim, and Hamdy A. Ashour, “Experimental Analysis of a Prototype Low Speed PMSG Unit With Different Loading Conditions,” in *2018 Twentieth International Middle East Power Systems Conference (MEPCON)*, Cairo University, Egypt, 2018, pp. 1134–1139.

[3] J. Meyer et al., “Overview and Classification of Interferences in the Frequency Range 2-150 kHz (Supraharmonics),” in SPEEDAM 2018 - Proceedings: International Symposium on Power Electronics, Electrical Drives, Automation and Motion, 2018, pp. 165–170.

[4] S. K. Rönnberg et al., “On waveform distortion in the frequency range of 2 kHz–150 kHz—Review and research challenges,” *Electr. Power Syst. Res.*, vol. 150, pp. 1–10, 2017.

[5] CENELEC SC 205A, “Study report II, electromagnetic interference between electrical equipment/systems in the frequency range below 150 kHz, SC 205A/Sec0339/R,” 2013.

[6] J. Matanza, S. Alexandres, and C. Rodriguez-Morcillo, “Performance evaluation of two narrowband PLC systems: PRIME and G3,” Comput. Stand. Interfaces, vol. 36, no. 1, pp. 198–208, 2013.

[7] R. Smolenski, J. Bojarski, A. Kempski, and P. Lezynski, “Time-Domain-Based Assessment of Data Transmission Error Probability in Smart Grids With Electromagnetic Interference,” IEEE Trans. Ind. Electron., vol. 61, no. 4, pp. 1882–1890, 2014.

[8] W. E. Sayed, H. Loschi, C. L. Lok, P. Lezynski and R. Smolenski, "Prospective Analysis of the effect of Silicon based and Silicon-Carbide based Converter on G3 Power Line Communication,", *2020 International Symposium on Electromagnetic Compatibility - EMC EUROPE*, 2020, pp. 1-6,
doi: 10.1109/EMCEUROPE48519.2020.9245727.

[9] W. E. Sayed, H. Loschi, M. A. Wibisono, N. Moonerr, P. Lezynski and R. Smolenski, "The Influence of Spread-Spectrum Modulation on the G3-PLC Performance", *2021 Asia-Pacific International Symposium on Electromagnetic Compatibility (APEMC)*, 2021, pp. 1-4,
doi: 10.1109/APEMC49932.2021.9597060.

[10] H. Loschi, R. Smolenski, P. Lezynski, D. Nascimento, and G. Demidova, “Aggregated conducted electromagnetic interference generated by DC/DC converters with deterministic and random modulation,” Energies, vol. 13, no. 14, 2020.

[11] F. Tounquet and C. Alaton, “Benchmarking Smart Metering Deployment in EU-28,” European Commission, no. December. p. 142, 2019.

[12] Sayed, W.E.; Lezynski, P.; Smolenski, R.; Madi, A.; Pazera, M.; Kempski, A. "Deterministic vs. Random Modulated Interference on G3 Power Line Communication", *Energies 2021*, 14, 3257.
https://doi.org/10.3390/en14113257

[13] Sayed, W.E.; Lezynski, P.; Smolenski, R.; Moonen, N.; Crovetti, P.; Thomas, D.W.P. "The Effect of EMI Generated from Spread-Spectrum-Modulated SiC-Based Buck Converter on the G3-PLC Channel", *Electronics 2021*, 10, 1416.
https://doi.org/10.3390/electronics10121416

[14] W. El Sayed, P. Crovetti, N. Moonen, P. Lezynski, R. Smolenski and F. Leferink, "Electromagnetic Interference of Spread-Spectrum Modulated Power Converters in G3-PLC Power Line Communication Systems," in *IEEE Letters on Electromagnetic Compatibility Practice and Applications*, vol. 3, no. 4, pp. 118-122, Dec. 2021,
doi: 10.1109/LEMCPA.2021.3121091.

[15] D. T. Hoang, P. Wang, D. Niyato, and E. Hossain, "Charging and discharging of plug-in electric vehicles (PEVs) in vehicle-to-grid (V2G) systems: A cyber insurance-based model," *IEEE Access*, vol. 5, pp. 732–754, 2017.

[16] K. Bernacki, D. Wybrańczyk, M. Zygmanowski, A. Latko, J. Michalak, and Z. Rymarski, "Disturbance and signal filter for power line communication," *Electronics.*, vol. 8, no. 4, 2019.

[17] K. Y. See, P. L. So, and A. Kamarul, "Feasibility study of adding a common-mode choke in PLC modem for EMI suppression," IEEE Trans. Power Deliv., vol. 22, no. 4, pp. 2136–2141, 2007.

[18] K. Vechalapu, S. Bhattacharya, E. Van Brunt, S. H. Ryu, D. Grider, and J. W. Palmour, "Comparative Evaluation of 15-kV SiC MOSFET and 15-kV SiC IGBT for Medium-Voltage Converter under the Same dv/dt Conditions," IEEE J. Emerg. Sel. Top. Power Electron., vol. 5, no. 1, pp. 469–489, 2017.

[19] S. Ji, Z. Zhang, and F. Wang, "Overview of high voltage sic power semiconductor devices: development and application," CES Trans. Electr. Mach. Syst., vol. 1, no. 3, pp. 254–264, 2020.

[20] L. Zhang, X. Yuan, X. Wu, C. Shi, J. Zhang, and Y. Zhang, "Performance Evaluation of High-Power SiC MOSFET Modules in Comparison to Si IGBT Modules," IEEE Trans. Power Electron., vol. 34, no. 2, pp. 1181–1196, 2019.

[21] X. Li et al., "Switching Loss Model of SiC MOSFET Promoting High Frequency Applications," in Proceedings of the International Symposium on Power Semiconductor Devices and ICs, 2019, vol. 2019-May, no. 2017, pp. 231–234.

[22] Y. Xie, C. Chen, Z. Huang, T. Liu, Y. Kang, and F. Luo, "High Frequency Conducted EMI Investigation on Packaging and Modulation for a SiC-Based High Frequency Converter," IEEE J. Emerg. Sel. Top. Power Electron., vol. 7, no. 3, pp. 1789–1804, 2019.

[23] V. Adrian, J. S. Chang, B. Gwee, and S. Tedjaseputro, "Spectral Analysis of Randomized Switching Frequency Modulation Scheme with a Triangular Distribution for DC-DC Converters," in 2009 International Conference on Computing, Engineering and Information, 2009, pp. 0–3.

[24] K. Cui, V. Adrian, Y. Sun, B. Gwee, and J. S. Chang, "A Low-Harmonics Low-Noise Randomized Modulation Scheme for Multi-Phase DC-DC Converters," in 15th IEEE International New Circuits and Systems Conference (NEWCAS), 2017, pp. 165–168.

[25] H. Loschi, P. Lezynski, R. Smolenski, D. Nascimento, and W. Sleszynski, "FPGA-Based System for Electromagnetic Interference Evaluation in Random Modulated DC / DC Converters," Energies 2020, vol. 13, no. 2389, pp. 1–14, 2020.

[26] Y. Lai, Y. Chang, and B.-Y. Chen, "Novel Random-Switching PWM Technique With Constant Sampling Frequency and Constant Inductor Average Current for Digitally Controlled Converter," IEEE Trans. Ind. Electron., vol. 60, no. 8, pp. 3126–3135, 2013.

[27] A. Knitter, J. ŁUszcz, and P. J. Chrzan, "Conducted EMI mitigation in switched mode DC-DC converters by spread spectrum techniques," Electr. Power Qulity Utlisation, vol. 2005, no. 2, pp. 166–171, 2005.

[28] R. Wang, Z. Lin, J. Du, J. Wu, and X. He, "Direct Sequence Spread Spectrum-Based PWM Strategy for Harmonic Reduction and Communication," IEEE Trans. Power Electron., vol. 32, no. 6, pp. 4455–4465, 2017.

[29] A. Bendicks, S. Frei, N. Hees, and M. Wiegand, "Systematic Reduction of Peak and Average Emissions of Power Electronic Converters by the Application of Spread Spectrum," IEEE Trans. Electromagn. Compat., vol. 60, no. 5, pp. 1571–1580, 2018.

[30] H. Park, M. Kim, and J.-H. Jung, "Spread-Spectrum Technique Employing Phase-Shift Modulation to Reduce EM Noise for Parallel–Series LLC Resonant Converter," IEEE TRANSACTIONS ON POWER ELECTRONICS, vol. 34, no. 2, pp. 1026–1031, 2019.

[31] H. P. Park, M. Kim, and J. H. Jung, "Spread spectrum technique to reduce EMI emission for an LLC resonant converter using a hybrid modulation method," IEEE Trans. Power Electron., vol. 33, no. 5, pp. 3717–3721, 2018.

[32] J. Chen, D. Jiang, W. Sun, Z. Shen, and Y. Zhang, "A Family of Spread-Spectrum Modulation Schemes Based on Distribution Characteristics to Reduce Conducted EMI for Power Electronics Converters," IEEE Trans. Ind. Appl., vol. 56, no. 5, pp. 5142–5157, 2020.

[33] R. Mukherjee, A. Patra, and S. Banerjee, "Impact of a frequency modulated pulsewidth modulation (PWM) switching converter on the input power system quality," IEEE Trans. Power Electron., vol. 25, no. 6, pp. 1450–1459, 2010.

[34] H. G. Li, W. Y. Cai, and S. Di Gong, "Chaotic spread spectrum for EMI reduction in DC-DC converter," in 2017 IEEE 6th Asia-Pacific Conference on Antennas and Propagation, APCAP 2017 - Proceeding, 2018, no. 2, pp. 1–3.

[35] S. Callegari, R. Rovatti, and G. Setti, "Spectral properties of chaos-based FM signals: Theory and simulation results," IEEE Trans. Circuits Syst. I Fundam. Theory Appl., vol. 50, no. 1, pp. 3–15, 2003.

[36] F. Pareschi, G. Setti, R. Rovatti, and G. Frattini, "Practical optimization of EMI reduction in spread spectrum clock generators with application to switching DC/DC converters," IEEE Trans. Power Electron., vol. 29, no. 9, pp. 4646–4657, 2014.

[37] F. Pareschi, G. Setti, R. Rovatti, and G. Frattini, "Short-term optimized spread spectrum clock generator for EMI reduction in switching DC/DC converters," IEEE Trans. Circuits Syst. I Regul. Pap., vol. 61, no. 10, pp. 3044–3053, 2014.

[38] H. Jing, Z. Weiying, and L. Jinhong, "Study on improving EMC of APFC converter with chaotic spread-spectrum technique," in Proceedings of 2017 IEEE 2nd Advanced Information Technology, Electronic and Automation Control Conference, IAEAC 2017, 2017, pp. 433–437.

[39] A. Peyghambari, A. Dastfan, and A. Ahmadyfard, "Selective Voltage Noise Cancellation in Three-Phase Inverter Using Random SVPWM," IEEE Trans. Power Electron., vol. 31, no. 6, pp. 4604–4610, 2016.

[40] Moon.C, Chen.C, and Lee.W, "A Random Modulation Spread-Spectrum Digital PWM for a Low System Clock Digital Buck Converter," IEEE Access, vol. 9, pp. 156663–156671, 2021.

[41] D. Chariag and L. Sbita, "Implementation of different randomized PWM schemes using Atmega328p microcontroller for EMI reduction in boost converter," Electr. Eng., vol. 102, no. 2, pp. 1063–1071, 2020.

[42] K. Cui, V. Adrian, B. H. Gwee, and J. S. Chang, "A Noise-Shaped Randomized Modulation for Switched-Mode DC-DC Converters," IEEE Trans. Circuits Syst. I Regul. Pap., vol. 65, no. 1, pp. 394–405, 2018.

[43] V. Adrian, J. S. Chang, and B. H. Gwee, "A randomized wrapped-around pulse position modulation scheme for dc-dc converters," IEEE Trans. Circuits Syst. I Regul. Pap., vol. 57, no. 9, pp. 2320–2333, 2010.

[44] Y. C. Lim, Y. G. Jung, J. G. Kim, S. Y. Oh, and S. Y. Oh, "A Two-Phase Separately Randomized Pulse Position PWM (SRP-PWM) Scheme with Low Switching Noise Characteristics Over the Entire Modulation Index," IEEE Trans. Power Electron., vol. 27, no. 1, pp. 362–369, 2012.

[45] A. Boudouda, N. Boudjerda, K. El Khamlichi Drissi, and K. Kerroum, "Combined random space vector modulation for a variable speed drive using induction motor," Electr. Eng., vol. 98, no. 1, pp. 1–15, 2016.

[46] M. Yu, M. Shi, W. Hu, and L. Yi, "FPGA-Based Dual-Pulse Anti-Interference Lidar System Using Digital Chaotic Pulse Position Modulation," IEEE PHOTONICS Technol. Lett., vol. 33, no. 15, pp. 757–760, 2021.

[47] K. Lee, G. Shen, W. Yao, and Z. Lu, "Performance Characterization of Random Pulse Width Modulation Algorithms in Industrial and Commercial Adjustable-Speed Drives," IEEE Trans. Ind. Appl., vol. 53, no. 2, pp. 1078–1087, 2017.

[48] A. A. K. Khan and M. Divya, "Random modulation schemes for industrial drives," in 2017 International Conference on Nascent Technologies in Engineering, ICNTE 2017 - Proceedings, 2017.

[49] A. M. Trzynadlowski et al., "Random Pulse Width Modulation Techniques for Converter-Fed Drive Systems-A Review," IEEE Trans. Ind. Appl., vol. 30, no. 5, pp. 1166–1175, 1994.

[50] K. S. Kim, Y. G. Jung, and Y. C. Lim, "A new hybrid random PWM scheme," IEEE Trans. Power Electron., vol. 24, no. 1, pp. 192–200, 2009.

[51] R. Gamoudi, D. E. Chariag, and L. Sbita, "A Review of Spread-Spectrum-Based PWM Techniques - A Novel Fast Digital Implementation," IEEE Trans. Power Electron., vol. 33, no. 12, pp. 10292–10307, 2018.

[52] F. Pareschi, R. Rovatti, and G. Setti, "EMI reduction via spread spectrum in DC/DC converters: State of the art, optimization, and tradeoffs," IEEE Access, vol. 3, pp. 2857–2874, 2015.

[53] F. Musolino and P. S. Crovetti, "Interference of Spread-Spectrum Modulated Disturbances on Digital Communication Channels," IEEE Access, vol. 7, pp. 158969–158980, 2019.

[54] F. Lin and D. Y. Chen, "Reduction of Power Supply EMI Emission by Switching Frequency Modulation," IEEE Trans. Power Electron., vol. 9, no. 1, pp. 132–137, 1994.

[55] J. M. Giron-Sierra, C. Insaurralde, M. Seminario, J. F. Jiménez, and P. Klose, "CANbus-based distributed fuel system with smart components," IEEE Trans. Aerosp. Electron. Syst., vol. 44, no. 3, pp. 897–912, 2008.

[56] J. Bojarski, R. Smolenski, P. Lezynski, and Z. Sadowski, "Diophantine equation based model of data transmission errors caused by interference generated by DC-DC converters with deterministic modulation," Bull. POLISH Acad. Sci. Tech. Sci., vol. 64, no. 3, pp. 575–580, 2016.

[57] K. Kilani, V. Degardin, P. Laly, M. Lienard, and P. Degauque, "Impulsive noise generated by a pulse width modulation inverter: Modeling and impact on powerline communication," ISPLC 2013 - 2013 IEEE 17th Int. Symp. Power Line Commun. Its Appl. Proc., pp. 75–79, 2013.

[58] M. Korki, N. Hosseinzadeh, and T. Moazzeni, "Performance Evaluation of a Narrowband Power Line Communication for Smart Grid with Noise Reduction Technique," IEEE Trans. Consum. Electron., vol. 57, no. 4, pp. 1598–1606, 2011.

[59] L. Di Bert, P. Caldera, D. Schwingshackl, and A. M. Tonello, "On Noise Modeling for Power Line Communications," in 2011 IEEE International Symposium on Power Line Communications and Its Applications On, 2011, pp. 283–288.

[60] J. Bojarski, R. Smolenski, A. Kempski, and P. Lezynski, "Pearson's random walk approach to evaluating interference generated by a group of converters," Appl. Math. Comput., vol. 219, no. 12, pp. 6437–6444, 2013.

[61] P. Pakonen, S. Vehmasvaara, M. Pikkarainen, B. A. Siddiqui, and P. Verho, "Experiences on narrowband powerline communication of automated meter reading systems in Finland," in PQ 2012: 8th International Conference - 2012 Electric Power Quality and Supply Reliability, Conference Proceedings, 2012, pp. 291–296.

[62] A. S. De Beer, A. Emleh, H. C. Ferreira, and A. J. H. Vinck, "Effects of LED lamps on the power-line communications channel," in ISPLC 2013 - 2013 IEEE 17th International Symposium on Power Line Communications and Its Applications, Proceedings, 2013, pp. 209–213.

[63] A. Emleh, A. S. De Beer, H. C. Ferreira, and A. J. H. Vinck, "The impact of the CFL lamps on the power-line communications channel," in ISPLC 2013 - 2013 IEEE 17th International Symposium on Power Line Communications and Its Applications, Proceedings, 2013, pp. 225–229.

[64] A. Emleh, A. S. De Beer, H. C. Ferreira, and A. Han Vinck, "Noise generated by modern lamps and the influence on the smart-grid communication network," in 2015 IEEE International Conference on Smart Grid Communications, SmartGridComm 2015, 2016, pp. 7–12.

[65] A. Emleh, A. S. D. Beer, H. C. Ferreira, and A. J. H. Vinck, "On mercury vapor lamps and their effect on the smart-grid plc channel," in 2015 IEEE International Workshop on Applied Measurements for Power Systems, AMPS 2015 - Proceedings, 2015.

[66] A. Emleh, A. S. De Beer, H. C. Ferreira, and A. J. Han Vinck, "The influence of fluorescent lamps with electronic ballast on the low voltage PLC network," in Proceedings of the 2014 IEEE 8th International Power Engineering and Optimization Conference, PEOCO 2014, 2014, no. March, pp. 276–280.

[67] P. A. J. Van Rensburg, A. J. Snyders, and H. C. Ferreira, "Modeling of Coupling Diversity for Extra-Low-Voltage Power-Line Communication Networked LED Lighting in Smart Buildings," IEEE J. Emerg. Sel. Top. Power Electron., vol. 6, no. 3, pp. 1224–1234, 2018.

[68] R. Smolenski, J. Bojarski, A. Kempski, and P. Lezynski, "Time-Domain-Based Assessment of Data Transmission Error Probability in Smart Grids With Electromagnetic Interference," IEEE Trans. Ind. Electron., vol. 61, no. 4, pp. 1882–1890, 2014.

[69] L. Fumagalli, E. Dstribuzione, G. Borgone, E. Dstribuzione, G. Faggioni, and E. Dstribuzione, "ELVIS (Enel Low Voltage Identification System): Improving narrowband PLC communication performance by means of electrical characteristics measurement of distribution line," in Int. Conf. on Electricity Distribution, 2015, no. June, pp. 15–18.

[70] Y. M. Hwang, J. H. Jung, J. K. Seo, J. J. Lee, and J. Y. Kim, "Energy-Efficient Transmission Strategy With Dynamic Load for Power Line Communications," IEEE Trans. Smart Grid, vol. 9, no. 3, pp. 2382–2390, 2018.

[71] N. Papandreou and T. Antonakopoulos, "Resource allocation management for indoor power-line communications systems," IEEE Trans. Power Deliv., vol. 22, no. 2, pp. 893–903, 2007.

[72] F. Fayad, D. Bardouil, F. Gauthier, A. Zeddam, and M. Tlich, "A denoising method for electromagnetic disturbances on PLC systems," in Proceedings of EMC Europe 2011 York - 10th International Symposium on Electromagnetic Compatibility, 2011, pp. 634–639.

[73] S. Aghajeri and H. Shafiee, "Synchronization in OFDM powerline communication systems in presence of narrowband interferences," in Proceedings - 7th International Symposium on Signal Processing and Its Applications, ISSPA 2003, 2003, vol. 2, pp. 359–362.

[74] Y. Sun and T. Pratt, "Narrowband plc simo-based interference suppression with zero-forcing," IEEE Trans. Power Deliv., vol. 28, no. 4, pp. 2022–2029, 2013.

[75] S. Bolognani, L. Peretti, L. Sgarbossa, and M. Zigliotto, "Improvements in power line communication reliability for electric drives by random PWM techniques," in IECON Proceedings (Industrial Electronics Conference), 2006, pp. 2307–2312.

[76] B. Auinger, B. Deutschmann, and G. Winkler, "Elimination of electromagnetic interference in communication channels by using spread spectrum techniques," in 2017 International Symposium on Electromagnetic Compatibility - EMC EUROPE 2017, EMC Europe 2017, 2017.

[77] P. S. Crovetti and F. Musolino, "Interference of Spread-Spectrum EMI and Digital Data Links under Narrowband Resonant Coupling," Electronics, vol. 6, no. 90, pp. 1–18, 2020.

[78] F. Musolino and P. S. Crovetti, "Interference of Spread-Spectrum Switching-Mode Power Converters and Low-Frequency Digital Lines," in 2018 IEEE International Symposium on Circuits and Systems (ISCAS), 2018, p. 5.

[79] P. Lezynski, R. Smolenski, H. Loschi, D. Thomas, and N. Moonen, "A novel method for EMI evaluation in random modulated power electronic converters," Measurement, vol. 151, no. 107098, p. 9, 2020.

[80] J. Bojarski, R. Smolenski, P. Lezynski, and Z. Sadowski, "Diophantine equation based model of data transmission errors caused by interference generated by DC-DC converters with deterministic modulation," BULLETIN OF THE POLISH ACADEMY OF SCIENCES TECHNICAL SCIENCES, vol. 64, no. 3, pp. 575–580, 2016, doi: 10.1515/bpasts-2016-0064.

[81] C. Cano, A. Pittolo, D. Malone, L. Lampe, A. M. Tonello, and A. Dabak, "State-of-the-art in Power Line Communications : from the Applications to the Medium," IEEE J. Sel. Areas Commun., vol. 8716, no. c, pp. 1–19, 2016.

[82] I. Fernandez et al., "Characterization of non-intentional emissions from distributed energy resources up to 500 kHz : A case study in Spain," Int. J. Electr. Power Energy Syst., vol. 105, no. April 2018, pp. 549–563, 2019.

[83] M. Schwarz and F. Gronwald, "EMI analysis of a generic power line communication OFDM data link," in Proceedings of EMC Europe 2011 York - 10th International Symposium on Electromagnetic Compatibility, 2011, pp. 625–628.

[84] A. Llano, I. Angulo, P. Angueira, T. Arzuaga, and D. De Vega, "Analysis of the Channel Influence to Power Line Communications Based on ITU-T G . 9904 (PRIME)," Energies 2016, vol. 9, no. 39, pp. 1–16, 2016.

[85] H. J. Choi and J. H. Jung, "Enhanced Power Line Communication Strategy for DC Microgrids Using Switching Frequency Modulation of Power Converters," IEEE Trans. Power Electron., vol. 32, no. 6, pp. 4140–4144, 2017.

Appendix A

Appendix A

A.1. Simulation Codes

A.1.1. Spectrum analyzer plotting

```
1
2  Fs=15000000;
3  resolutonReqd = 200;
4  % Calculate number of FFT points (NFFT)
5  % fs/NFFT = resolutionReqd
6  NFFT = Fs/ resolutonReqd;
7
8  % Set overlap to 0
9  overlap = 0;
10
11 [pxx1,f] = pwelch(dm1,rectwin(NFFT),overlap,NFFT,Fs);
12 dbuV1 = 10*log10(pxx1/1e-3)+107;
13
14 [pxx2,f] = pwelch(dm2,rectwin(NFFT),overlap,NFFT,Fs);
15 dbuV2 = 10*log10(pxx2/1e-3)+107;
16
17 [pxx3,f] = pwelch(dm3,rectwin(NFFT),overlap,NFFT,Fs);
18 dbuV3 = 10*log10(pxx3/1e-3)+107;
19
20 [pxx4,f] = pwelch(dm4,rectwin(NFFT),overlap,NFFT,Fs);
21 dbuV4 = 10*log10(pxx4/1e-3)+107;
22
23 [pxx5,f] = pwelch(dm5,rectwin([]),overlap,NFFT,Fs);
24 dbuV5 = 10*log10(pxx5/1e-3)+107;
25
26 [pxx6,f] = pwelch(dm6,[],[],NFFT,Fs);
27 dbuV6 = 10*log10(pxx6/1e-3)+107;
28
29
30 plot(f/1000,dbuV1)
31 hold on
32 plot(f/1000,dbuV2)
33 hold on
34 plot(f/1000,dbuV3)
35 hold on
36 plot(f/1000,dbuV4)
37 hold on
38 plot(f/1000,dbuV5)
39 hold on
```

```
plot(f/1000,dbuV6)

xlim([40 90])
xlabel('Frequency (kHz)')
ylabel('Magnitude(dBuV)')
grid
```

A.1.2. Matlab Shannon Heartley code

```

C0=0;
C1=0;
C2=0;
C3=0;
C4=0;
C5=0;
C6=0;
C7=0;
C8=0;
C9=0;
C10=0;
C11=0;
C12=0;
C13=0;
C14=0;
C15=0;
C16=0;
C17=0;
C18=0;
C19=0;
C20=0;
C21=0;
C22=0;
C23=0;
C24=0;
C25=0;
C26=0;
C27=0;
C28=0;
C29=0;
C30=0;

%the G3-PLC bandwidth
Bmin=35000;
Bmax=91000;
B = Bmax - Bmin;
% the middel frequency of all Spreaded spectrum modulation
F0=63000;
%Step frequency of measurment
df=100;

%PLC signal spectrum in dBuV
S=PLC;
%Background spectrum in dBuV
%AV
 N_0=AWGN;
% data for Random
```

```
%Spread spectrum modulation noise at K=1
%dBuV
S_EMI_1=Ran_K_1
%Spread spectrum modulation noise at K=5
%dBuV
S_EMI_2=Ran_K_5
%Spread spectrum modulation noise at K=10
%dBuV
S_EMI_3=Ran_K_10
%Spread spectrum modulation noise at K=50
%dBuV
S_EMI_4=Ran_K_50
%Spread spectrum modulation noise at K=100
%dBuV
S_EMI_5=Ran_K_100
%Spread spectrum modulation noise at K=500
%dBuV
S_EMI_6=Ran_K_500
%Spread spectrum modulation noise at K=1000
%dBuV
S_EMI_7=Ran_K_1000
%Spread spectrum modulation noise at K=3000
%dBuV
S_EMI_8=Ran_K_3000
%Spread spectrum modulation noise at K=6000
%dBuV
S_EMI_9=Ran_K_6000
%Spread spectrum modulation noise at K=10000
%dBuV
S_EMI_10=Ran_K_10000

%*****************************************************
%*****************************************************
%*****************************************************
%The results for Triangle
%Spread spectrum modulation noise at K=1
%dBuV
S_EMI_11=Saw_K_1
%Spread spectrum modulation noise at K=5
%dBuV
S_EMI_12=Saw_K_5
%Spread spectrum modulation noise at K=10
%dBuV
S_EMI_13=Saw_K_10
%Spread spectrum modulation noise at K=50
%dBuV
S_EMI_14=Saw_K_50
%Spread spectrum modulation noise at K=100
%dBuV
S_EMI_15=Saw_K_100
%Spread spectrum modulation noise at K=500
%dBuV
S_EMI_16=Saw_K_500
%Spread spectrum modulation noise at K=1000
%dBuV
S_EMI_17=Saw_K_1000
%Spread spectrum modulation noise at K=3000
%dBuV
```

```
S_EMI_18=Saw_K_3000
%Spread spectrum modulation noise at K=6000
%dBuV
S_EMI_19=Saw_K_6000
%Spread spectrum modulation noise at K=10000
%dBuV
S_EMI_20=Saw_K_10000


%*******************************************************
%*******************************************************
%*******************************************************
%The results for Sinusoidal
%Spread spectrum modulation noise at K=1
%dBuV
S_EMI_21=Sin_K_1
%Spread spectrum modulation noise at K=5
%dBuV
S_EMI_22=Sin_K_5
%Spread spectrum modulation noise at K=10
%dBuV
S_EMI_23=Sin_K_10
%Spread spectrum modulation noise at K=50
%dBuV
S_EMI_24=Sin_K_50
%Spread spectrum modulation noise at K=100
%dBuV
S_EMI_25=Sin_K_100
%Spread spectrum modulation noise at K=500
%dBuV
S_EMI_26=Sin_K_500
%Spread spectrum modulation noise at K=1000
%dBuV
S_EMI_27=Sin_K_1000
%Spread spectrum modulation noise at K=3000
%dBuV
S_EMI_28=Sin_K_3000
%Spread spectrum modulation noise at K=6000
%dBuV
S_EMI_29=Sin_K_6000
%Spread spectrum modulation noise at K=10000
%dBuV
S_EMI_30=Sin_K_10000
N_S = size(S);


%Conversion from dBuV to V
for k=1:N_S
S(k)=10^((S(k)-120-2)/20);
S_EMI1(k)=10^((S_EMI_1(k)-120-2)/20);
S_EMI2(k)=10^((S_EMI_2(k)-120-2)/20);
S_EMI3(k)=10^((S_EMI_3(k)-120-2)/20);
S_EMI4(k)=10^((S_EMI_4(k)-120)/20);
S_EMI5(k)=10^((S_EMI_5(k)-120)/20);
S_EMI6(k)=10^((S_EMI_6(k)-120)/20);
S_EMI7(k)=10^((S_EMI_7(k)-120)/20);
S_EMI8(k)=10^((S_EMI_8(k)-120)/20);
S_EMI9(k)=10^((S_EMI_9(k)-120)/20);
```

```
S_EMI10(k)=10^((S_EMI_10(k)-120-1)/20);

S_EMI11(k)=10^((S_EMI_11(k)-120+7)/20);
S_EMI12(k)=10^((S_EMI_12(k)-120)/20);
S_EMI13(k)=10^((S_EMI_13(k)-120+1.5)/20);
S_EMI14(k)=10^((S_EMI_14(k)-120)/20);
S_EMI15(k)=10^((S_EMI_15(k)-120)/20);
S_EMI16(k)=10^((S_EMI_16(k)-120-1)/20);
S_EMI17(k)=10^((S_EMI_17(k)-120-1)/20);
S_EMI18(k)=10^((S_EMI_18(k)-120)/20);
S_EMI19(k)=10^((S_EMI_19(k)-120+1.1)/20);
S_EMI20(k)=10^((S_EMI_20(k)-120+1)/20);

S_EMI21(k)=10^((S_EMI_21(k)-120-1)/20);
S_EMI22(k)=10^((S_EMI_22(k)-120)/20);
S_EMI23(k)=10^((S_EMI_23(k)-120+1)/20);
S_EMI24(k)=10^((S_EMI_24(k)-120+1.5)/20);
S_EMI25(k)=10^((S_EMI_25(k)-120+1)/20);
S_EMI26(k)=10^((S_EMI_26(k)-120)/20);
S_EMI27(k)=10^((S_EMI_27(k)-120)/20);
S_EMI28(k)=10^((S_EMI_28(k)-120)/20);
S_EMI29(k)=10^((S_EMI_29(k)-120)/20);
S_EMI30(k)=10^((S_EMI_30(k)-120-2)/20);

N0(k)=10^((N_0(k)-120)/20);
end


%Capacity calculation with direct way based on Shannon equation

 for k=1:N_S
      alpha(k)= (S(k).^2)/((N0(k)).^2);%SNR of AWGN

      SNR1(k)=S(k)^2/(S_EMI1(k)^2);
      SNR2(k)=S(k)^2/(S_EMI2(k)^2);
      SNR3(k)=S(k)^2/(S_EMI3(k)^2);
      SNR4(k)=S(k)^2/(S_EMI4(k)^2);
      SNR5(k)=S(k)^2/(S_EMI5(k)^2);
      SNR6(k)=S(k)^2/(S_EMI6(k)^2);
      SNR7(k)=S(k)^2/(S_EMI7(k)^2);
      SNR8(k)=S(k)^2/(S_EMI8(k)^2);
      SNR9(k)=S(k)^2/(S_EMI9(k)^2);
      SNR10(k)=S(k)^2/(S_EMI10(k)^2);

      SNR11(k)=S(k)^2/(S_EMI11(k)^2);
      SNR12(k)=S(k)^2/(S_EMI12(k)^2);
      SNR13(k)=S(k)^2/(S_EMI13(k)^2);
      SNR14(k)=S(k)^2/(S_EMI14(k)^2);
      SNR15(k)=S(k)^2/(S_EMI15(k)^2);
      SNR16(k)=S(k)^2/(S_EMI16(k)^2);
      SNR17(k)=S(k)^2/(S_EMI17(k)^2);
      SNR18(k)=S(k)^2/(S_EMI18(k)^2);
      SNR19(k)=S(k)^2/(S_EMI19(k)^2);
      SNR20(k)=S(k)^2/(S_EMI20(k)^2);

      SNR21(k)=S(k)^2/(S_EMI21(k)^2);
      SNR22(k)=S(k)^2/(S_EMI22(k)^2);
      SNR23(k)=S(k)^2/(S_EMI23(k)^2);
```

```
223         SNR24(k)=S(k)^2/(S_EMI24(k)^2);
224         SNR25(k)=S(k)^2/(S_EMI25(k)^2);
225         SNR26(k)=S(k)^2/(S_EMI26(k)^2);
226         SNR27(k)=S(k)^2/(S_EMI27(k)^2);
227         SNR28(k)=S(k)^2/(S_EMI28(k)^2);
228         SNR29(k)=S(k)^2/(S_EMI29(k)^2);
229         SNR30(k)=S(k)^2/(S_EMI20(k)^2);
230
231       % Capacity loss for the intersection between the PLC signal and the EMI noise
232
233         C0 = C0 + log2(1 + alpha(k))*df;% capacity loss of the AWGN
234
235         C1=C1 + log2(1 + SNR1(k))*df;
236         C2=C2 + log2(1 + SNR2(k))*df;
237         C3=C3 + log2(1 + SNR3(k))*df;
238         C4=C4 + log2(1 + SNR4(k))*df;
239         C5=C5 + log2(1 + SNR5(k))*df;
240         C6=C6 + log2(1 + SNR6(k))*df;
241         C7=C7 + log2(1 + SNR7(k))*df;
242         C8=C8 + log2(1 + SNR8(k))*df;
243         C9=C9 + log2(1 + SNR9(k))*df;
244         C10=C10 + log2(1 + SNR10(k))*df;
245
246         C11=C11 + log2(1 + SNR11(k))*df;
247         C12=C12 + log2(1 + SNR12(k))*df;
248         C13=C13 + log2(1 + SNR13(k))*df;
249         C14=C14 + log2(1 + SNR14(k))*df;
250         C15=C15 + log2(1 + SNR15(k))*df;
251         C16=C16 + log2(1 + SNR16(k))*df;
252         C17=C17 + log2(1 + SNR17(k))*df;
253         C18=C18 + log2(1 + SNR18(k))*df;
254         C19=C19 + log2(1 + SNR19(k))*df;
255         C20=C20 + log2(1 + SNR20(k))*df;
256
257         C21=C21 + log2(1 + SNR21(k))*df;
258         C22=C22 + log2(1 + SNR22(k))*df;
259         C23=C23 + log2(1 + SNR23(k))*df;
260         C24=C24 + log2(1 + SNR24(k))*df;
261         C25=C25 + log2(1 + SNR25(k))*df;
262         C26=C26 + log2(1 + SNR26(k))*df;
263         C27=C27 + log2(1 + SNR27(k))*df;
264         C28=C28 + log2(1 + SNR28(k))*df;
265         C29=C29 + log2(1 + SNR29(k))*df;
266         C30=C30 + log2(1 + SNR30(k))*df;
267   end
268
269
270
271
272
273
274
275
276     y1=(C0-C1)/C0;
277     y2=(C0-C2)/C0;
278     y3=(C0-C3)/C0;
279     y4=(C0-C4)/C0;
280     y5=(C0-C5)/C0;
```

```
    y6=(C0-C6)/C0;
    y7=(C0-C7)/C0;
    y8=(C0-C8)/C0;
    y9=(C0-C9)/C0;
    y10=(C0-C10)/C0;

    y11=(C0-C11)/C0;
    y12=(C0-C12)/C0;
    y13=(C0-C13)/C0;
    y14=(C0-C14)/C0;
    y15=(C0-C15)/C0;
    y16=(C0-C16)/C0;
    y17=(C0-C17)/C0;
    y18=(C0-C18)/C0;
    y19=(C0-C19)/C0;
    y20=(C0-C20)/C0;

    y21=(C0-C21)/C0;
    y22=(C0-C22)/C0;
    y23=(C0-C23)/C0;
    y24=(C0-C24)/C0;
    y25=(C0-C25)/C0;
    y26=(C0-C26)/C0;
    y27=(C0-C27)/C0;
    y28=(C0-C28)/C0;
    y29=(C0-C29)/C0;
    y30=(C0-C30)/C0;


 C_50V=[C1;C2;C3;C4;C5;C6;C7;C8;C9;C10;C0]/1000;
 C_100V=[C11;C12;C13;C14;C15;C16;C17;C18;C19;C20;C0]/1000;
 C_150V=[C21;C22;C23;C24;C25;C26;C27;C28;C29;C30;C0]/1000;
 y_50V=[y1;y2;y3;y4;y5;y6;y7;y8;y9;y10;0]*100;
 y_100V=[y11;y12;y13;y14;y15;y16;y17;y18;y19;y20;0]*100;
 y_150V=[y21;y22;y23;y24;y25;y26;y27;y28;y29;y30;0]*100;
 F = [300000;60000;30000;6000;3000;600;300;100;50;30;0];

figure(1);
semilogx(F,C_50V,'-','LineWidth',1.5,'Color','b');
hold on
semilogx(F,C_100V,'-','LineWidth',1.5,'Color','r');
hold on
semilogx(F,C_150V,'-','LineWidth',1.5,'Color','g');
xlabel('Sampling frequency (f_n)')
ylabel('Capacity of the channel (kbit/s)')
title('Capacity of PLC Channel')
grid on;

figure(2);
semilogx(F,y_50V,'-','LineWidth',1.5,'Color','b');
hold on
semilogx(F,y_100V,'-','LineWidth',1.5,'Color','r');
hold on
semilogx(F,y_150V,'-','LineWidth',1.5,'Color','g');
xlabel('Sampling frequency (f_n)');
ylabel('Capacity loss factor (%)')
title('Capacity Loss of PLC Channel')
grid on;
```

Appendix B

Appendix B

B.1. PLC data Sheet

PL360-EK Quick Start User Guide

Overview

PL360-EK is an evaluation kit for the PL360 modem, a multi-protocol device to implement standard and customized PLC solutions. PL360-EK includes a SAM4CMS16C ARM Cortex-M4 microcontroller, which provides a full-featured platform to develop a complete communication system over PLC technology.

Getting Started

Attention: Before starting, it is necessary to register the kit and obtain access to online resources from Microchip. Please follow the instructions in the welcome letter attached to this kit.

Power-Up

By default, the boards are configured to be supplied with 230Vac. Please verify that the mains voltage level is also 230Vac, otherwise, check the *PL360 EK User Guide* to know how to change the voltage configuration to 115Vac. Afterward, plug the power cord cable to an AC power socket.

The kit is delivered with a preprogrammed application in SAM4CMS16C Flash memory (G3-PLC PHY Tester for CENELEC-A band) which allows sending and receiving PLC messages using PHY layer. When the board is powered-up, the LCD will display some text and LEDs will show activity.

Running PHY Tester Demo

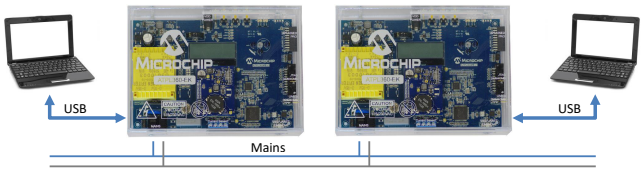

1. Download *Microchip PLC PHY Tester* from the online resources site and install it
2. Power-up PL360-EK board 1 and connect it to a PC using a micro USB cable
3. Launch the PHY Tester PC Tool, select serial port of board 1 and baud rate (230400 bps)
4. Follow on-screen instructions and configure a Tx test
5. Power-up PL360-EK board 2 and connect it to a PC using a micro USB cable
6. Launch the PHY Tester PC Tool, select serial port of board 2 and baud rate (230400 bps)
7. Follow on-screen instructions and configure an Rx test
8. Start Rx test in PL360-EK board 1
9. Start Tx test in PL360-EK board 2
10. Transmitted frames from board 2 are received in board 1

For more information about usage and configuration of the PLC PHY tester tool, please check the user manual embedded in the tool: **Help** tab > **User Manual**.

Navigating the Kit

Important: In order to explore all the features of this kit, please check the firmware user guides provided with the online contents of the EK.

Online Resources

PL360-EK is complemented with a set of online resources. To access these resources, it is necessary to register the kit as it is described in the welcome letter. These online resources include:

- Board schematics, layout and BOM of all boards included in the kit
- Last version of supported firmware stacks for power line communications
- Set of PC tools to evaluate the performance of Microchip PLC solutions

Firmware Projects

PL360-EK currently supports G3-PLC and PRIME protocols. Each firmware stack includes several projects and examples of use. For more information about the firmware projects and how to build and debug the different examples, please read the appropriate documentation provided with the online contents of the kit:

- *G3-PLC Firmware Stack*
- *PRIME 1.3 FW Stack for Service Nodes* and *PRIME 1.3 FW Stack for Base Nodes*
- *PRIME 1.4 FW Stack for Service Nodes* and *PRIME 1.4 FW Stack for Base Nodes*

Tools

Some of the projects included in the firmware release require a PC application:

- G3-PLC/PRIME Manager PC tool: enables users to easily interface with the highest layer of the provided PLC stacks
- PHY Tester tool: provides users with complete access to PHY layer configuration. Excellent tool for point-to-point tests
- PHY Sniffer: captures, analyzes and displays PLC traffic. Excellent tool for network supervision and debugging

For more information about the tools read the documentation of the firmware stack.

Coupling Boards

Coupling boards are a set of easily interchangeable boards, each one designed to achieve optimal performance in a specific band of transmission. PL360-EK includes two coupling boards:

- PLCOUP006, designed to communicate in the frequency band between 151 and 471 kHz
- PLCOUP007, designed to communicate in the band between 35 and 91 kHz (CENELEC-A)

To communicate in a frequency band, PL360-EK requires the appropriate coupling board and firmware configuration. For more information about the coupling boards, read the *PL360-EK User Guide*.

Revision History

Revision	Date	Description
50002752A	04/2018	Initial Release

B.2. Cree DC-DC development board data Sheet

KIT8020CRD8FF1217P-1
CREE Silicon Carbide MOSFET Evaluation Kit

User's Manual

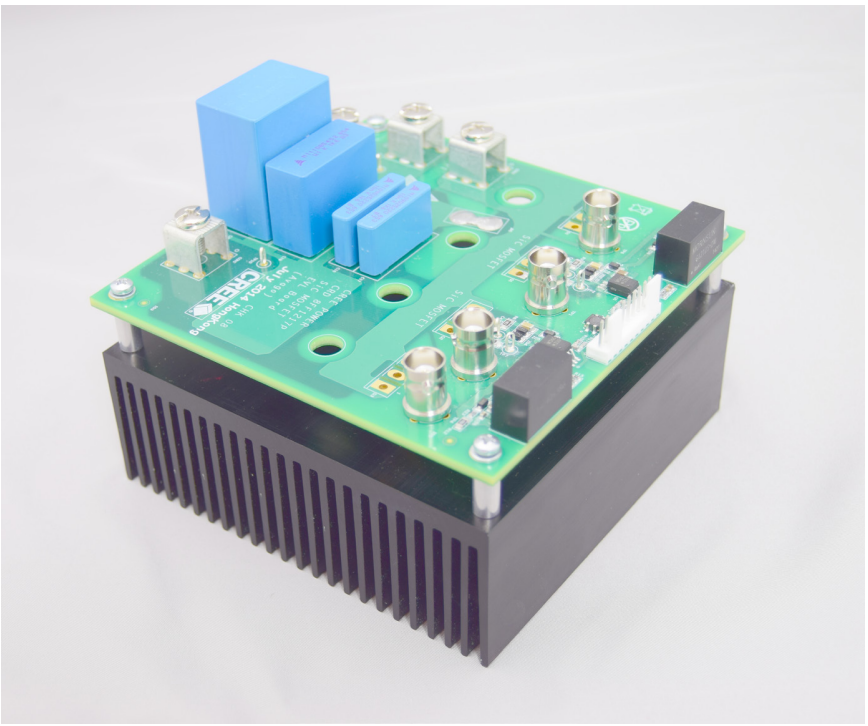

This document is prepared as a user reference guide to install and operate CREE evaluation hardware.

Safety Note: Cree designed evaluation hardware is meant to be an evaluation tool in a lab setting for Cree components and to be handled and operated by highly qualified technicians or engineers. The hardware is not designed to meet any particular safety standards and the tool is not a production qualified assembly

1. Introduction

This Evaluation kit is meant to demonstrate the high performance of CREE 1200V SiC MOSFET and SiC Schottky diodes (SBD) in the standard TO-247 package. It can be easily configured for several topologies from the basic phase-leg configuration. The evaluation (EVL) board can be used for the following purposes:

- Evaluate the SiC MOSFET performance during switching events and steady state operation.
- Easily configure different topologies with SiC MOSFET and SiC diodes
- Functional testing with SiC MOSFET, for example double pulse test to measure switching losses (E_{on} and E_{off}).
- PCB layout example for driving the Cree MOSFET.
- Gate drive reference design for a TO-247 packaged Cree MOSFET.
- Comparative testing between Cree devices and IGBTs.

This user manual will include information on the EVL board architecture, hardware configuration, Cree SiC power devices and an example application when using this board.

2. Package Contents

Item No.	*QTY*	*P/N*	*Description*
1	1	CRD8FF1217P-1	Avago Driver version Eval board
2	4	AOS2182471	Ceramic tile
3	1	57908	Heat sink with mounting holes
4	2	C2M0080120D	80 mohm MOSFET
5	2	C4D20120D	20A Diode
6	1		Copper shorting strip
7	2	74270011	Ferrite Bead
8	8	91166a210	M3 washer, Zn-S, 7mm OD, 3.2mm ID
9	4	92005a129	M3x22mm, Zn-S, Board mounting Screw
10	4	94669a727	Stand offs, Al spacer, 6mm OD x 14mm
11	4	92005a120	M3x10mm, Zn-S, Device mounting screw
12	1		User Guide

3. EVL Board Overview

The EVL board's general block diagram is shown in Figure 1. There is a phase-leg which can include two SiC MOSFETs (Q1 and Q2) with half bridge phase-leg configuration and two anti-parallel SiC schottky diodes (D1 and D3) with Q1 and Q2. The gate drive block with electrical isolation is designed on the board to drive SiC MOSFET Q1 and Q2. There are four power trace connectors (CON1, CON2, CON3 and CON5) and one 10 pin signal/supply voltage connector (CON4) on board.

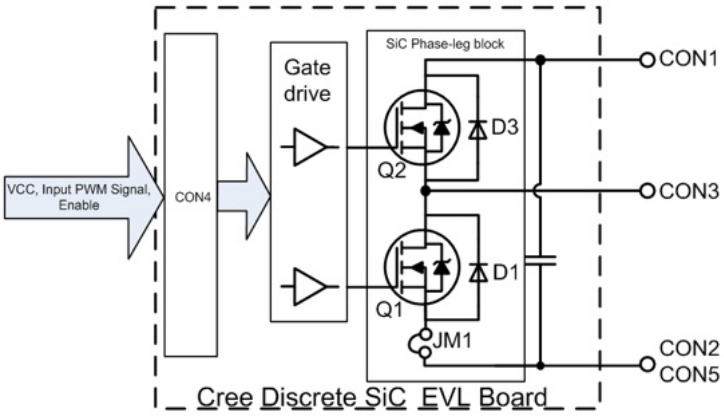

Figure 1. General block diagram of Cree Discrete SiC EVL board

Please note that JM1 as shown in Figure 1 is open circuit. It is necessary to short this with a wire or insert a shunt as shown in section 6.2 to complete the circuit before operation.

CRD8FF1217P-1 includes two 2.5A gate driver integrating opto-coupler from Avago ACPL-W346 and two 2W isolation DC/DC converters from Mornsun G1212S-2W for both high side and low side isolated power. The 2W DC/DC converter with +12V Vcc input generates +24V Vcc_out output voltage with 6KVDC isolation that is supplying voltage to W346 on push-pull gate drive of the secondary side as shown in Figure 2. In this circuit, a 5V zener in parallel with 1uF capacitor is used to generate -5V Vgs voltage for the SiC MOSFET turn-off and turn-on Vgs voltage is equal to 24V-5V=19V. Note that SiC MOSFET can be turned off with zero voltage, and the -5V turn-off voltage helps with faster turn-off and lower turn-off losses and also improves dv/dt induced self turn-on and noise immunity during transient periods with more margin for Vgs turn-on threshold voltage. You can implement any PWM signal to drive the SiC phase leg block, if the board is operating in synchronous mode with high side MOSFET and low side MOSFET, the input signals must have additional dead time to avoid shoot through.

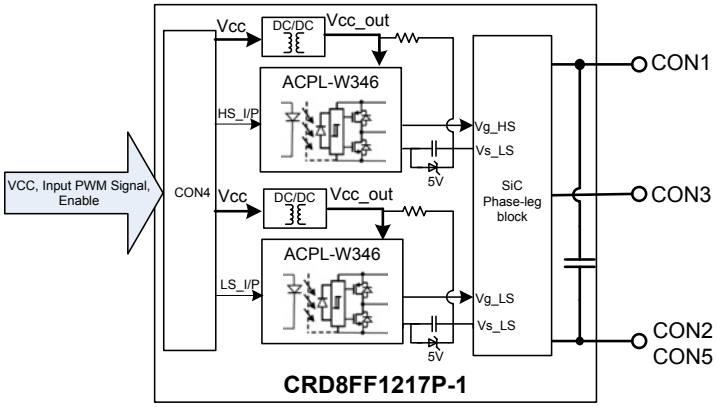

Figure 2. CRD8FF1217P-1 Block diagram with ACPL-W346

The EVL board size is 124mmx120mmx40mm (not including heatsink). Different types of heatsinks can be assembled depending on your cooling requirements. Figure 3 shows the board attached with the heatsink provided in the kit. However, the users can use any type of heatsink that can work with the standard TO-247 package.

Figure 3. Cree EVL board assembly (see Appendix for assembly instructions).

4. Configurations

The EVL board can be flexible to implement difference topologies when using the different configurations of SiC MOSFETs and SiC diodes. It is possible to test several topologies with this board: synchronous Buck, non-synchronous Buck (or high-side Buck), synchronous Boost, non-synchronous Boost, half phase-leg bridge converter, H bridge converter (2x EVL boards) and bi-directional buck-boost converters. Table 1 summarizes the possible topologies that can be implemented using this EVL board. For the phase-leg configuration, it can either use discrete anti-parallel SiC SBD or body diode of SiC MOSFET, thus body diode of SiC MOSFET can be evaluated without anti-parallel diode with option one in the below table.

With double EVL boards, H-bridge converter and bi-directional DC/DC converter can be configured. For H-bridge, with different control architecture, the phase shift full bridge, resonant LLC ZVS converter and single phase DC/ AC converter can all be achieved. For bi-directional DC/DC converter, it can achieve either Buck from port 1 to port 2 or Boost from port2 to port 1. Furthermore, with three EVL boards, it can even be set up as a three-phase DC/AC inverter for some motor drive or inverter applications.

Table. 1 The EVL board topology configuration

Option One: Syn. Buck converter or Phase-leg bridge topology without anti-parallel diodes	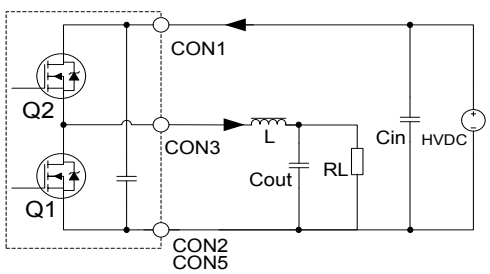	• Step down voltage or phase leg topology w/o anti-parallel diodes • SiC Body diode used • Connect inductor L with CON3 as output • CON1: INPUT • CON3: OUTPUT

		• CON2, CON5: GND
Option Two: Phase-leg bridge topology with anti-parallel SiC SBD	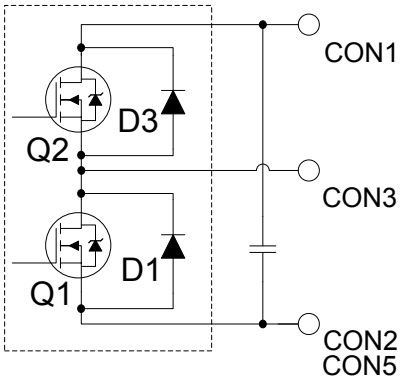	• Phase-leg, switching with external anti-parallel diode • SiC SBD used • CON1, CON3: Input/output depends on which topology apply to board • CON2, CON5: GND
Option Three: Non-syn Buck converter	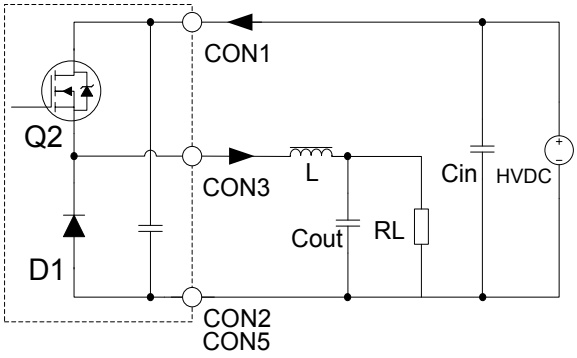	• Step down voltage • Connect inductor L with CON3 as output • CON1: INPUT • CON3: OUTPUT • CON2, CON5: GND
Option Four: Syn. Boost converter	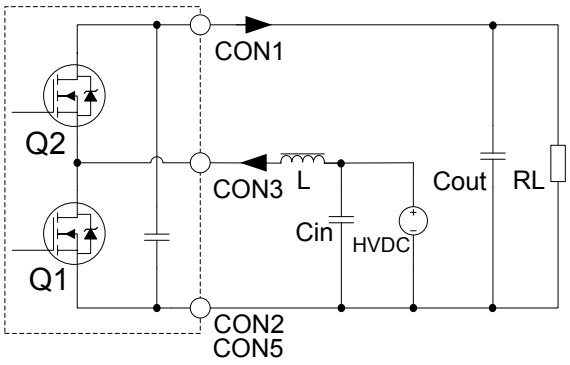	• Step up voltage • Connect inductor L with CON3 as input • CON1: OUTPUT • CON3: INPUT • CON2, CON5: GND
Option Five: Non-syn Boost converter	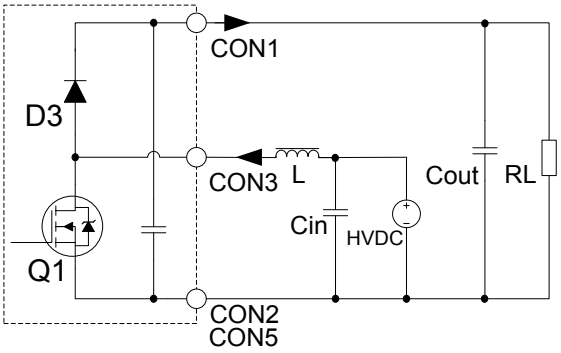	• Step up voltage • Connect inductor L with CON3 as input • CON1: OUTPUT • CON3: INPUT • CON2, CcON5: GND

Option Six: Diode bridge	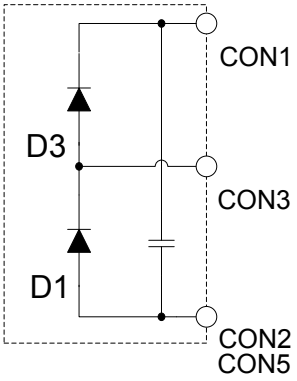	• Bridge diode with SiC SBD • CON1: OUTPUT (Positive) • CON3: INPUT • CON2, CON5: OUTPUT (Negative)
Option Seven: H bridge topology configuration using two EVL boards	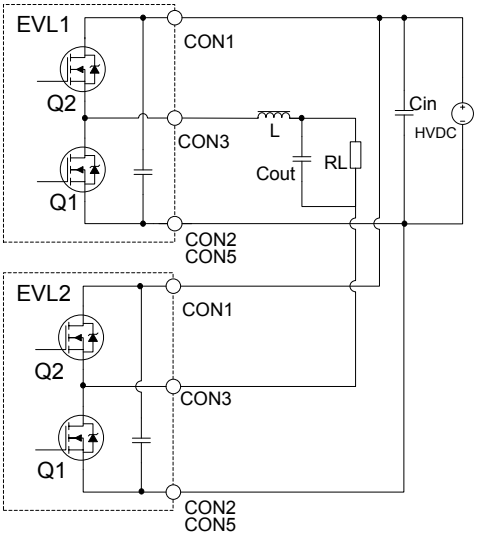	• Full bridge converter with Phase shift or resonant • single phase DC/AC inverter
Option Eight: Bi-directional DC/DC converter	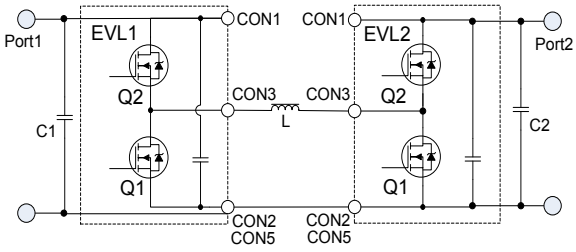	• Port 1 is input and port 2 is output with Buck converter, Q2 of EVL2 is constantly turn-on, and Q1 of EVL2 is constantly turn-off • Port 1 is output and port 2 is input with Boost converter, Q2 of EVL1 is constantly turn-on and Q1 of EVL2 is constantly turn-off

5. Hardware Description

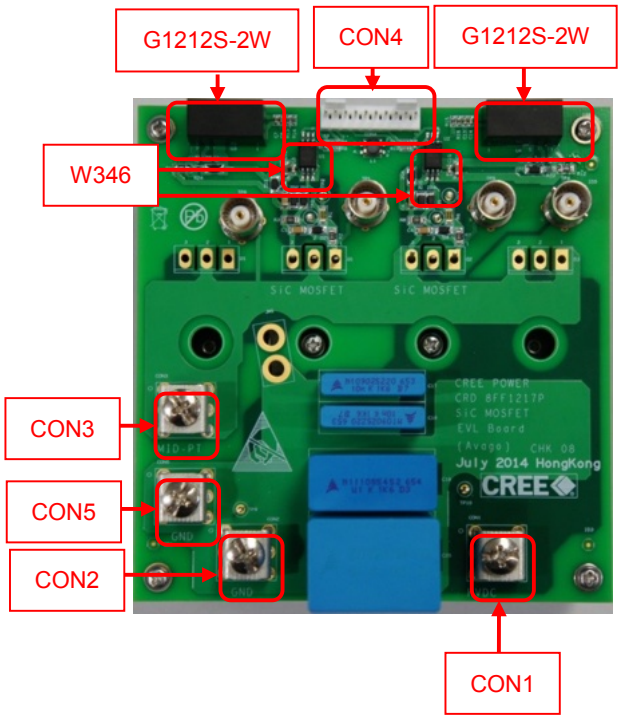

Figure 4. EVL board showing key connectors and components.

The above figures give top view of the EVL board. The picture highlights key test points and connectors on the boards.

5.1 Test points

To make testing more effective and easy, the BNC connectors are added on the board to measure both Vgs and Vds waveforms for SiC MOSFET Q1 and Q2. A current test point with two unpopulated through-hole contacts is available to measure the drain current through the low side switch. A jumper wire (not provided in the kit) with a short loop (JM1) can be inserted to the test point and measure current using current probe. Another option is to use accurate coaxial shunt resistors, (not provided in the kit) from T&M Research (www.tandmresearch.com) to make the measurement. This option can minimize the stray inductance on the switching loops and achieve accurate switching loss measurement. Lastly, one can also simply short JM1 with the small shorting strips provided in the kit, if it's not necessary to measure the current waveform. Also, some test points are added between gate resistors for measuring the voltage across the gate resistors. Thus it can estimate the gate current Ig to the SiC MOSFET.

5.2 Connectors

For the connectors, CON1, CON2, CON3 and CON5 are power trace connectors, and their definitions are depending on the different topology as described in table 1. CON4

is for the signal/logic inputs and supply voltage for ICs. The definition of CON4 for each pin is shown in table 2.

Table. 2 Pin definitions for connector CON4

Connector CON4 Pin	CRD8FF1217P-1
Pin1	N/A
Pin2	N/A
Pin3	N/A
Pin4	N/A
Pin5	VCC: +12Vdc
Pin6	VCC_RTN: GND for +12Vdc
Pin7	Input_HS: signal input for Q2
Pin8	Input_HS_RTN: signal ground for Q2
Pin9	Input_LS: signal input for Q1
Pin10	Input_LS_RTN: signal ground for Q1

5.3 Board design

SiC device is a fast switching device, and it is important to maximize SiC's high performance and minimize ringing with fast switching. The EVL board introduces some design approaches to minimize the ringing on the board:

- The gate drive and logic signal are put on top of the PCB board, while the main power trace and switching devices are put on the bottom layer. There is no crossover or overlap between gate signal and switching power trace, which can minimize high dv/dt and di/dt noise influence from the switching node to gate signal.
- Four de-coupling film capacitors with value 10nF, 10nF, 0.1uF and 5uFare placed close to the SiC devices, and it can reduce high frequency switching loop and bypass noise within switching loop.
- The layout of gate drive circuitry is designed with symmetric trace distance, which can introduce balance impendence on the gate drive. Also, the gate drive is placed as close as possible to the SiC MOSFETs.
- The power trace layout is optimized to reduce the switching loops.

6. CREE Devices

SiC devices including SiC MOSFET and SiC Schottky diodes are recognized as next generation wide bandgap devices. It can provide fast switching with less loss compared to conventional Si devices. Cree is the world's leading manufacturer of silicon-carbide Schottky diodes and MOSFETs for efficient power conversion. Two sample 20A, 1200V rated SiC MOSFET devices and two 20A, 1200V rated Schottky diodes are provided in the kit. However, other samples ranging from 5A to 50A can be ordered online (www.cree.com/power)

Acknowledgments

First of all, I would like to express my sincere gratitude to SCENT project funded by European Union's Horizon 2020 research and innovation program under the Marie Sklodowska-Curie grant agreements, for letting me be part of this incredible leaders network.
I would like to express my sincere thanks to my supervisors , Prof.Robert Smolenski, Prof. Frank Leferink and Prof.Dave Thomas for giving me the opportunity to work in SCENT project and guiding me through this thesis. You have transferred to me so much more than purely scientific knowledge.I am extremely thankful and indebted to them for sharing expertise, and sincere and valuable help to me.

I would also like to thank Dr.Piotr Lezynski for his valuable guidance throughout my studies. You provided me with the tools that I needed to choose the right direction and successfully complete my dissertation. In addition, thanks for your help with providing me with the required devices i needed to complete my practical implementation test-bed. I did'nt forgot your help and guidance during the EMC tests during my secondment in Ekoenergetyka company. You transferred a great practical knowledge, especially in the EMC testing field.

Dr.Niek Moonem, without you, I wouldn't be able to finish my research work,thank you for helping me to become confident in the work done, really you garbed me from the dark to the light during very hard time. Thanks for your motivation and support for all of my research ideas. I didn't forgot your research guidance in our common journals, in addition, to your extensive review for all my research papers. Thanks for your patience and time.

I would like to thank Prof.Paolo Crovetti from the Department of Electronics and Telecommunications Torino, Politecnico di Torino, for guiding me with his knowledge in the communication field. Without him i have never be able to finish the analysis of the output practical results.

I would like to thank all my colleges in University of Zielona Gora Hermes Loschi, Amr Madi, Douglas Nascimento and Lok Choon Long , for their daily support. During my four years of my PhD, we went together through a lot of courses, meetings and conversations , which were vital in inspiring me to think outside the box, from multiple perspectives to form a comprehensive and objective critique. Moreover, i want to thank all my colleges in SCENT project for their supporting ideas and outreach activities for my research work through all the social media channels and SCENT project website.

Especial thanks for Dr. Marco Raaben our project manger, for his support during the whole period of the project. He guided us to all the required administrative work of the project, going through a lot of deliverers, millstones , summer schools and secondments.

Finally, I would like to thank my wife Toqa for her patience during the period of the PhD, you bore a lot of hard times with me. I would like to thank my parents for their wise counsel and sympathetic ear. You are always there for me. Finally, I could not have completed this dissertation without the support of my friends, who provided stimulating discussions as well as happy distractions to rest my mind outside of my research.

Waseem El-Sayed
May 25, 2023

Biography

Waseem El Sayed Was born in 1991, in Alexandria, Egypt. He finished his B.Sc. and M.Sc. studies in electrical and control engineering from the Arab Academy for Science and Technology and Maritime Transport (AASTMT), Egypt in 2013, and 2018 respectively. In April 2019, he started his Ph.D. studies as Earlier Stage Researcher number 1 in the "SCENT - Smart Cities EMC Network for Training" project, he recruited as a Ph.D. student in the Institute of Automatic Control, Electronics and Electrical Engineering at the University of Zielona Gora, Poland as well as the faculty of Electrical Engineering, Mathematics and Computer Science (EEMCS) in the University of Twente, Netherlands and George Green Institute for Electromagnetic Research (GGIER) at the University of Nottingham. .

List of publications related to this thesis

Conferences

1 Waseem El Sayed, Hermes Loschi, Robert Smolenski, Piotr Lezynski, Choon Long Lok ,"Performance Evaluation of the Effect of Power Converters Modulation on Power line Communication",*XIV Konferencja Naukowa Sterowanie w Energoelektronice i Napedzie Elektrycznym 2019*

2 Hermes Loschi, Robert SMOLENSKI, Piotr LEZYNSKI, Waseem El SAYED, Choon Long LOK, "EMC Issues: Prospective Review on the Switch Control Strategies for Converters" *XIV Konferencja Naukowa Sterowanie w Energoelektronice i Napedzie Elektrycznym 2019*

3 H. Loschi, R. Smolenski, P. Lezynski, W. El Sayed and D. Nascimento, "Reduction of Conducted Emissions in DC/DC Converters with FPGA-based Random Modulation", *2020 International Symposium on Electromagnetic Compatibility - EMC EUROPE*, 2020, pp. 1-6, doi: 10.1109/EMCEUROPE48519.2020.9245684.

4 W. E. Sayed, H. Loschi, C. L. Lok, P. Lezynski and R. Smolenski, "Prospective Analysis of the effect of Silicon based and Silicon-Carbide based Converter on G3 Power Line Communication,", *2020 International Symposium on Electromagnetic Compatibility - EMC EUROPE*, 2020, pp. 1-6, doi: 10.1109/EMCEUROPE48519.2020.9245727.

5 W. E. Sayed, H. Loschi, M. A. Wibisono, N. Moonerr, P. Lezynski and R. Smolenski, "The Influence of Spread-Spectrum Modulation on the G3-PLC Performance", *2021 Asia-Pacific International Symposium on Electromagnetic Compatibility (APEMC)*, 2021, pp. 1-4, doi: 10.1109/APEMC49932.2021.9597060.

6 M. A. Wibisono, B. t. Have, W. Elsayed, N. Moonen, D. Hamdani and F. Leferink, "Impact of a Speed-Controlled Water Pump on Power Line Communication of Smart Energy Meters", *2021 Asia-Pacific International Symposium on Electromagnetic Compatibility (APEMC)*, 2021, pp. 1-4, doi: 10.1109/APEMC49932.2021.9596941.

7 W. E. Sayed, H. Loschi, A. Madi, N. Moonen, R. Smolenski and F. Leferink, "Low-Frequency Envelope of DC/DC Converters due Differences in the Control Hardware Features," *2021 Asia-Pacific International Symposium on Electromagnetic Compatibility (APEMC)*, 2021, pp. 1-4, doi: 10.1109/APEMC49932.2021.9596732.

8 W. El Sayed, P. Crovetti, P. Lezynski, R. Smolenski, A. Madi and F. Grassi, "The Influence of Commercial PC Switched Mode Power Supply Interference on the PRIME PLC Performance",*2021 IEEE International Joint EMC/SI/PI and EMC Europe Symposium, 2021*, pp. 632-636, doi: 10.1109/EMC/SI/PI/EMCEurope52599.2021.9559175.

Journal papers

1 Sayed, W.E.; Lezynski, P.; Smolenski, R.; Moonen, N.; Crovetti, P.; Thomas, D.W.P. "The Effect of EMI Generated from Spread-Spectrum-Modulated SiC-Based Buck Converter on the G3-PLC Channel", *Electronics 2021*, 10, 1416.
https://doi.org/10.3390/electronics10121416

2 Sayed, W.E.; Lezynski, P.; Smolenski, R.; Madi, A.; Pazera, M.; Kempski, A. "Deterministic vs. Random Modulated Interference on G3 Power Line Communication", *Energies 2021*, 14, 3257.
https://doi.org/10.3390/en14113257

3 W. El Sayed, P. Crovetti, N. Moonen, P. Lezynski, R. Smolenski and F. Leferink, "Electromagnetic Interference of Spread-Spectrum Modulated Power Converters in G3-PLC Power Line Communication Systems," in *IEEE Letters on Electromagnetic Compatibility Practice and Applications*, vol. 3, no. 4, pp. 118-122, Dec. 2021,
doi: 10.1109/LEMCPA.2021.3121091.

4 Beshir, A.H.; Wan, L.; Grassi, F.; Crovetti, P.S.; Liu, X.; Wu, X.; El Sayed, W.; Spadacini, G.; Pignari, S.A., " Electromagnetic Interference of Power Converter with Random Modulation on the Power Line Communication System", *Electronics 2021*, 10, 2979.
https://doi.org/10.3390/electronics10232979

5 Hermes Loschi, Douglas Nascimento, Robert Smolenski, Waseem El Sayed, Piotr Lezynski,"Shaping of converter interference for error rate reduction in PLC based smart metering systems", *Measurement*, Volume 203, 2022, 111946,ISSN 0263-2241.
https://doi.org/10.1016/j.measurement.2022.111946.

6 Angel Pena-Quintal, Waseem El Sayed, Mark Sumner, Senior, Steve Greedy, Dave Thomas, Robert Smolenski, "On Spread Spectrum for DC grids: Low Frequency Conducted EMI Mitigation and Signal Integrity Disruption in Serial Communication Links", *IEEE Transactions on Electromagnetic Compatibility*,
DOI: 10.1109/TEMC.2023.3273111